Aus dem Forschungszentrum Borstel
Leibniz-Zentrum für Medizin und Biowissenschaften
Laborgruppe Immunepigenetik (Laborgruppenleiter: Dr. Prim B. Singh)
Abteilung Immunologie und Zellbiologie (Direktorin: Prof. Dr. Dr. Silvia Bulfone-Paus)

The role of HP1β on genomic stability and cellular senescence

DISSERTATION
zur Erlangung des Doktorgrades
der Mathematisch-Naturwissenschaftlichen Fakultät
der Christian-Albrechts-Universität
zu Kiel

vorgelegt von
Mustafa Billur

Kiel, Oktober 2010

Leibniz Gemeinschaft

Referent/in:	Prof. Dr. Dr. Silvia Bulfone-Paus
Korreferent/in:	Prof. Dr. Thomas Roeder
Tag der mündlichen Prüfung:	08/11/2010
Zum Druck genehmigt:	

"It is, in fact, nothing short of a miracle that modern methods of teaching have not yet entirely strangled that sacred spirit of curiosity and inquiry, for this delicate plant needs freedom no less than stimulation."

Albert Einstein

Contents

List of abbreviations 1

List of figures 3

List of tables 5

Chapter 1. Introduction 6

1.1 Heterochromatin and Epigenetics 7

1.1.1 Heterochromatin 7

1.1.2 Epigenetics 8

1.1.2.1 Noncoding RNAs 9

1.1.2.2 Chromatin remodelling and histone variants 9

1.1.2.3 DNA methylation 10

1.1.2.4 Histone modifications 10

1.2 Heterochromatin protein 1 (HP1) 12

1.2.1 HP1β 14

1.2.2 HP1β, centromeres and sister chromatid cohesion 17

1.2.3 HP1β and telomeres 20

1.2.4 HP1β and oncogene-induced senescence (OIS) 22

1.2.5 HP1β knockout mice 24

1.3 The goal of the study 25

Chapter 2. Materials and Methods 27

2.1 Materials 28

2.1.1 Primers 28

2.1.2 Plasmids 28

2.1.3 Antibodies 28

2.1.3.1 Primary antibodies 29

2.1.3.2 Secondary antibodies 30

2.1.4 Buffers, media and solutions 30

2.1.4.1 Standard media and solutions 30

2.1.4.2 Flow-FISH solutions 31

2.1.4.3 Telomere-FISH and Giemsa staining solutions 31

2.1.4.4 ChIP solutions 32

2.1.4.5 GST pull down solutions 32

2.1.4.6 Protein purification solutions 33

2.1.4.7 Coomassie stain solutions 33

2.1.4.8 SDS-PAGE and Western blotting solutions 33

2.1.4.9 Metaphase spread preparation solutions 34

2.1.5 Bacterial strains 34

2.1.6 Kits 34

2.2 Methods ... 35
2.2.1 Molecular biology ... 35
2.2.1.1 Preparation of plasmid DNA ... 35
2.2.1.2 Isolation of total RNA from tissue ... 35
2.2.1.3 Measuring concentration of nucleic acids ... 35
2.2.1.4 Reverse transcription of RNA (cDNA synthesis) ... 35
2.2.1.5 Transformation of plasmid DNA into *E.coli* ... 35
2.2.1.6 Agarose gel electrophoresis ... 36
2.2.1.7 Restriction digest ... 36
2.2.1.8 Site-directed mutagenesis ... 36
2.2.1.9 Genotyping PCR ... 37
2.2.1.10 Chromatin Immunoprecipitation (ChIP) ... 38
2.2.1.11 Dot/Slot-blotting of ChIP DNA ... 39
2.2.1.12 Random primer end labelling of telomeric DNA with radioactive ^{32}P-dCTP ... 39
2.2.1.13 Hybridization of dot-blotted ChIP DNA with a ^{32}P-labelled telomeric probe and image analysis ... 39
2.2.1.14 Measurement of telomere length by FLOW-FISH ... 40
2.2.1.15 Telomere-FISH and Giemsa staining ... 41
2.2.2 Protein biochemistry ... 41
2.2.2.1 Protein expression in *E.coli* ... 41
2.2.2.2 GST fusion protein purification ... 42
2.2.2.3 Hexahistidin fusion protein purification ... 42
2.2.2.4 Measuring protein concentration ... 42
2.2.2.5 SDS-PAGE ... 43
2.2.2.6 Coomassie staining ... 43
2.2.2.7 Western blotting ... 43
2.2.2.8 GST pulldown assays ... 43
2.2.2.9 Preparation of paraffin sections and immunohistochemistry ... 44
2.2.2.10 Indirect immunofluorescence ... 45
2.2.3.11 Preparation of chromosome spreads and indirect immunofluorescence staining ... 45
2.2.2.12 Isothermal titration calorimetry (ITC) ... 45
2.2.3 Cell biology ... 47
2.2.3.1 Production of primary mouse embryonic fibroblasts (MEFs) ... 47
2.2.3.2 MEF cell culture ... 47
2.2.3.3 Cell counting ... 47
2.2.3.4 3T9 assay ... 48
2.2.3.5 Transient transfection of EGFP-TPP1, -POT1a and -POT1b ... 48
2.2.4 Animal experiments ... **48**
2.2.4.1 Induction of K-ras^{V12} in K-ras$^{+/V12}$;RERTn$^{+/ERT}$;*Cbx1*$^{+/-}$ transgenic mice ... 48

Chapter 3. Results ... 49
3.1 Investigation of the effect of *Cbx1* null mutation on genomic stability ... 50
3.2 Investigation of the effect of *Cbx1* null mutation on telomere function ... 52
3.2.1 Investigation of the effect of *Cbx1* null mutation on the telomeric "shelterin" ... 52
3.2.2 Investigation of the effect of *Cbx1* null mutation on cellular distribution of "shelterin" proteins ... 54

3.2.3 Investigation of the effect of *Cbx1* null mutation on telomere length 55
3.3 Investigation of the effect of *Cbx1* null mutation on sister chromatid cohesion 57
3.4 Investigation of the effect of *Cbx1* mutation on oncogene-induced senescence in K-ras(+V12);RERT(ert/ert) mouse model system 61
3.5 Investigation of the effect of *Cbx1* mutation on oncogene-induced senescence *in vitro* 71
3.6 Investigation of the binding of HP1β to histone H3 72
3.7 Investigation of the binding affinity of HP1β to histone H3 and H3K9me3 75

Chapter 4. Discussion 82
4.1 The *Cbx1* gene and the regulation on genomic stability 83
4.2 Investigation of the effect of *Cbx1* null mutation on telomere function 84
4.3 The *Cbx1* mutation and sister chromatid cohesion 87
4.4 Investigation of the effect of *Cbx1* mutation on oncogene-induced senescence 89
4.5 The binding of HP1β to histone H3 93

Chapter 5. References 99

Abstract 111
Zusammenfassung 112
Acknowledgements 113
Curriculum Vitae 115
Publications 116
Eidesstattliche Erklärung 117
Appendix 118

List of abbreviations

Ab	antibody
ALT	alternative lengthening of telomeres
bp	base pair
BSA	bovine serum albumin
Bub1	budding uninhibited by benomyl-1
CAF	chromatin assembly factor
CBX	chromobox
CD	chromodomain
cDNA	complementary DNA
CENP	centromere protein
ChIP	chromatin immunoprecipitation
CREST	calcinosis, Raynaud's phenomenon, esophageal dysmotility, sclerodactyly, telangiectasias
CSD	chromoshadow domain
DCR	decoy receptor
dCTP	deoxycytosine triphosphate
DMEM	Dulbecco's modified eagle medium
DNA	deoxyribonucleic acid
DNMT	DNA methyltransferase
dNTP	deoxynucleotide triphosphate
dsRNA	double-stranded RNA
DTT	dithiothreitol
EDTA	ethylene diamine tetraacetic acid
EGFP	enhanced green fluorescent protein
EGTA	ethylene glycol tetraacetic acid
FCS	fetal calf serum
FISH	fluorescent in situ hybridization
FITC	fluorescein isothiocyanate
GST	glutathione S-transferase
h	hour
HAT	histone acetyl transferase
HDAC	histone deacetylase
HKMT	histone lysine methyltransferase
HP1	heterochromatin protein-1
H-ras	harvey rat sarcoma (virus)
IgG	immunoglobulin G
ITC	isothermal titration calorimetry
kb	kilobase
KCM	potassium chromosome medium
KO	knock out
K-ras	kirsten rat sarcoma (virus)
LB	Luria-Bertani medium
MAD	mitotic-arrest deficient protein
MEF	mouse embryonic fibroblast
min	minutes
miRNA	micro RNA
mRNA	messenger RNA
NP-40	nonylphenylpolyethylene glycol
N-ras	neuroblastoma rat sarcoma
OD	optical density
OIS	oncogene-induced senescence
ON	overnight
^{32}P	phosphorus isotope 32
PAGE	polyacrylamide gel electrphoresis
PBS	phosphate-buffered saline
PCR	polymerase chain reaction
PEV	position effect variegation
PMSF	phenylmethylsulfonyl fluoride
PNA	peptide nucleic acid
PO	peroxidase
POT	protection of telomeres
PP2A	protein phosphatase 2A
PRMT	protein arginine methyltransferase
RAP	repressor/activator protein
RB	retinoblastoma
RNA	ribonucleic acid
RNAi	RNA interference
rpm	revolutions per minute
RT	room temperature
s	seconds
SAC	spindle assembly checkpoint

SAHF	senescence-associated heterochromatic foci
SCC	sister chromatid cohesion
SDS	sodium dodecyl sulfate
SGO	shugoshin
SIR	silent information regulatory
siRNA	small interfering RNA
SMC	structural maintenance of chromosomes
SOC	super optimal broth with catabolite repression
SSC	saline sodium citrate
TAE	tris acetate EDTA
TBS	tris-buffered saline
TE	tris EDTA
TEG	tris EGTA
TEMED	tetramethylethylenediamine
TIF	transcriptional intermediary factor
TIN2	TRF1 interacting nuclear factor2
TPP	TINT1/PTOP/PIP1
TRF	telomere repeat binding factor
Triton X-100	polyethylene glycol p-(1,1,3,3-tetramethylbutyl)-phenyl ether
Tween-20	polyoxyethylene (20) sorbitan monolaurate
UV	ultraviolet
WT	wild type

The international system of units (SI) has been used throughout this thesis.

List of figures

Figure 1 Covalent histone modifications 11
Figure 2 Tertiary structures of HP1β chromodomain, chromoshadow domain and chromoshadow domain dimer 14
Figure 3 Aromatic cage formation 15
Figure 4 The structural organization of a mitotic chromosome 17
Figure 5 The structure of the cohesin complex 18
Figure 6 Structure of the mammalian telomeres and "shelterin" complex 21
Figure 7 Steps involved in a typical ChIP experiment 38
Figure 8 Steps involved in a typical GST pull down experiment 44
Figure 9 Schematic diagram of ITC_{200} instrument used in calorimetry experiments 46
Figure 10 3T9 assay of primary MEFs 50
Figure 11 Telomere FISH analysis on metaphases from *Cbx1*$^{-/-}$ primary MEFs 51
Figure 12 ChIP experiments for the analysis of telomeric heterochromatin 53
Figure 13 Western blot with TRF1, TRF2 and HP1β on crude cell lysates 54
Figure 14 Intracellular localizations of POT1a, POT1b and TPP1 in G1 interphase nuclei 55
Figure 15 A typical FACS blot obtained in a FLOW-FISH experiment 56
Figure 16 Mean telomere lengths of early and late passages of WT and *Cbx1*$^{-/-}$ MEFs 56
Figure 17 Localization of SMC3 on WT and *Cbx1*$^{-/-}$ metaphase chromosomes 58
Figure 18 Localization of BUB1 on WT and *Cbx1*$^{-/-}$ metaphase chromosomes 59
Figure 19 Localization of SGO1 on WT and *Cbx1*$^{-/-}$ metaphase chromosomes 60
Figure 20 Sequencing results of RT-PCR products from K-ras mice 62
Figure 21 Number of adenocarcinomas found in K-ras mice with *Cbx1*$^{+/-}$ mutation compared to WT 63
Figure 22 IHC staining of lung tumours with p16 antibody 65
Figure 23 IHC staining of lung tumours with DcR2 antibody 66
Figure 24 IHC staining of lung tumours with pKi-67 antibody 67
Figure 25 IHC staining of lung tumours with HP1α antibody 68
Figure 26 IHC staining of lung tumours with HP1β antibody 69
Figure 27 IHC staining of lung tumours with HP1γ antibody 70
Figure 28 Growth curve analysis of the cells transduced with a ras expression vector 71
Figure 29 The percentages of SA-b-gal positive cells after transduction with a ras expression vector 72
Figure 30 An overview of mutations and recombinant HP1β proteins used in pull down experiments 73
Figure 31 Coomassie stained SDS gels showing the results of GST pull down experiments 74
Figure 32 Binding of wild type HP1β to H3K9me3 at 25°C and 37°C 77
Figure 33 Binding of wild type HP1β to histone H3 at 25 °C and 37 °C 77
Figure 34 Binding of HP1β T51A to H3K9me3 at 25 °C and 37 °C 78
Figure 35 Binding of HP1β T51A to histone H3 at 25 °C and 37 °C 78
Figure 36 Binding of HP1β V23M to H3K9me3 at 25 °C and 37 °C 79

Figure 37 Binding of HP1β V23M to histone H3 at 25 ˚C and 37 ˚C 79
Figure 38 Binding of HP1β F45E to H3K9me3 at 25 ˚C and 37 ˚C 80
Figure 39 Binding of HP1β F45E to histone H3 at 25 ˚C and 37 ˚C 80
Figure 40 Binding of HP1β I161E to H3K9me3 at 25 ˚C and 37 ˚C 81
Figure 41 Binding of HP1β I161E to histone H3 at 25 ˚C and 37 ˚C 81
Figure 42 A model for the interaction of the WT human HP1β bound to H3K9me2 95

List of tables

Table 1 Enzymes that are responsible for site specific histone modifications 11
Table 2 Composition of SDS gels 43
Table 3 TEG medium composition 47
Table 4 Comparison of the frequencies of chromosome aberrations 51
Table 5 Analysis of lungs from K-ras$^{+/V12}$;RERTn$^{+/ERT}$ and K-ras$^{+/V12}$;RERTn$^{+/ERT}$;*Cbx1*$^{+/-}$mice 63
Table 6 An overview of the results of all GST pull down experiments performed 74
Table 7 An overview of thermodynamic parameters obtained from all ITC experiments performed 76

Chapter 1

Introduction

1.1 Heterochromatin and epigenetics

1.1.1 Heterochromatin

In eukaryotic cells, genomic DNA is folded with histone and non-histone proteins to form chromatin. Chromatin is divided into two major compartments called euchromatin and heterochromatin. Euchromatin or "true" chromatin is referred as the transcriptionally active region of chromatin where heterochromatin is considered to be transcriptionally inert, consisting primarily of highly repetitive sequences, such as satellite sequences, transposable elements, centromeric and telomeric sequences which participate critically in the formation of chromosomal structures essential for proper chromosome function (Hughes and Hawley, 2009). Heterochromatin itself is further classified into two distinct groups as constitutive and facultative (Brown, 1966). Facultative heterochromatin is defined as euchromatic regions that become packaged into a compact heterochromatin-like form generated in a developmental manner (*e.g.* autosomal imprinted genomic loci) which retain the potential to interconvert between heterochromatin and euchromatin (Gilbert *et al.*, 2003) whereas constitutive heterochromatin describes large segments of the genome, primarily arrays of tandemly repeated sequences which are packaged in a permanently inactive form (Gilbert and Allan, 2001).

It was Emil Heitz who first distinguished heterochromatin from euchromatin 82 years ago on the basis of a series of cytogenetic observations (Heitz, 1928). He stained cells from several species of moss with carmine acetic acid and observed a type of chromatin in the nucleus that remained condensed throughout the cell cycle, which was different from euchromatin that underwent cycles of condensation and decondensation at different stages of the cell cycle. His observations were followed by those of Hermann Joseph Muller's, who first described the phenomenon of **p**osition **e**ffect **v**ariegation (PEV) in *Drosophila* (Muller, 1930). Muller used X-rays as a mutagen and observed, in mutant flies, a variegating eye phenotype with some patches of red and some patches of white facets. Variegation was due to the change in the position of a typically distal gene, "white" to a more proximal position within the pericentric heterochromatin due to an X-ray induced chromosomal inversion. The evidence that genes that were more proximal to heterochromatin were silenced first, with subsequent silencing of

distal genes later came from the studies of Demerec, Slisynska (Demerec and Slisynska, 1937) and Schultz (Schultz, 1939) and led eventually to the idea of linear spreading of heterochromatin along the chromosomes, an idea that still has an influence on the theories of chromatin-mediated silencing. Genetic screens for dominant second-site mutations on flies exhibiting a PEV phenotype were extremely useful for the identification of loci likely to encode (hetero-) chromatin components or enzymes that modify those components (Reuter and Spierer, 1992). As a result of these analyses, about 30 modifiers of PEV have been isolated and characterized so far that are either suppressors (Su(var)) or enhancers (E(var)) of PEV. Heterochromatin protein 1 (HP1 – Su(var)2-5) and the histone methyltransferase Su(var)3-9 are among the most important chromatin components revealed by this approach, which will be explained in more detail below (James and Elgin, 1986; Tschiersch *et al.*, 1994).

1.1.2 Epigenetics

The word epigenetics was coined by Conrad Hal Waddington (1905-1975) in 1942 as *"the branch of biology which studies the causal interactions between genes and their products, which bring the phenotype into being"* (Waddington, 1942) although the root term "epigenesis" dates back to Aristotle (384-322 BC) where he used it in opposition to "preformation" and argued that there were no preformed equivalents in the fertilized egg for later developing structures. Waddington elegantly put these terms into the context of development in his 1939 book "An Introduction to Modern Genetics" (Waddington, 1939) where he wrote that as *"the interaction of these constituents [of the fertilized egg] gives rise to new types of tissue and organ which were not present originally,...development must be considered as 'epigenetic'."* In light of many more discoveries that have dramatically increased our understanding of the molecular mechanisms underlying regulation of eukaryotic gene expression, the current definition of epigenetics has been evolved into: *"the study of mitotically and/or meiotically heritable changes in gene function that cannot be explained by changes in DNA sequence"* (Riggs *et al.*, 1996).

Several interrelated epigenetic mechanisms have been identified so far including noncoding RNAs, chromatin remodelling, histone variant composition, DNA methylation and histone modifications, which will be further explained below.

1.1.2.1 Noncoding RNAs

The RNAi machinery (*e.g.* dicer, argonaute, siRNA, miRNA) is an evolutionarily conserved set of proteins that breaks down double-stranded RNA (dsRNA) species into smaller siRNA molecules (short interfering RNA). These small siRNAs inhibit mRNA translation into proteins and thereby reduce gene expression. Notably, a transcriptional gene silencing mechanism has been discovered in fission yeast *S. pombe*, where mutations of any component of the RNAi machinery resulted in defects in chromosome segregation that is likely due to a defect in centromeric heterochromatin (Hall *et al.*, 2002; Reinhart and Bartel, 2002; Volpe *et al.*, 2002). Further work in yeast and fruit flies has indicated strongly a role for the RNAi machinery in the assembly of silent heterochromatin domains (Grewal, 2010).

1.1.2.2 Chromatin remodelling and histone variants

According to current concepts, chromatin composition can be changed by the recruitment of chromatin "remodelling" complexes (Ho and Crabtree, 2010). These remodelling complexes are able to mobilize nucleosomes and/or alter nucleosomal structure resulting in conformational changes that regulate the accessibility of several transcriptional factors and regulators to DNA. Remodelers can be generalized into two families, namely ISWI and SWI/SNF (Ho and Crabtree, 2010); ISWI complexes are thought to mobilize nucleosomes, allowing them to move along the DNA, while SWI/SNF complexes are thought to alter the structure of the nucleosome itself (Tsukiyama *et al.*, 1995; Varga-Weisz *et al.*, 1997). There are also other remodelling complexes like Swr1 (Mizuguchi *et al.*, 2004) and SRCAP (Ruhl *et al.*, 2006) that are dedicated to the replacement of core histones with specialized histone variants. Some examples the histone variants known today include histone H3.3 that replaces histone H3.1 in regions of high transcriptional activity, CENP-A which is the centromere specific H3 variant, H2A.Z which is correlated with open promoters in yeast and H2A.X which is primarily associated with sensing DNA damage and augments the recruitment of DNA repair complexes (Sarma and Reinberg, 2005; Cairns, 2009).

1.1.2.3 DNA methylation

The methylation of the cytosines in CpG dinucleotides in mammalian genomic DNA represents the archetypal epigenetic mechanism, having been studied for many decades since it was posited that DNA methylation could regulate gene activity (Riggs, 1975; Holliday and Pugh, 1975). DNA methylation involves the addition of a methyl group at cytosine residues of the DNA template by DNMTs (DNA methyltransferases). This modification does not change the primary DNA sequence but impacts on gene activity and expression in a heritable fashion (Razin and Riggs, 1980). The addition of a methyl group in vertebrates occurs mostly on the cytosine within CG dinucleotides (CpG) although there is evidence that also non-CpG methylation exists, primarily within CA nucleotides, which is detected mainly in stem cells (Schübeler, 2009). 60-90 % of all CpGs are methylated in mammals whereas "CpG islands", CpG-enriched sequences that frequently coincide with gene promoter regions, are generally unmethylated (Bird, 1986). In higher eukaryotes, CpG methylation is associated with a repressed chromatin environment and is involved in various processes such as gene repression, imprinting, X-chromosome inactivation, suppression of repetitive genomic elements, and carcinogenesis (Bird, 2002).

1.1.2.4 Histone modifications

The fundamental chromatin unit, or nucleosome, contains 146 bp of DNA, which is wrapped around an octamer of histones (Luger *et al.*, 1997). All higher order levels of compaction (*e.g.* the 30 nm fibre) are assembles out of this fundamental nucleosome particle. Accordingly, there is a current high interest how post-translational modifications of the constituent histones of the nucleosome might be involved in the epigenetic regulation of gene activity. It is known that histones are modified by covalent modifications at specific positions within the amino-terminus of the core histones (the "histone tails") that protrude from the nucleosome (Figure 1). These modifications include lysine acetylation, methylation, ubiquitination and sumoylation, arginine methylation, serine and threonine phosphorylation, glutamate ADP-ribosylation, and proline isomerization. Lysine residues can be mono-, di- or tri- methylated

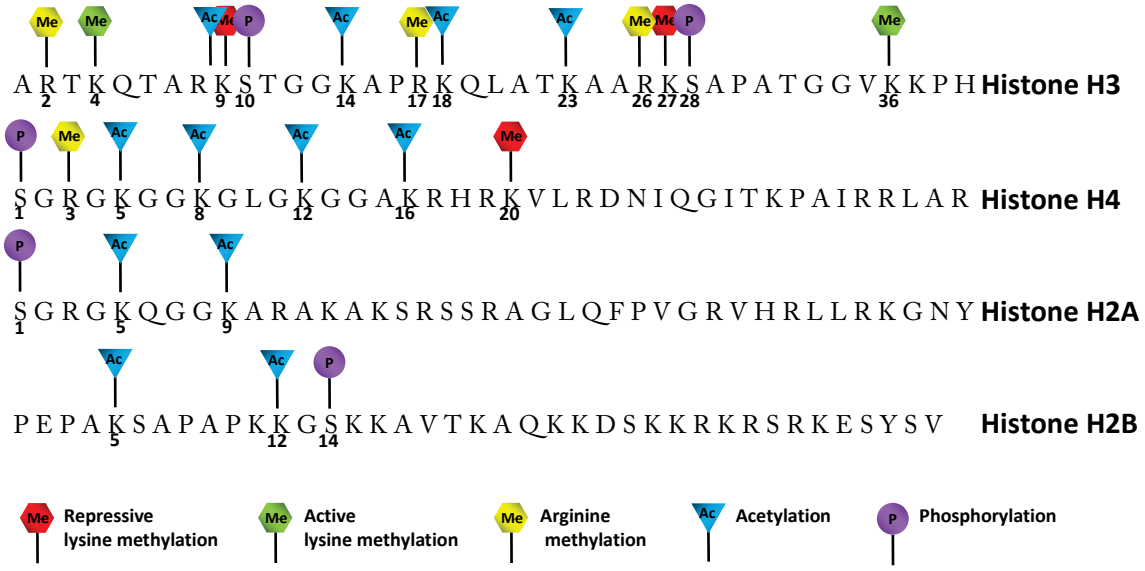

Figure 1 Some of the most studied covalent modifications and their positions on histones are depicted.

	Lysine acetylation	Serine & threonine phosphorylation	Arginine methylation	Lysine methylation
Establishers	**HATs**	**Kinases**	**PRMTs**	**HKMTs**
Examples	Gcn5, Src1, TAF1, CBP & p300, Sas3, MOZ & MORF, PCAF & hGcn5, Rtt109, Esa1, Hat1, HBO1, Mof, Sas2	Snf1, Jil-1, Rsk2, Msk1, Ip11, Aurora B, Sps1, CKII, Mst1, Haspin, ATM, DNA-PK	CARM1, PRMT1	Set1, SET7/SET9, SUV39H1&SUV39H2, G9a, Eu-HMTase1, ESET&SETDB1, Clr4, EZH2, DOT1, SUV420, SET9
Removers	**HDACs**	**PPtases**	**Deiminases**	**Amine oxidases, hydroxylases**
Examples	RPD3, Hda1, HDAC1-10	Glc7, PP1, PP2A	JMJD6	JARID1A-C, LSD1, Lid, UTX, JMJD3, JHDM1-3

Table 1 Enzymes that are responsible for site specific histone modifications. "Establishers" are the enzymes that are responsible for the transfer of the stated modifications on the amino acids, whereas "removers" remove these modifications. HAT: Histone acetyltransferase, PRMT: Protein arginine methyltransferase, HKMT: Histone lysine methyltransferase, HDAC: Histone deacetylase, PPtase: Protein phosphatase.

whereas arginine residues can be modified into symmetric or asymmetric dimethylated states, or into a monomethylated state (Gelato and Fischle, 2008). These modifications can also be reversed and many enzymes and complexes have been identified and characterized that modify histones or return histone residues to an unmodified state (Bhaumik *et al.*, 2007) (Table 1).

Existence of such distinct histone modifications are thought to generate synergistic or antagonistic interaction affinities for chromatin-associated proteins that in turn dictate dynamic transitions between transcriptionally active (on) or transcriptionally silent (off) chromatin states. In general, histone acetylation and H3K4, –K36, -K79 methylation are related to a transcriptionally active state, whereas H3K9, -K27 and H4K20 methylation are indicative of a silent state. This notion has led to the proposal of a "histone code" hypothesis where histone modifications are thought to change higher order chromatin structures and thus regulate accessibility of genomic information (Strahl and Allis, 2000). Although an interesting hypothesis, it remains unproven particularly because generalisations are somewhat difficult to make as histone modification patterns vary considerably between organisms (especially between lower and higher eukaryotes).

1.2 Heterochromatin protein 1 (HP1)

In addition to enzymatic activities that can reversibly modify the histones, the "histone code" hypothesis posits that there are "adapter" proteins that recognize the modifications and "translate" the code into biological function. Of these adapter proteins, one of the first to be characterized was the non-histone chromosomal protein, **h**eterochromatin **p**rotein **1** (HP1) (Eissenberg and Elgin, 2000). HP1 was first identified in *D. melanogaster* as a mutation Su(var)205, that dominantly suppresses PEV (James and Elgin, 1986; Eissenberg *et al.*, 1990). The subsequent cloning of the wild type gene product showed it to be a chromatin protein that predominantly localizes to pericentromeric heterochromatin (James *et al.*, 1989). HP1 is a phylogenetically highly conserved protein with homologues in diverse organisms including both plants and animals (Singh *et al.*, 1991) with the exception of budding yeast, in which PEV relies on **s**ilent **i**nformation **r**egulatory (SIR) proteins. Studies in many organisms have shown that HP1 homologues are involved in the establishment and maintenance of higher-order chromatin structures by

specifically recognizing and binding to (*tri-* and *di-*) methylated histone H3K9 (Bannister *et al.*, 2001; Lachner *et al.*, 2001). Artificial recruitment of HP1 to a gene promoter region results in gene repression in many organisms, establishing the role of HP1 in gene silencing (Ayyanathan *et al.*, 2003; Li *et al.*, 2003).

The HP1 family of proteins are encoded by a class of genes known as the chromobox (*Cbx*) genes. In mammals, there are three homologues of *D. melanogaster* HP1, termed HP1α (*Cbx5*), HP1β (*Cbx1*), and HP1γ (*Cbx3*) (Jones *et al.*, 2000). They share a high degree of sequence similarity and localize, to a lesser or greater extent, to constitutive heterochromatin: HP1α and HP1β are usually found enriched at sites of constitutive heterochromatin such as centromeres and telomeres, whereas HP1γ has a more uniform distribution (Minc *et al.*, 1999; Minc *et al.*, 2000; Dialynas *et al.*, 2007). Although HP1 proteins are concentrated at pericentric heterochromatin in most organisms, they are also found at euchromatin, where their binding correlates with the repression of genes (Fanti *et al.*, 2003; Grewal and Moazed, 2003). For example, HP1α and HP1γ were shown to be recruited by the hormone-induced repression of a viral promoter fused to a transgene reporter inserted into mouse euchromatin (Ayyanathan *et al.*, 2003). HP1γ has also been found to associate with actively transcribed gene regions and to play a role in efficient transcriptional elongation (Vakoc *et al.*, 2005; Lomberk *et al.*, 2006).

HP1 proteins are part of a larger superfamily of proteins containing **chr**omatin **o**rganization **mo**difier (chromo) domain (CD), which is an evolutionarily conserved region of 30-60 amino acids found in the amino-terminal half of these proteins. Many members of this superfamily are known to function in gene regulation and heterochromatin formation, such as the Polycomb protein PC1, a silencer of homeotic genes (Paro and Hogness, 1991). The CD of HP1 shares greater than 60 % amino acid sequence identity with the Polycomb CD and substitution of these chromodomains in HP1 and PC1 with each other changes their nuclear localization patterns indicating a role of the CD in both target-site binding and target preference (Platero *et al.*, 1995). HP1 proteins are also characterized by the presence of a second unique conserved domain in the C-terminal half of the protein, known as the **c**hromo**s**hadow **d**omain (CSD) (Aasland and Stewart, 1995). CSD shares amino-acid sequence identity with the

CD, but has different functions. It can dimerize to form a hydrophobic pocket that can accommodate a pentapeptide PxVxL sequence motif, found in several HP1-interacting partners such as such as **t**ranscriptional **i**ntermediary **f**actors (TIFs) and **c**hromatin **a**ssembly **f**actor 1 (CAF1) (Brasher *et al.*, 2000; Thiru *et al.*, 2004; Nielsen *et al.*, 1999; Murzina *et al.*, 1999) (Figure 2).

1.2.1 HP1β

Among the three mammalian HP1 isoforms HP1β is the best characterized. It is a small protein of around 25 kDa and has the typical N-terminal CD/C-terminal CSD structure with a poorly conserved hinge region in between. Although the structure of the intact HP1β has not yet been determined, three dimensional structures of the CD and CSD have been elucidated by NMR spectroscopy and X-ray crystallography (Figure 2) (Ball *et al.*, 1997; Brasher *et al.*, 2000; Huang *et al.*, 2006). The similarity of the CD and CSD at the level of the primary sequence (identity 24 %) is reflected in a concomitant similarity at the tertiary level with each globule consisting of an anti-parallel, three-stranded, β-sheet that backs onto one (CD) or two (CSD) α-helices. Recombinant HP1β CSD dimerizes in solution with the dimer focused upon helix α2, which interacts symmetrically and at an angle of 35° with helix α2 of the adjacent CSD subunit and forms a non-polar pit that can accommodate pentapetides with the consensus sequence motif PxVxL that is found in several HP1-interacting proteins (Figure 2).

Figure 2 Tertiary structures of HP1β chromodomain (green), chromoshadow domain (pink) and the chromoshadow domain dimer (pink & blue) are depicted (Billur *et al.*, 2010). At the level of primary sequence, CD and CSD are 24 % identical and this similarity is also reflected upon the tertiary level with each globule consisting of an anti-parallel, three-stranded, β-sheet that backs onto one (CD) or two (CSD) α-helices. The CSD dimer interface centers on helix α2, which interacts symmetrically and at an angle of 35° with helix α2 of a neighboring subunit and forms a "nonpolar" pit that can accommodate pentapeptides with the consensus sequence motif PxVxL.

HP1β localizes to constitutive heterochromatin through a variety of interactions with chromatin. One involves a dynamic interaction of the HP1β CD with the H3K9me3 determinant of the histone code with a K_D of 1.9 μM that results from the enzymatic activities of Suv39h1/h2 histone methyltransferases (Rea *et al.*, 2000, Cheutin *et al.*, 2003, Festenstein *et al.*, 2003). In cells taken from *Suv39h1/h2* double-null mutant mice, the enrichment of both H3K9me3 and H4K20me3 at centromeric heterochromatin is lost, and HP1β is found homogeneously distributed throughout both the eu- and heterochromatin (Peters *et al.*, 2001; Kourmouli *et al.*, 2004; Kourmouli *et al.*, 2005; Schotta *et al.*, 2004). Enrichment of HP1β at heterochromatin could be reconstituted in these cells by exogenously expressed Suv39h1 but not by a Suv39h1 mutant that lacks H3K9 histone methyltransferase activity. Together with other studies, this has led to the development of a model where HP1β–H3K9me3 binding leads to further methylation of H3K9 on adjacent nucleosomes through the interaction of HP1β with Suv39h1, thereby resulting in the spreading of a repressive heterochromatic chromosomal domain (Bannister *et al.*, 2001). The NMR solution structure of the HP1β CD–H3K9me3 complex and the crystal structure of *D. melanogaster* HP1 CD with the H3 tail peptide revealed that the binding site for the H3K9me3 peptide is the groove in the HP1β CD and that a short stretch of amino acids in the histone tail (E5 - S10) were involved in this binding (Jacobs *et al.*, 2002; Nielsen *et al.*, 2002). An induced fit mechanism has been shown to be utilized

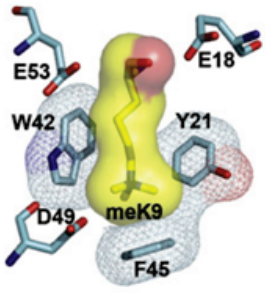

Figure 3 A notional "aromatic cage" is formed from three conserved aromatic residues: Y21, W42 and F45. The interaction between the methylammonium moiety and the aromatic cage is largely electrostatic and mediated by cation-π interactions where the positively charged (cation) moiety is attracted to the negative electrostatic potential of the aromatic groups' π-system (Billur *et al.*, 2010).

where the HP1β N-terminus wraps around the H3K9me3 peptide as binding takes place. As a result of this, three conserved aromatic residues (Y21, W42 and F45) are brought together to form a notional "aromatic cage" in which the positively charged methylammonium functional moiety of H3K9me3 fits in largely through electrostatic interactions forming a cation-π bond (Figure 3) (Dougherty, 2007). Non-conservative substitutions at any of these

aromatic residues have been shown to cause a 200-500 fold reduction in the binding affinity of HP1 CD for the H3K9me3 peptide (Jacobs *et al.*, 2002). It has been shown that the phosphorylation of the adjacent serine residue (S10) in the H3K9me3 peptide also reduces the affinity of HP1β CD for the histone tail by 100 fold and this is probably caused by the interference of this residue with the side chains of T51 and E53. As a result of this phosphorylation, most of the chromatin-bound HP1β is excluded into the cytoplasm at metaphase and this is thought to be required for chromatin to undergo maximal compaction during formation of metaphase chromosomes (Fischle *et al.*, 2005; Hirota *et al.*, 2005).

Another key interaction of HP1β which has been studied in some detail is the binding to histone H3 histone-fold domain. The binding of HP1β to the histone-fold region (amino acids 48–136) of recombinant, non-modified, histone H3 has been shown to be resistant to 0.6 M NaCl concentration and is not perturbed by a 200-fold excess of H3K9me3 peptide (Nielsen *et al.*, 2001; Dialynas *et al.*, 2006). Mutational analysis on HP1β and *D. melanogaster* HP1 indicates that a single residue, valine 23, is probably responsible for both H3K9me3 and histone H3 binding (Nielsen *et al.*, 2002; Jacobs *et al.*, 2001). Binding to histone H3 fold probably occurs only if the histone H3 fold is accessible and the fact that HP1β binds poorly to mononucleosomes but strongly to oligonucleosomal arrays that contain various nucleosome assembly/disassembly intermediates is in support of this hypothesis (Dialynas *et al.*, 2006). Passage through S-phase seems to be required for the stable incorporation of HP1β into heterochromatin as evidenced by the failure of cells blocked in S-phase to incorporate HP1β into heterochromatin (Dialynas *et al.*, 2006). S-phase results in the disruption of chromatin and may explain the observation that HP1β preferentially binds to H3-H4 subparticles in S-phase extracts. H3-H4 subparticles can also be isolated from bulk heterochromatin using GST-HP1β "pull downs" and have been shown being not to be particularly enriched in the H3K9me3 determinant of the histone code (Dialynas *et al.*, 2006) indicating that the binding of HP1β to histone H3 fold does not require the presence of H3K9me3 on the same histone.

1.2.2 HP1β, centromeres and sister chromatid cohesion

Centromeres were originally defined by Flemming in 1880 as a cytologically visible "primary" constriction in the chromosome (Flemming, 1880). The current definition is that the centromere consists of the DNA plus chromatin proteins that are responsible for kinetochore formation (Torras-Llort *et al.*, 2009). The kinetochore itself defines a small, transiently assembled structure whose function is to attach chromosomes to spindle microtubules, generate force for chromosome movements, and produce a signal that delays anaphase onset until all chromosomes are attached to the spindle microtubules (Figure 4) (Pidoux and Allshire, 2005). In most eukaryotes the kinetochore forms only on a subset of the long arrays of repetitive DNA associated with centromeres and these 'regional' centromeres are specified by epigenetic mechanisms instead of the primary DNA sequence. It has been shown that the centromeric heterochromatin in humans has a conserved organization with a typical association with specific histone methylation patterns, high levels of DNA methylation, low recombination frequency and repression of transcription (Blower *et al.*, 2002). Both centromeric chromatin and flanking pericentromeric heterochromatin are required for chromosome segregation and *de novo* chromosome assembly and they are distinct epigenetic entities with their own characteristics. Whereas centromeric chromatin is continuous and contains the histone variant

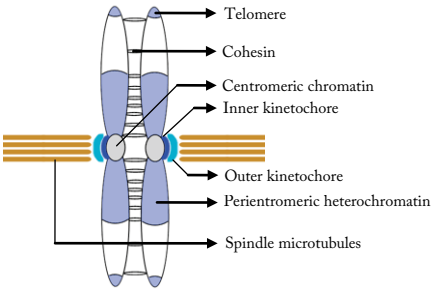

Figure 4. The structural organization of a mitotic, metacentric chromosome. Centromeric chromatin underlies the kinetochore, which contains inner and outer plates that form microtubule attachment sites. Pericentromeric heterochromatin flanks centromeric chromatin, and contains a high density of cohesin, which mediates sister chromatid cohesion (redrawn from Allshire and Karpen, 2008).

CENP-A as well as H3K4me2, the flanking pericentric heterochromatin is defined by H3K9me2 and H3K9me3 and exerts a repressive effect on gene transcription, which appears to be relevant for the activity of the centromere (Sullivan and Karpen, 2004; Lam *et al.*, 2006). The HP1 and Su(var)3-9 proteins are also located at the heterochromatic pericentromeric regions in *Drosophila* and mammals (James *et al.*, 1989; Wreggett *et al.*, 1994; Aagaard *et al.*, 1999; Minc *et al.*, 1999). In fission yeast, the absence of either Swi6 (HP1) or Clr4 (Su(var)3-9) has been shown to result

in the alleviation of outer repeat (and mating type) silencing, and Swi6 is specifically located at these regions (Allshire *et al.*, 1995; Ekwall *et al.*, 1995; Partridge *et al.*, 2000; Nakayama *et al.*, 2000; Noma *et al.*, 2001).

Sister chromatid cohesion is required to ensure faithful chromosome segregation by ensuring biorientation of chromosomes on the mitotic or meiotic spindle (Lee and Orr-Weaver, 2001). Cohesion depends on a multi-subunit, ring-shaped cohesin complex which consists of a heterodimer of **s**tructural **m**aintenance of **c**hromosomes (SMC) subunits, SMC1 and SMC3, the kleisin subunit SCC1 (also known as Mcd1/Rad21), and SCC3 (also known as SA/STAG) (Peters *et al.*, 2008) (Figure 5). Loading of this complex on chromatin occurs in early G1 in vertebrates which establishes cohesion during S phase (Uhlmann and Nasmyth, 1998; Watrin *et al.*, 2006). As a result of the so-called prophase pathway that involves Aurora B and Polo kinases, as well as a number of additional cohesin-interacting factors, most cohesin dissociates from chromatin at the onset of mitosis (Losada *et al.*, 2002; Dai *et al.*, 2006). However, a small population of cohesin, enriched mainly at the centromeric region, remains on chromatin until the onset of anaphase when it is finally removed through the cleavage of the SCC1 N-terminus by separase (Waizenegger *et al.*, 2000; Wirth *et al.*, 2006). Protection of centromeric cohesin

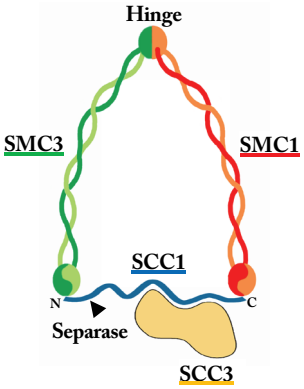

Figure 5. The structure of the cohesin complex (yeast nomenclature) which is a heterodimer formed between SMC1 and SMC3 subunits. Each subunit composed of a ca. 50 nm long intramolecular antiparallel coiled coil, forms a rod-shaped protein with a globular "hinge" domain at one end and an ATP nucleotide-binding domain at the other. At the onset of anaphase, separase cleaves the SCC1 subunit and removes cohesin from chromosomes.

from the prophase pathway is established by the centromere-specific SGO1 protein, a member of a class of proteins known as shugoshins (means "guardian spirit" in Japanese), whose founding member is the Mei-S332 protein in *D. melanogaster* (Kerrebrock *et al.*, 1995; Kitajima *et al.*, 2005; McGuinness *et al.*, 2005; Salic *et al.*, 2004). SGO1 proteins possess a conserved coiled-coil domain that binds the ABC PP2A holoenzyme (**A**TP **b**inding **c**assette **p**rotein **p**hosphatase

2A), which is also localized to centromeres in mitotic cells and is required for maintaining cohesion in early mitosis in human cells and in meiosis I in yeast (Kitajima *et al.*, 2006; Riedel *et al.*, 2006; Tang *et al.*, 2006). It is thought that PP2A counteracts cohesin phosphorylation by Polo thereby preventing the cohesin's release. An additional mechanism that has evolved in eukaryotes to prevent chromosome missegregation is the **s**pindle **a**ssembly **c**heckpoint (SAC). SAC activity delays the metaphase-to-anaphase transition until all chromosomes establish proper attachments to spindle microtubules and align at the metaphase plate. There are several evolutionary conserved core components of the SAC, including: BUB1, BUB3, MAD1, MAD2, BUBR1 (MAD3 in yeast), MPS1 and Aurora B. It has been shown that the proper localization of SGO1 at centromeres requires both the spindle checkpoint protein BUB1, Aurora B and also HP1α (Kitajima *et al.*, 2005; Tang *et al.*, 2004; Yamagishi *et al.*, 2008). In human cells treated with an siRNA against HP1α, SGO1 localization was abolished and the centromeric cohesin was largely dissociated in the SGO1-lacking chromosomes (Yamagishi *et al.*, 2008). Besides SGO1 has also been shown to directly interact with GST-tagged HP1α, HP1β and HP1γ indicating a role for HP1 proteins in the localization of SGO1 (Serrano *et al.*, 2009). Recently, Kawashima *et al.* have shown that Bub1 is responsible for the phosphorylation of a conserved serine residue at position 121 of histone H2A in fission yeast and demonstrated that this single phosphorylation event is required for the correct localization and function of SGO1 and that this pathway is conserved from yeast to human (Kawashima *et al.*, 2010; Javerzat, 2010).

As explained, the role of heterochromatin in cohesion formation and proper sister chromatid segregation has been under investigation for some time. However, there have been conflicting results concerning the role of HP1 proteins in regulating chromosome cohesion. In fission yeast, the methyltransferase Clr4 (Suv39h1 homologue) and Swi6 (HP1 homologue) have been shown to be required for the enrichment of cohesin at centromeres in interphase and to be essential for centromeric cohesion in both mitosis and meiosis (Bernard *et al.*, 2001; Nonaka *et al.*, 2002; Kitajima *et al.*, 2003). Specifically, Swi6 mutants lack cohesin in the outer centromeric repeat region and, as a consequence, show chromosome segregation defects. Supporting the conservation of this mechanism in higher eukaryotes, mouse cells deficient for Suv39h1 and

Suv39h2 histone methyltransferases, in which there is no apparent enrichment of HP1 in pericentric heterochromatin, showed reduced cohesion in the pericentric major satellite (Peters *et al.*, 2001; Guenatri *et al.*, 2004). However another group, using the same Suv39h1/h2 deficient cells, showed that neither the association of cohesin with major satellite repeats in interphase nor the enrichment of cohesin on mitotic centromeres is detectably reduced compared to wt cells (Koch *et al.*, 2008). Moreover, mutants of Su(var)39 in *Drosophila* show a slight reduction in the amount of cohesin in the 1.688 pericentric satellite (Peng and Karpen, 2007) but *Drosophila* larvae expressing reduced or mutant versions of HP1 show no apparent defects in pericentromeric cohesion (Fanti *et al.*, 1998). Finally, Serrano *et al.* showed that depletion of all three HP1 isoforms by siRNA in human cells did not perturb cohesin loading onto chromatin in interphase and the presence of cohesin in the pericentric regions of metaphase chromosomes (Serrano *et al.*, 2009). Thus, the role of mammalian HP1 proteins in chromosome cohesion remains an open question.

1.2.3 HP1β and telomeres

Telomeres are nucleoprotein structures with two specific functions: they ensure that DNA replication includes the very ends of the chromosomes, overcoming the "end-replication problem", and also form a protective "cap" to prevent the natural ends of linear chromosomes from degradation and from being detected as double-strand DNA breaks by the DNA repair machinery (Lue, 2004; Chan and Blackburn, 2004; Palm and de Lange; 2008). In mammals, telomeres consist of double-stranded G-rich repeats ending in a single-stranded 3´overhang (the G-strand overhang), which provides the substrate for telomerase. The G-strand overhang can also fold back and invade the double-stranded region of telomeres, forming a protective structure known as the T-loop (Griffith *et al.*, 1999; de Lange, 2004) (Figure 6). The majority of eukaryotes, including mammals, use the repeated sequence TTAGGG at their chromosome ends and the length of these repeats varies greatly between different mammals. Human telomeres are around 10–15 kilobases (kb) long at birth, whereas the telomeres of laboratory mice and rats are 20–50 kb long (de Lange et *al.*, 1990; Hastie *et al.*, 1990; Kipling and Cooke, 1990; Lejnine *et al.*, 1995). The length of the telomeres is maintained by the enzyme telomerase, which is a reverse

transcriptase that adds telomeric repeats *de novo* after each cell division, counteracting the end-replication problem in those cell types in which it is expressed (Chan and Blackburn, 2002; Collins and Mitchell, 2002). An alternative way of maintaining telomere length has also been described, such as ALT (**al**ternative **l**engthening of **t**elomeres), which relies on homologous recombination between telomeric sequences (Dunham *et al.*, 2000; Muntoni and Reddel, 2005).

The protective cap function of telomeres is essential for organisms as the slightest defect in this structure results in a damage response that leads to a cell cycle checkpoint arrest and/or attempts to repair the chromosome end by non-homologous end joining leading to end-to-end fusion of chromosomes followed by chromosome breakage (Riha *et al.*, 2006). In order to maintain this function, a number of proteins have evolved that bind to telomeres and play vital roles. This complex is termed "shelterin" in mammals and consists of six specialized proteins: **t**elomeric **r**epeat binding **f**actor 1-2 (TRF1-TRF2), **r**epressor and **a**ctivator **p**rotein 1 (RAP1), **T**RF1 **i**nteracting **n**uclear protein 2 (TIN2), **p**rotection **o**f **t**elomeres 1 (POT1) and TPP1 (formerly known as **T**INT1, **P**TOP, or **P**IP1) (Figure 6) (Palm and de Lange, 2008; O'Sullivan and Karlseder, 2010). The components of shelterin specifically localize to telomeres; they are abundant at telomeres throughout the cell cycle and they do not function elsewhere in the

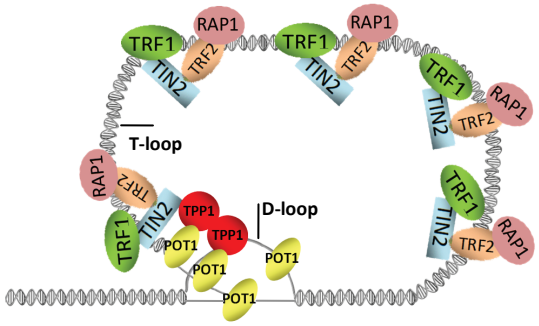

Figure 6 Mammalian telomeres end in a 3′ overhang of the G-rich strand that is the substrate for telomerase-mediated telomere elongation. The G-strand overhang can fold back and invade the double-stranded region of the telomere, thereby generating a looped structure known as the telomere loop (T-loop). The overhang then forms base pairs with the C-rich strand, displacing the G-strand at this site into a displacement loop (D-loop).

nucleus. TRF1 and TRF2 bind the double stranded part of telomeres, whereas POT1 can bind the single stranded TTAGGG repeats present at the 3' overhang and in the D-loop of the T-loop configuration. These TRF1 and TRF2 DNA binding modules are bridged by TPP1 and TIN2 and are crucial for chromosome end protection and telomere length regulation. TRF1 and TRF2 are constitutively present at telomeres and the proportion of TRF1 and TRF2 loaded on telomeres is important for telomere length regulation. RAP1 does not bind TTAGGG repeats and its telomeric localization is dependent on interaction

with TRF2. RAP1 has recently been implicated in the inhibition of non-homologous end joining *in vitro* and *in vivo* (Bae and Baumann, 2007; Sarthy *et al.*, 2009). There are two paralogues of POT1 in mouse: POT1a and POT1b. Disruption of these two genes in mouse embryonic fibroblasts has been shown to result in reduced proliferation, a severe telomeric DNA damage response, chromosome reduplication, increased sister telomere recombination and resection of the telomeric C-strand to give long G-overhangs (Hockemeyer *et al.*, 2006; Wu *et al.*, 2006). TPP1, on the other hand, connects POT1 with TIN2 through its centrally located POT1 interaction domain and depletion of TPP1 leads to removal of all detectable POT1 from telomeres. Furthermore, impaired TPP1 function leads to unprotected telomeres and telomere length phenotypes like the ones seen in POT1 deficient cells (Hockemeyer *et al.*, 2007; Lazzerini and de Lange, 2007; Liu *et al.*, 2004; Xin *et al.*, 2007; Ye *et al.*, 2004).

In addition to the shelterin complex, telomeric sequences are also bound by nucleosomes that are enriched in histone modifications characteristic of constitutive heterochromatin domains (García-Cao *et al.*, 2004; Makarov *et al.*, 1993) including trimethylation of H3K9 and H4K20 by the histone methyltransferases Suv39h1/h2 and Suv420h1/h2 and are therefore rich in heterochromatin proteins HP1α, HP1β and HP1γ. The overexpression of HP1β in human cells has been shown to result in reduced association of human telomerase reverse transcriptase with the telomere and a higher frequency of end-to-end chromosomal fusions, indicating that the concentration of HP1β in the nucleus can affect telomere function (Sharma *et al.*, 2003). Similar telomere dysfunction and enhanced genomic instability has previously been observed in *Drosophila* larvae that are null mutant for HP1 (Perrini *et al.*, 2004). It has also been shown that the reduction of all three isoforms of HP1 proteins in mice causes abnormal telomere elongation (Garcia-Cao *et al.*, 2004) indicating a potential regulatory function of these proteins at the ends of mammalian chromosomes.

1.2.4 HP1β and oncogene-induced senescence (OIS)

Cellular senescence was originally described as the process of cell cycle arrest that accompanies the exhaustion of replicative potential in cultured human fibroblasts (Hayflick and Moorhead, 1961). It is now defined as an irreversible proliferation arrest that occurs in response to various cell

stresses, including activated oncogenes (oncogene-induced senescence), critically short telomeres (replicative senescence) or DNA damage. Senescence is also thought to be an important tumour suppression mechanism with a distinct role in organismal ageing. Senescence can be distinguished from quiescence, a form of cell cycle arrest that is reversible following exposure to appropriate cellular signals, by its irreversibility. Senescent cells have a typical flat and enlarged morphology (Serrano *et al.*, 1997), are positive for **s**enescence-**a**ssociated **β**-**gal**actosidase (SA-β-Gal) (Dimri *et al.*, 1995) and have a characteristically changed pattern of gene expression particularly in genes involved in regulation of the cell cycle, extra-cellular matrix remodelling, cytokine signalling and inflammation (Fridman and Tainsky, 2008). Most strikingly, senescent cells possess **s**enescence-**a**ssociated **h**eterochromatic **f**oci (SAHF) that are manifest as large blocks of HP1-containing heterochromatin domains in the nucleus (Narita *et al.*, 2003).

Oncogene-**i**nduced **s**enescence (OIS) was initially described more than a decade ago when a senescence phenotype was unexpectedly observed on overexpression of an oncogenic version of H-ras (H-ras^{G12V}) in normal cells grown *in vitro* (Serrano *et al.*, 1997). These cells stopped dividing and suffered morphological and molecular changes that were indistinguishable from senescence. In OIS there was also an upregulation of p16^{INK4A} and p19^{ARF} tumour suppressors which are thought to be responsible for the cell cycle arrest. It is now known that OIS in primary cells is mediated by the two main tumour suppressor pathways of the cell: the p19^{ARF}/p53 and/or the p16^{INK4A}/Retinoblastoma (pRb) pathways (Gil and Peters, 2006; Kim and Sharpless, 2006). *In vivo* evidence for this tumour suppressor mechanism was found when cellular senescence, with the concomitant increase in senescence markers, was observed in a variety of mouse and human premalignant tumours while malignant tumours lack the markers and continued to proliferate (Braig *et al.*, 2005; Chen *et al.*, 2005; Collado *et al.*, 2005; Lazzerini Denchi *et al.*, 2005; Michaloglou *et al.*, 2005). These data placed senescence as a tumour suppressor mechanism operating in the premalignant stages of tumorigenesis to prevent progression of oncogenically stressed cells. In particular, Collado and colleagues showed that the expression of oncogenic K-ras (Kras^{V12}) triggered senescence during the early stages of tumorigenesis driven by this oncogene and identified premalignant (adenomas) as well as malignant (adenocarcinomas)

tumours in the lungs of these mice (Guerra *et al.*, 2203; Collado *et al.*, 2005). They showed that premalignant lesions in the lung contained abundant senescent cells positive for OIS markers (SA-β-gal, p15, p16, Dec1, DcR2 and HP1γ) and concluded that a substantial number of cells in premalignant tumours undergo OIS. In contrast, cells in malignant adenocarcinomas continued to proliferate and did not express these OIS markers. Subsequent studies using similar mouse models based on endogenous K-ras have produced contradictory results. Therefore more studies are needed for the accurate role of K-ras oncogene in OIS (Collado and Serrano, 2010).

A specific role for p16 in OIS is the maintenance of the growth arrest through activation of pRb. This $p16^{INK4A}$/pRb pathway has been shown to be crucial for the formation of SAHF, highly condensed regions of chromatin with a typical accumulation of H3K9me3 and heterochromatin proteins, including HP1, **h**igh-**m**obility **g**roup **A** (HMGA) proteins and macroH2A (Narita *et al.*, 2003; Narita *et al.*, 2006; Zhang *et al.*, 2005). It has been reported that access of the transcription factor E2F to its target genes is prevented by SAHF formation resulting in a stable repression of the transcription of S-phase promoting genes and thereby contributing to a robust cell cycle arrest (Narita *et al.*, 2003; Narita *et al.*, 2006; Dimova and Dyson, 2005). Besides, Suv39h1 histone methyltransferase activity was shown to be required for Ras-induced OIS in lymphocyte cells; in Suv39h1-deficient lymphomas, pRb was not able to activate the senescence pathway and promote senescence. The fact that pRb physically interacts with both HP1 and Su(var)39h1 suggests a role of HP1 proteins in OIS (Nielsen *et al.*, 2001; Trimarchi and Lees, 2002).

1.2.5 HP1β knockout mice

In a first attempt to elucidate the function of HP1β *in vivo*, the murine *Cbx1* gene encoding HP1β was disrupted in the Singh laboratory using gene targeting which resulted in a perinatal lethal phenotype (Aucott *et al.*, 2008). *Cbx1*$^{-/-}$ neonates exhibited no gross morphological abnormalities in the major organs. However, it was observed that the lung alveoli remained collapsed after birth due to the inability of the diaphragm to respond to the activating signals from the intramuscular nerve as evidenced by a significant reduction in the number of

acetylcholine receptor clusters per μm of the nerve. *Cbx1*$^{-/-}$ mutant brains showed aberrant cerebral cortex development, reduced proliferation of neuronal precursors, widespread cell death and edema. *In vitro* cultures of neurospheres from *Cbx1*$^{-/-}$ mutant brains revealed a dramatic genomic instability as evidenced by a statistically significant increase in premature centromere division, increased ploidy, micronuclei formation and diplochromosomes compared to WT cells. Strikingly, the *Cbx1*$^{-/-}$ phenotype is more severe than the viable double null *Suv39h1/h2* phenotype and, in addition, the overall H3K9me3 and H4K20me3 levels and distribution are unchanged in *Cbx1*$^{-/-}$ neurons. Based on these observations, it has been proposed that the essential interaction of HP1β, whose loss results in the lethality, lies outside its interaction with the H3K9me3 determinant of the "histone code" that is imposed by the Suv39h1/h2 HMTases. Instead, it has been posited that the loss of an immobile fraction of HP1β that binds tightly to the H3 histone fold might be responsible for the dramatic genomic instability seen in *Cbx1*$^{-/-}$ cortical neurons (Billur *et al.*, 2010). It would seem that despite many years of study on HP1β, its true physiological function still remains to be elucidated.

1.3 The goal of the study

This study builds on the observations on the *Cbx1* (gene encoding the HP1β protein) null mutant mice. *Cbx1* function is essential for organismal survival. The null mutants die at around birth and *in vitro* cultures of neurospheres from *Cbx1*$^{-/-}$ brains revealed a dramatic genomic instability as evidenced by a statistically significant increase in premature centromere division, increased ploidy, micronuclei formation and diplochromosomes compared to WT cells (Aucott *et al.*, 2008). Based on this phenotype one major goal of this study is to describe, in concrete cellular and molecular terms, the role of HP1β on genomic stability. To that end, the effects of *Cbx1* null mutation on telomere function and sister chromatid cohesion are investigated. A second goal is to investigate the role of HP1β in OIS, using both *in vivo* and *in vitro* model systems. Finally, in order to characterise the critical interaction of HP1β, which is likely to result in the lethality seen in the *Cbx1* mutants, the binding affinity of HP1β (and its mutants), to recombinant histone H3 is measured using isothermal titration

calorimetry (ITC) and this binding affinity is compared to the affinity of HP1β to the H3K9me3 peptide.

Chapter 2

Materials and Methods

2.1 Materials

2.1.1 Primers

All primers were purchased from Eurofins MWG Operon (Ebersberg, Germany).

Primer Name	Primer Sequence (5' – 3')
CPAU2	GCCGCAGACATGATAAGATACATTGATG
CPAL2	AAAACCTCCCACACCTCCCCCTGAA
RNA3	GTCAGTACACATACAGACTT
ERT2	TCCATGGAGCACCCAGTGAA
POL3	TGAGCGAACAGGGCGAA
UTR-K-RAS-1	CACTGGACACTGAGGGTCA
UTR-K-RAS-2	CATACTGGGTCTGCCTTA
CLNEO	GATGCCTGCTTGCCGAATAT
M31genoty2.for	ACAGTCAGAAAAGCCACGAGGC
M31genoty3.rev	GTCAGGCCGAGGGTCACTATCG
K-ras V12 for	CTGCTGAAAATGACTGAGTATAAA
K-ras V12 rev	TCCTTGCTAACTCCTGAGCC

2.1.2 Plasmids

GST-HP1α: Expresses full length mouse heterochromatin protein-1 α as a GST fusion protein in pGEX-4T-1 vector (provided by Dr. P. B. Singh, see Appendix for sequence)

GST-HP1β: Expresses full length mouse heterochromatin protein-1 β as a GST fusion protein in pGEX-3X vector (provided by Dr. P. B. Singh, see Appendix for sequence)

GST-HP1γ: Expresses full length mouse heterochromatin protein-1 γ as a GST fusion protein in pGEX-3X vector (provided by Dr. P. B. Singh, see Appendix for sequence)

His-HP1β: Expresses full length mouse heterochromatin protein-1 β as a hexahistidin fusion protein in pQE-30 vector (provided by Dr. P. B. Singh, see Appendix for sequence)

pCAG-EGFP-TPP1: Expresses TPP1 as fused to EGFP (kindly provided by Dr. Y. Shinkai, Kyoto, Japan)

pCAG-EGFP-POT1a: Expresses POT1a as fused to EGFP (as above)

pCAG-EGFP-POT1b: Expresses POT1b as fused to EGFP (as above)

2.1.3 Antibodies

2.1.3.1 Primary antibodies

Anti-H3K9me3:	Rabbit polyclonal antibody against trimethylated lysine 9 on histone H3 (Abcam, Cambridge, UK)
Anti-H3K9me2:	Mouse monoclonal antibody against dimethylated lysine 9 on histone H3 (Abcam, Cambridge, UK)
Anti-H4K20me3:	Rabbit polyclonal antibody against trimethylated lysine 20 on histone H4 (Abcam, Cambridge, UK)
Anti-SMC3:	Rabbit polyclonal antibody against SMC3 (Abcam, Cambridge, UK)
Anti-BUB1:	Rabbit polyclonal antibody against human BUB1 (kindly provided by J. M. van Deursen, Rochester, USA)
Anti-SGO1:	Rabbit polyclonal antibody against SGO1 (kindly provided by Dr. J. Peters, Vienna, Austria)
Anti-CREST:	Human antiserum against CREST (kindly provided by Dr. A. Kromminga, Hamburg, Germany)
Anti-HP1α:	Mouse monoclonal antibody against HP1α (Millipore, Schwalbach, Germany)
Anti-HP1β:	Rat polyclonal antibody against HP1β (Dr. P. B. Singh, Borstel, Germany)
Anti-HP1γ:	Mouse monoclonal antibody against HP1γ (Millipore, Schwalbach, Germany)
Anti-pKi67:	Rabbit polyclonal antibody against pKi-67 (kindly provided by Prof. H. Zentgraf, Heidelberg, Germany)
Anti-p16:	Rabbit polyclonal antibody against p16 (Santa Cruz biotechnology, Heidelberg, Germany)
Anti-DcR2:	Rabbit polyclonal antibody against human DcR2 (Assay Designs, Michigan, USA)
Anti-TIN2:	Rabbit polyclonal antibody against TIN2 (Abcam, Cambridge, UK)
Anti-GFP:	Rabbit polyclonal antibody against green fluorescent protein (MBL, MA, USA).
Anti-TRF1:	Rabbit polyclonal antibody against TRF1 (Abcam, Cambridge, UK)
Anti-TRF2:	Rabbit polyclonal antibody against TRF2 (Abcam, Cambridge, UK)

2.1.3.2 Secondary antibodies

Alexa Fluor 488: Goat anti rabbit IgG (H+L) alexa fluor 488 dye conjugate (Invitrogen, Carlsbad/CA, USA)

Alexa Fluor 594: Goat anti rabbit IgG (H+L) alexa fluor 594 dye conjugate (Invitrogen, Carlsbad/CA, USA)

Anti-human-FITC: Goat anti human IgG (H+L) FITC conjugate (Serotec, Martinsried, Germany)

Anti-mouse-PO: Goat anti mouse IgG (H+L) horseradish peroxidase conjugate (Dianova, Hamburg, Germany)

Anti-rabbit-PO: Goat anti rabbit IgG (H+L) horseradish peroxidase conjugate (Dianova, Hamburg, Germany)

Anti-goat-PO: Rabbit anti goat IgG (H+L) horseradish peroxidase conjugate (Dianova, Hamburg, Germany)

Anti-Rat-PO: Rabbit anti rat IgG (H+L) horseradish peroxidase conjugate (Dianova, Hamburg, Germany)

2.1.4 Buffers, media and solutions

All fine chemicals were purchased from Merck (Darmstadt, Germany) unless otherwise stated.

2.1.4.1 Standard media and solutions

Phosphate buffered saline (PBS)
150 mM NaCl, 8 mM Na_2HPO_4, 2 mM KH_2PO_4, (pH 7.5). Stored at RT.

Tris-buffered saline (TBS)
150 mM NaCl, 10 mM Tris-HCl, (pH 7.5). Stored at RT.

LB medium
1 % (w/v) Tryptone (Roth, Karlsruhe, Germany), 0.5 % (w/v) yeast extract (Roth, Karlsruhe, Germany), 1 % (w/v) NaCl (pH 7.5). Stored at 4 °C.

LB agar
0.5 % (w/v) Agar in LB medium. Stored at 4 °C.

SOC medium
Invitrogen (Carlsbad/CA, USA). Stored at 4 °C.

NZY+ medium
0.96 % (w/v) NZ amine (casein hydrolysate), 0.48 % (w/v) yeast extract, 0.48 % (w/v) NaCl, 0.11 % (w/v) $MgCl_2$, 0.14 % (w/v) $MgSO_4$, 0.34 % (w/v) glucose, (pH 7.5). Stored at 4 °C.

Psi Medium
0.48 % (w/v) $MgSO_4$, 0.75 % (w/v) KCl in LB medium. Stored at 4 °C.

2.1.4.2 Flow-FISH solutions

Cell suspension buffer
0.1 % BSA, 10 mM Hepes-bufffer (Roth, Karlsruhe, Germany), 5 % Glucose (Sigma-Aldrich, Munich, Germany). Stored at 4 °C.

Hybridization mix „unst" and „tel"
20 mM Tris-Base, 20 mM NaCl, 1 % BSA, 75 % deionized formamide (Sigma-Aldrich, Munich, Germany), 0.3 µg/ml Telo-PNA-FITC (Panagene, Daejeon, Korea) (only in tel). Freshly prepared.

Wash buffer 1
75 % formamide, 20 mM Tris-Base, 1 % BSA, 1 % Tween-20 (Sigma-Aldrich, Munich, Germany). Freshly prepared.

Wash buffer 2
1 % BSA, 1 % Tween-20 (Sigma-Aldrich, Munich, Germany), 10 mM Hepes (Roth, Karlsruhe, Germany), 5 % Glucose (Sigma-Aldrich, Munich, Germany) Freshly prepared.

LDS solution
0.1 µg/ml LDS751 (Invitrogen, Carlsbad/CA, USA), 10 µg/ml RNase A (Roth, Karlsruhe, Germany), 0.1 % BSA, in PBS. Freshly prepared.

2.1.4.3 Telomere-FISH and Giemsa staining solutions

Hybridization buffer
10 mM NaH_2PO_4, (pH 7.4), 10 mM NaCl, 20 mM Tris, (pH 7.5), 70 % formamide

Fixative solution
Methanol:glacial acetic acid (3:1). Freshly prepared.

Pepsin solution
2.5 ml of 10 % Pepsin stock in 50 ml 10 mM HCl (0.005 % solution).

Washing solution
Washing Solution 1: PBS/0.1 % (v/v) Tween-20

Washing Solution 2 : 2×SSC/0.1 % (v/v) Tween-20

Trypsin solution
0.015 g Trypsin in 100 ml PBS

Giemsa solution
5 % (v/v) Giemsa in H_2O, freshly prepared and sterile filtrated.

2.1.4.4 ChIP solutions

Fixation solution
1 % (w/v) formaldehyde in DMEM (Sigma-Aldrich, Munich, Germany). Freshly prepared.

20/2 TE buffer
2 mM EDTA (Sigma-Aldrich, Munich, Germany), 20 mM Tris-HCl (pH 8.0). Stored at 4 °C.

ChIP dilution buffer
0.01 % (w/v) SDS, 1.1 % (v/v) Triton X-100, 1.2 mM Tris-HCl (pH 8.0), 167 mM NaCl. Stored at 4 °C.

Elution buffer
0.1M $NaHCO_3$, 1 % SDS. Freshly prepared.

High salt buffer
0.1 % (w/v) SDS, 1 % (v/v) Triton X-100, 2 mM EDTA (Sigma-Aldrich, Munich, Germany), 20 mM Tris-HCl (pH 8.0), 500 mM NaCl. Stored at 4 °C.

Low salt buffer
0.1 % (w/v) SDS, 1 % (v/v) Triton X-100, 2 mM EDTA (Sigma-Aldrich, Munich, Germany), 20 mM Tris-HCl (pH 8.0), 150 mM NaCl. Stored at 4 °C.

LiCl buffer
0.25M LiCl, 1 % (v/v) NP-40, 1 % (w/v) Sodium deoxycholate, 1 mM EDTA (Sigma-Aldrich, Munich, Germany), 10 mM Tris-HCl (pH 8.0). Stored at 4 °C.

SDS lysis buffer
1 % (w/v) SDS, 10 mM EDTA (Sigma-Aldrich, Munich, Germany), 50 mM Tris-HCl (pH 8.0). Stored at 4 °C

2.1.4.5 GST pull down solutions

0.3 M assay buffer
20 mM Tris-HCl, 0.3 M NaCl, 0.1 mM EGTA (Sigma-Aldrich, Munich, Germany), 2 mM $MgCl_2$, 1 mM PMSF (Sigma-Aldrich, Munich, Germany), 0.5 % (v/v) Triton X-100, Complete Protease inhibitors (Roche, Mannheim, Germany) and 0.5 % (v/v) Gelatine (Sigma-Aldrich, Munich, Germany), (pH 7.6).

Bead washing and blocking buffer
150 mM NaCl, 20 mM Tris-HCl, 1 % (v/v) Gelatine (Sigma-Aldrich, Munich, Germany) (pH 7.6).

2.1.4.6 Protein purification solutions

Lysis buffer
1 mM PMSF (Sigma-Aldrich, Munich, Germany), 1 mM DTT (Sigma-Aldrich, Munich, Germany), 100 mM $MgCl_2$, 1 mg/ml lysozyme (Fluka, St.Gallen, Switzerland), 2500 U/l culture Benzonase (Sigma-Aldrich, Munich, Germany), NP-40 (0.5 %, v/v) in PBS (pH 7.3). Freshly prepared.

Elution buffer
50 mM Tris-HCl, 10 mM reduced glutathione (Sigma-Aldrich, Munich, Germany) (pH 8.0). Freshly prepared.

NPI-10
50 mM NaH_2PO_4, 300 mM NaCl, 10 mM imidazole, (pH 8.0).

NPI-20
50 mM NaH_2PO_4, 300 mM NaCl, 20 mM imidazole, (pH 8.0).

NPI-300
50 mM NaH_2PO_4, 300 mM NaCl, 300 mM imidazole, (pH 8.0).

2.1.4.7 Coomassie stain solutions

Coomassie stain solution
0.25 % (w/v) Coomassie brilliant blue (BioRad, Munich, Germany), 45 % (v/v) methanol, 10 % (v/v) acetic acid.

Coomassie destain solution
30 % (v/v) methanol, 10 % (v/v) acetic acid.

Coomassie fixative solution
30 % (v/v) methanol, 3 % (v/v) glycerol.

2.1.4.8 SDS-PAGE and western blotting solutions

SDS sample buffer
25 mM Tris-HCl, 50 mM DTT (Sigma-Aldrich, Munich, Germany), 10 % (v/v) glycerol, 2 % (w/v) SDS, 0.02 % (w/v) Bromphenol blue (Sigma-Aldrich, Munich, Germany) (pH 6.8).

Electrophoresis buffer
25 mM Tris-HCl, 192 mM glycin, 0.1 % (w/v) SDS.

Upper tris buffer

0.4 % (v/v) SDS, 0.5 M Tris-HCl (pH 6.8).

Lower tris buffer
0.4 % SDS, 1.5 M Tris-HCl (pH 8.8).

Transfer buffer
20 mM Tris, 15 mM glycin, 20 % (v/v) methanol, (pH 8.3).

AP buffer
1 M Tris/HCl, 1 M NaCl, 50 mM $MgCl_2$, (pH 9.5).

Ponceau-S solution
0.2 % (w/v) Ponceau-S, 0.2 % (v/v) acetic acid.

2.1.4.9 Metaphase spread preparation solutions

Hypotonic buffer
75 mM KCl, 0.1 % Tween-20.

Potassium chromosome medium (KCM)
120 mM KCl, 20 mM NaCl, 10 mM Tris-HCl, 0.5 mM EDTA, 0.1 % (v/v) Triton X-100 (pH 7.5).

2.1.5 Bacterial strains

Name	Genotype	Manufacturer
E.coli M15[pREP4]	Km^r, rpsL, rpoB, gyrA, NaI^s, Str^s, Rif^s, Thi^-, Mtl^-, Ara^+, Gal^+,Mtl^-, F^-, $RecA^+$, Uvr^+, Lon^+	Qiagen
E.coli XL-10 Gold	$Tetr^R\Delta$ (mcrA)183 Δ(mcrCB-hsdSMR-mrr) 173 endA1 supE44 thi-1 recA1 gyrA96 relA1 lac The [F' proAB $lacI^qZ\Delta M15$ Tn10 (Tet^R) Amy Cam^R]	Stratagene
E.coli BL21-CodonPlus-RIL	B F^- ompT hsdS(r_B^- m_B^-) dcm^+ Tet^r gal endA Hte [argU ileY leuW Cam^r]	Stratagene

2.1.6 Kits

QIAprep Spin Miniprep Kit (Qiagen, Hilden, Germany), Plasmid Midi Kit (Qiagen, Hilden, Germany), QiaQuick PCR purification kit (Qiagen, Hilden, Germany), QuikChange II XL Site-Directed Mutagenesis Kit (Stratagene, Santa Clara, USA), Ladderman Labeling Kit (Takara Bio, Saint-Germain-en-Laye, France), DC Protein Assay Kit (BioRad, Munich, Germany).

2.2 Methods

2.2.1 Molecular biology

2.2.1.1 Preparation of plasmid DNA

Small scale plasmid DNA was prepared using "QiaprepSpin Miniprep" kit from a 2 ml ON culture in LB medium, following the manufacturer's instructions. Plasmid was eluted in 50 µl water and stored at -20 °C.

Large scale plasmid DNA was prepared using "Plasmid Midi" kit from a 100 ml ON culture in LB medium, following the manufacturer's instructions. Plasmid DNA was eluted in 50 µl water and stored at -20 °C.

2.2.1.2 Isolation of total RNA from tissue

Lung tissues were grinded using a mortar, and total RNA from the tissue was prepared using "RNeasy Mini" kit following the manufacturer's instructions. RNA was eluted in 30 µl water and stored at -20 °C.

2.2.1.3 Measuring concentration of nucleic acids

The concentration of nucleic acids was determined by measuring the OD at 260 nm with spectrophotometer Ultraspec 1000 (Pharmacia Biotech, Uppsala, Sweden). A measured OD_{260} value of 1 equals a double stranded DNA concentration of 50 µg/ml. A measured OD_{260} value of 1 equals a RNA concentration of 40 µg/ml. To determine the protein contamination in the samples, OD_{280} nm value was also measured in parallel. For DNA samples the OD_{260} / OD_{280} value must ≥1.8 and for RNA samples ≥2.0.

2.2.1.4 Reverse transcription of RNA (cDNA synthesis)

3 µg of freshly purified total-RNA and 1 µg Oligo-dT18-primer were added to 10 µl water and were incubated for 10 min at 70 °C. After briefly cooling on ice, RNase-inhibitors, RT-Buffer, DTT, dNTPs and 200 U Reverse Transcriptase Superscript II (Invitrogen, Carlsbad/CA, USA), were added to the reaction mixture following the manufacturer's protocol and were incubated at 42 °C for 1 h. The enzyme was deactivated by 3 min incubation at 95 °C, cDNA was diluted 1:10 in water and stored at -20 °C.

2.2.1.5 Transformation of plasmid DNA into *E.coli*

XL-10 Gold: After gently thawing the cells on ice, 2 µl of β-mercaptoethanol was added to 45 µl bacteria and incubated 10 min on ice with gentle swirling every 2 min 2 µl of *Dpn-I* treated DNA was added to this mix and incubated further for 30 min on ice. The cells were heat-shocked by 30 s incubation in a 42 °C water bath following 2 min incubation on ice. 0.5 ml NZY+ Broth preheated to 42 °C was added following 1 h incubation at 37 °C on a shaker. The reaction was then spread on LB agar plates with appropriate antibiotics.

M15[pREP4]: After gently thawing the cells on ice, 2 µl of DNA were added to 40 µl of bacteria and incubated 20 min on ice. The cells were heat-shocked by 90 s incubation a in 42 °C water bath following with 2 min incubation on ice. 0.5 ml Psi Broth preheated to 42 °C was then added following 1 h incubation at 37 °C on a shaker. The reaction was then spread on LB agar plates with appropriate antibiotics.

BL21-CodonPlus-RIL: After gently thawing the cells on ice, 2 µl of β-mercaptoethanol was added to 100 µl bacteria and incubated 10 min on ice with gentle swirling every 2 min 1–50 ng of expression plasmid DNA containing the gene of interest was added to this mix and incubated further for 30 min on ice. The cells were heat shocked with 20 s incubation in 42 °C water bath following 2 min incubation on ice. 0.9 ml SOC medium preheated to 42 °C was then added following 1 h incubation at 37 °C on a shaker. The reaction was then spread on LB agar plates with appropriate antibiotics.

2.2.1.6 Agarose gel electrophoresis

For the separation of nucleic acid fragments, agarose gels based on TAE-Buffer system were used. 0.4 µg/ml ethidium bromide was added to the gel mixture for the visualization of DNA on a UV transilluminator (Intas, Göttingen, Germany). Samples were mixed with 10 % (v/v) DNA sample buffer (10X) and loaded on a gel. The gel was run with 5 V/cm in horizontal electrophoresis equipment (Bio-Rad, Munich, Germany). 1 kb and 100 bp ladders (Fermentas, St. Leon-Rot, Germany) were used as standards.

2.2.1.7 Restriction digest

250 ng – 1 µg DNA was mixed with 4-10 U restriction endonuclease in the suitable buffer (as stated by the manufacturer) and incubated for 10 min – 1 h at 37 °C on a shaker.

2.2.1.8 Site-directed mutagenesis

Single and double amino acid mutations of HP1β proteins were done using "QuikChange II XL Site-Directed Mutagenesis Kit" following manufacturer's instructions. The basic procedure utilizes a supercoiled double-stranded DNA vector with an insert of interest and two synthetic oligonucleotide primers, both containing the desired mutation, which were designed using manufacturer's primer design software. The oligonucleotide primers, each complementary to opposite strands of the vector, are extended during temperature cycling by *Pfu* Ultra HF DNA polymerase, without primer displacement. Extension of the oligonucleotide primers generates a mutated plasmid containing staggered nicks. Following temperature cycling, the product is treated with *Dpn I*. The *Dpn I* endonuclease is specific for methylated and hemimethylated DNA and is used to digest the parental DNA template and to select for mutation containing synthesized DNA. DNA isolated from almost all *E. coli* strains is *dam* methylated and therefore susceptible to *Dpn I* digestion. The nicked vector DNA incorporating the desired mutations was then transformed into XL10-Gold ultracompetent cells.

2.2.1.9 Genotyping PCR

Genomic DNA from transgenic mice was prepared by the lysis of ear tissue samples in DirectPCR reagent (Peqlab, Erlangen, Germany) following the manufacturer's instructions.

HP1β genotyping PCR: K-ras$^{+/V12}$;RERTn$^{+/ERT}$ mice were screened for *Cbx1*$^{+/-}$ mutation with M31genoty2.for and M31genoty3.rev primers and "Expand LT PCR" Kit (Roche, Mannheim, Germany) using the following conditions:

94°C – 2 min	
94°C – 1 min	33X
62°C – 1 min	
72°C – 4 min	
72°C – 15 min	
16°C – 10 min	

Buffer 3	2 µl
M31genoty2.for (20 pmol/µl)	1 µl
M31genoty3.rev (20 pmol/µl)	1 µl
dNTPs (20 mM stock)	0.2 µl
Taq enzyme	0.1 µl
H_2O	14.7 µl
Template	1 µl

PCR products were run on a 1,2 % agarose gel. WT genotype, gave a band of 258 bp and HP1β$^{+/-}$ genotype gave a band of 1,36 kb.

K-ras genotyping PCR: K-ras(+V12);RERT(ert/ert) mice were screened for K-Ras mutation with UTR-K-RAS-1, UTR-K-RAS-2 and CLNEO primers using following conditions:

94°C – 2 min	
94°C – 40 s	34X
60°C – 40 s	
72°C – 1 min	
72°C – 10 min	
4°C – ∞	

$MgCl_2$ (25 mM)	2 µl
Buffer TAQ (10X)	5 µl
UTR-K-RAS-1 10 µM	2.5 µl
UTR-K-RAS-2 10 µM	5 µl
CLNEO 10 µM	2.5 µl
dNTPs 2.5 mM	1 µl
Taq enzyme	0.25 µl
H_2O	29.75 µl
Template	1 µl

PCR products were run on a 2 % agarose gel. WT genotype, gave a band of 270 bp, K-ras^{V12} homozygous genotype gave a band of 500 bp and K-ras^{V12} heterozygous genotype gave 2 bands of 500 bp and 270 bp.

RERT genotyping PCR: K-ras(+V12);RERT(ert/ert) mice were screened for RERT mutation with RNA3, ERT2 and POL3 primers using following conditions:

94°C – 2 min	
94°C – 40 s	34X
55°C – 40 s	
72°C – 1 min	
72°C – 10 min	
4°C – ∞	

$MgCl_2$ (25 mM)	2 µl
Buffer TAQ (10X)	5 µl
RNA3 10 µM	5 µl
POL3 10 µM	2.5 µl
ERT2 10 µM	2.5 µl
dNTPs 2.5 mM	1 µl
Taq enzyme	0.25 µl
H_2O	29.75 µl
Template	1 µl

PCR products were run on a 2 % agarose gel. WT genotype, gave a band around 400 bp, RERT homozygous genotype gave a band around 700 bp and RERT heterozygous genotype gave 2 bands around 400 bp and 700 bp.

2.2.1.10 Chromatin immunoprecipitation (ChIP)

ChIP assay was performed as described by Bullwinkel *et al.*, 2006 (Figure 7). Mouse embryonic fibroblasts grown to sub-confluency were washed twice with PBS, cross-linked for 10 min by 1 % formaldehyde in serum-free medium at 37 °C, washed again with ice-cold PBS containing complete EDTA free protease inhibitor cocktail, scraped off the culture dish and resuspended in 2.5 ml SDS lysis buffer containing the same protease inhibitors. The cell lysate was sonicated six times for 10 s on ice (in 2 min intervals) with a microtip on a Branson sonifier 250 (Branson Ultrasonics Corporation, CT, USA) at an output setting of 3–4, resulting in DNA fragments with an average length of approximately 800 bp. Insoluble material was removed by centrifugation (5 min at 1000 *g* followed by 5 min at 13000 *g*) and the supernatant was diluted 1:10 in ChIP dilution buffer containing protease inhibitors. Protein G sepharose slurry was prepared by equilibration of protein G sepharose 4 Fast Flow, (GE Healthcare, Munich, Germany) in PBS, containing 0.75 mg/ml BSA and 0.1 mg/ml baker's yeast RNA (Sigma-Aldrich, Munich, Germany) with a final bead volume content of 20 %. Preclearing of the ChIP samples was performed for 2 h by addition of 60 µl protein G sepharose slurry. 75 µl of the precleared lysate (equals to 0.3 % of the initial sonicated cell lysate) was transferred into a new tube and labelled as input DNA which was kept at 4 °C until reverse crosslinking step, whereas 1 ml of this precleared lysate was used for the experimental samples and incubated ON at 4 °C with appropriate antibodies or no antibody as control. The DNA-protein-antibody complex was precipitated with 60 µl protein G sepharose slurry for 1 h. After washing once with wash buffer containing 150 mM NaCl, once with wash buffer containing 500 mM NaCl, once with lithium chloride buffer and twice with TE, complexes were eluted twice in 100 µl elution buffer and 150 µl of the eluted sample supernatant (equals to 3 % of the initial sonicated cell lysate) was transferred into a new tube and 5 M NaCl was added to a final concentration of 0.2 M. Finally, crosslinks were removed by incubation for 4 h at 65 °C. After addition of EDTA (10 mM final concentration) and Tris-HCl (pH 6.5, 40 mM final concentration) proteins were digested by 1 µl (10 mg/ml) proteinase K (Sigma-Aldrich, Munich, Germany). DNA was recovered by QiaQuick PCR purification columns (Qiagen, Hilden, Germany). For the quantification of precipitated ChIP DNA, input DNA was used.

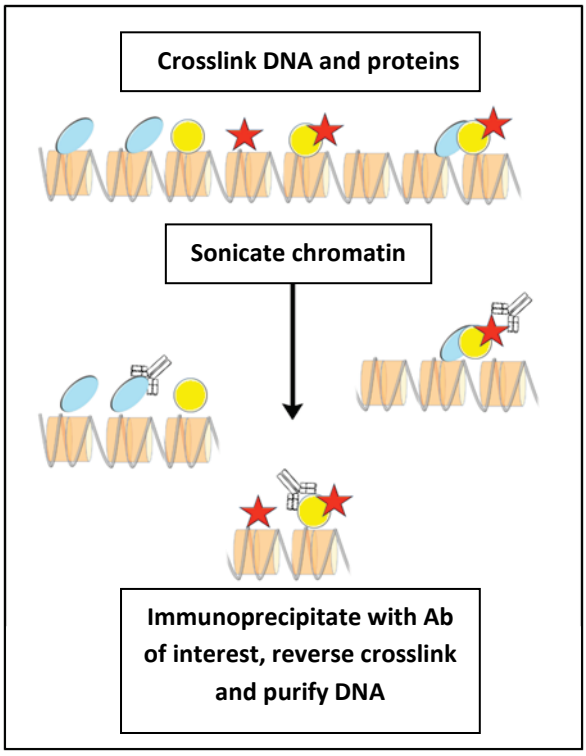

Figure 7 Steps involved in a typical ChIP experiment.

2.2.1.11 Dot/Slot-blotting of ChIP DNA

ChIP DNA was dot/slot-blotted on Hybond N^+ nylon membranes (GE Healthcare, Munich, Germany) with an apparatus (Schleicher & Schuell, Dattel, Germany) using a modified protocol implementing the manufacturer's protocol. Briefly, a piece (10 cm x 13 cm) of positively charged nylon membrane and Whatman filter paper (GE Healthcare, Munich, Germany) was cut and soaked for 10 min in distilled water in a glass dish of 0.5 cm depth. The blotting manifold was assembled with the filter paper and nylon membrane on top, and the membrane was prewashed with distilled water by pipetting 500 µl of water per well. Samples were prepared in a buffer with a final concentration of 0.4 M NaOH and 10 mM EDTA and denatured by boiling at 100 °C for 10 min. After a brief chill on ice, samples were centrifuged briefly to collect evaporated water and applied to the membrane while the dot-blot manifold was connected to vacuum pump. The wells were then rinsed with 500 µl 1 M NaOH, the manifold dismantled and the nylon membrane was UV crosslinked with the autocrosslink option of the UV Stratalinker 1800 (Stratagene, CA, USA).

2.2.1.12 Random primer end labelling of telomeric DNA with radioactive ^{32}P-dCTP

The random primer labelling was done using the "Ladderman Labelling Kit" using the manufacturer's instructions. Removal of unincorporated ^{32}P labeled dCTP (GE Healthcare, Munich, Germany) was done using Illustra MicroSpin S-200 HR Columns (GE Healthcare, Munich, Germany) following manufacturer's instructions. Briefly, 1 µg template DNA and 2 µl random primer were mixed and distilled water was added to a total volume of 14 µl. The mixture was heated at 95 °C for 3 min and cooled on ice for 5 min. 1 µl of *Bca* DNA polymerase was then added and the mixture was incubated at 53 °C for 10 min followed by the addition of EDTA to a final concentration of 30 mM. Reaction mixture was then added on illustra MicroSpin S-200 HR columns and centrifuged for 2 min at 2700 rpm. The eluate was used for the hybridization experiments.

2.2.1.13 Hybridization of dot-blotted ChIP DNA with a ^{32}P-labelled telomeric probe and image analysis

After a brief rinse in 6X SSC, nylon membrane with dot-blotted ChIP DNA was preincubated in 10 ml Church buffer for 10 min at 68 °C. After this preincubation step, the buffer was removed, nylon membrane was put in a hybridization bag whose 3 sides were sealed and 4 ml of fresh Church buffer together with ^{32}P-labelled telomeric probe was added to the membrane. The open side of the bag was heat-sealed using the heat sealing machine Polystar 100 GE (Rische+Herfurth GmbH, Hamburg, Germany) and hybridized overnight at 68 °C with gentle shaking in a water bath. Next day, nylon membrane was washed 3 times in 2X SSC/0.1 % SDS for 5 min at RT followed by two washes in 2XSSC/0.1 % SDS for 10 min at 68 °C. After final wash, the nylon membrane was exposed overnight to a storage phosphor screen (GE Healthcare, Munich, Germany), in an X-Omatic Regular intensifying cassette (Kodak, Stuttgart, Germany). Next day, the phosphor screen was scanned with Phosphorimage SI (GE Healthcare, Munich, Germany) using manufacturer's software with 50 µm resolution.

The image was analyzed using Image Quant 6.0 Software (GE Healthcare, Munich, Germany) for the quantification of signal intensities. Final values were calculated by subtracting "No antibody control" intensity (as background signal) from all samples and by normalizing (dividing by input DNA value), which then gave the final value of "Telomeric DNA in ChIP" in arbitrary units.

Telomeric DNA in ChIP [a.u.] = (Sample intensity - background intensity) / Input DNA intensity

2.2.1.14 Measurement of telomere length by FLOW-FISH

These experiments have been done in collaboration with Dr. U. Brassat and Prof. T. Brummendorf (UKE, Hamburg). The mean telomere lengths were measured using FLOW-FISH technique which basically implements the use of FITC-labelled telomeric PNA probes ($CCCTAA_3$) (Panagene, Daejeon, Korea) for the hybridization to the telomeres of cells to be measured. In principal this technique involves the discrimination of 2N interphase cells from 4N cells by using the DNA stain LDS751 (Invitrogen, Carlsbad/CA, USA) and including only 2N cells in the measurement of mean telomere length by FACS. As internal control, bovine thymocytes were used as these control cells are easily distinguished from the murine test cells due to their size and therefore provide a convenient reference point for telomere fluorescence measurements. The telomere lengths of the control cells were previously measured using telomere restriction fragment (TRF) analysis, and found to be 19.515 kb. Comparison of the fluorescence signals obtained from control cells and experimental cells made it possible to measure the absolute mean telomere length. In this procedure, cells were harvested and resuspended in cell suspension buffer. Frozen and fixed bovine thymocytes were also thawed out and resuspended in cell suspension buffer. For each sample, $2x10^5$ MEFs and $1x10^5$ bovine thymocytes (thy) were counted and used. Each measurement was done in triplicates in 1.5 ml reaction tubes, with ("tel") and without ("unst") FITC-labelled telomeric probe in order to allow subtraction of autofluorescence of cells in the same light scatter window. The cells were then centrifuged at 20000 *g* for 30 s, supernatants discarded and the pellets were resuspended in 300 µl (=100 µl/$1x10^5$) hybridization mix "tel" or "unst". DNA was denatured by incubating the samples at 87 °C for 15 min in water bath, with a following 1,5 h incubation in the dark at RT for the hybridization of telomeric probe. The samples were then washed 4 times with 1 ml wash buffer 1 for the removal of excess probe. Between the washes, the cells were resuspended well by pipetting up and down, centrifuged at 2000 *g* for 5 min at 4 °C and the supernatants were discarded. After final wash step, samples were washed for the last time in wash buffer 2, centrifuged at 900 *g* for 10 min at 4 °C and all but 50 µl of the supernatant was discarded. Thereafter, DNA was stained by adding 300 µl LDS solution to the samples and incubating in the dark for 20 min at RT in FACS tubes. The samples were kept on ice until the measurement was done. The fluorescent signal emitted from LDS751 was measured in Fl3 and the signal emitted from FITC was measured in Fl1 channel of the FACSCalibur (Beckman-Coulter, CA, USA). For the calculation of the absolute mean telomere length, the following formula has been used:

Mean Telomere Length [kb] = ((MEF „tel“ – MEF – „unst“) / (Thy „tel“ – Thy „unst“)) x 19.515 (TL of thymocytes)

2.2.1.15 Telomere-FISH and Giemsa staining

Telomere FISH was done in collaboration with Prof. T. Pandita (WUSM, St. Louis) using manufacturer's (Panagene, Daejeon, Korea) protocol. Briefly, one day before the experiment, cells were passaged at a split ratio of 1:5 to achieve maximal cell division rate. On the next day, Colcemid (PAA, Pasching, Austria) was added to flasks to a final conc. of 0.1 µg/ml and incubated for 3 h. The cells at metaphase were then shaken off by hitting the bottom of the cell culture dish a couple of times and the supernatant including cells at metaphase was transferred into 50 ml tubes. Following centrifugation at 1200 rpm for 10 min at 4 °C, supernatant was discarded and the cell pellet was resuspended in 30 ml 75 mM KCl and incubated at RT for 30 min. The cells were fixed initially by adding 2 ml of fixative solution (4 °C) twice and mixing carefully by turning the tube. After harvesting the cells at 1500 rpm for 5 min, 10 ml of fixative solution was added twice followed by centrifugation at 1500 rpm for 5 min. Following last centrifugation step, 700 µl of fixative solution was added to cell pellet and suspension was dropped on slides. Preparation of metaphases until this step was same for telomere FISH and Giemsa staining. After this point, for Giemsa staining slides were then heated up to 100 °C on a heating plate and incubated in trypsin solution for 40 s. Following a brief wash in H_2O and PBS, slides were then incubated for 10 min in Giemsa solution. Chromosomal abnormalities were analyzed using a light microscope. 200 metaphases per genotype were analyzed for the determination of chromosomal aberrations and Chi-squared tests were used to test the significance of the observed differences between the genotypes. For telomere FISH experiments, slides were dried at 67 °C for 10 min, incubated in PBS for 15 min, fixed in 4 % formaldehyde/PBS for 4 min, washed twice in PBS for 5 min, treated with pepsin solution for 4 min and washed three times in PBS for 5 min. Slides were then dehydrated using cold ethanol series (1 min each in 70 %, 80 %, 100 % ethanol) and dried on air. 15 µl of telomere PNA probe was then added to slides, which were then coverslipped and allowed to denature at 80 °C for 5 min. Hybridization was done at RT for 2 h. After hybridization, slides were washed in washing solution-1 for 20 min at 57 °C following a second wash in washing solution 2 at RT for 5 min. Slides were then coverslipped with a drop of Vectashield antifade medium with DAPI (Vector laboratories, Burlingame, USA).

2.2.2 Protein biochemistry

2.2.2.1 Protein expression in *E.coli*

40 ml of LB medium containing appropriate antibiotics were inoculated with a freshly picked single bacterial colony and grown at 37 °C overnight with vigorous shaking in water bath. Next day, overnight culture was diluted 1:50 in 2 l of fresh LB medium and grown at 37 °C with vigorous shaking until an OD_{600} value of 0.6 was reached. Expression was induced by adding IPTG (Fluka, St. Gallen, Switzerland) to the culture to a final concentration of 1 mM. Cultures were grown for 5 h at 37 °C with vigorous shaking followed by centrifugation

at 4000 *g* for 20 min at 4 °C. The supernatant was discarded and the bacterial pellets were stored at –80 °C until purification.

2.2.2.2 GST fusion protein purification

Bacterial pellets were allowed to thaw out for 15 min at RT and then completely resuspended by pipetting up and down in 30 ml cold lysis buffer on ice. After 30 min incubation on ice, samples were sonicated 4 x 10 s with a Branson sonifier 250 (50 % duty, level 3), with 20 s intervals on ice. The protein was then solubilized by 15 min incubation on a roller at 4 °C. After a centrifugation step at 12000 rpm for 20 min at 4 °C, pellets were discarded and the supernatant was loaded on GSTrapFF 1 ml columns (GE Healthcare, Munich, Germany) which were already equilibrated with 5 ml of PBS (pH 7.3) using a microperpex peristaltic pump (LKB Broma, Sweden) with a flow rate of 0.2 ml/min while keeping the sample on ice. The column was then washed with 20 ml of cold PBS with a flow rate of 1 ml/min and the GST-fusion protein was eluted with 5 ml elution buffer with a flow rate of 1 ml/min.

2.2.2.3 Hexahistidin fusion protein purification

Bacterial pellets were allowed to thaw out for 15 min at RT and then completely resuspended by pipetting up and down in 40 ml cold NPI-10 buffer together with 10 ml lysozyme (10 mg/ml) on ice. After 30 min incubation on ice, samples were sonicated 4 x 10 s on a Branson sonifier 250 (50 % duty, level 3), with 20 s intervals on ice. The protein was then solubilized by 15 min incubation on a roller at 4 °C. After a centrifugation step at 15000 *g* for 20 min at 4 °C, pellets were discarded and the supernatant was incubated with 2-4 ml Ni-NTA Superflow Resin (Qiagen, Hilden, Germany) for 1 h at 4 °C. The beads were then loaded on a polypropylene plastic column (Qiagen, Hilden, Germany), washed twice with buffer NPI-20 and fusion protein was eluted using 5 ml NPI-300 buffer.

2.2.2.4 Measuring protein concentration

Protein concentrations were determined both by using "DC Protein Assay Kit" (BioRad, Munich, Germany) following the manufacturer's instructions, which is a colorimetric assay similar to Lowry (Lowry *et al.*, 1951), and by measuring the OD_{280} value of protein samples with the spectrophotometer Ultraspec 1000 (Pharmacia Biotech, Uppsala, Sweden) and using the Beer-Lambert formula:

$$\mathbf{A = c \times l \times \varepsilon}$$

(**A:** OD_{280} value, **ε:** extinction coefficient, **c:** concentration in mol/l, **l:** optical path length in cm)

2.2.2.5 SDS-PAGE

Separation of proteins according to their molecular weight was done with SDS polyacrylamide gel electrophoresis (PAGE). Briefly, samples in SDS sample buffer were denatured by incubating at 95 °C for 10 min and loaded on 3 % loading gel. Separation was done on a 5-15 % running gel depending on the molecular mass of the protein (for gel composition see Table 2). The gel was run using a vertical SDS-PAGE apparatus (BioRad, Munich, Germany) with a current of 20-25 mA. "Precision Plus Protein Standard All Blue" (BioRad, Philadelphia, USA) was used as molecular weight standard.

	Loading gel 3.3 % (w/v) polyacrylamide	Running gel 5-15 % (w/v) polyacrylamide
40 % acrylamide/ bisacrylamide (1:29)	8.35 % (v/v)	12.38 – 37.16 % (v/v)
Lower tris buffer	-	24.8 % (v/v)
Upper tris buffer	26.1 % (v/v)	-
Ammonium persulfate	0.42 % (w/v)	0.82 % (w/v)
TEMED	0.42 % (v/v)	0.08 % (v/v)

Table 2 Composition of SDS gels used.

2.2.2.6 Coomassie staining

After SDS-PAGE, the gel was washed twice for 5 min in water followed by 10 min incubation in Coomassie staining solution at 85 °C. Excess Coomassie stain was then destained by incubating the gel in Coomassie destain solution for 3 h. The gel was then fixed by incubation in Coomassie fixing solution overnight. On the next day, the gel was dried between two cellophane sheets (BioRad, Munich, Germany) for long term storage.

2.2.2.7 Western blotting

After SDS-PAGE, proteins were transferred overnight onto a nitrocellulose membrane (Schleicher&Schuell, Dassel, Germany) using a Mini Protean II Blotting apparatus filled with transfer buffer (BioRad, Munich, Germany) with a constant current of 50 mA. After verification of the transfer with Ponceau-S staining for 3 min, the unspecific binding was blocked by incubating the blot in 5 % skimmed milk powder/TBST for 30 min. Following this step, the blot was incubated with primary antibodies in 0.5 % skimmed milk powder/TBST for 1 h and after washing 3x in TBST, AP-conjugated species specific secondary antibody incubation in 0.5 % skimmed milk powder/TBST for 30 min was done. The colour reaction indicating the binding of the antibody was visualized using NBT/BCIP (Promega, Madison, USA) diluted in AP buffer and the reaction was stopped with water after protein bands were visible.

2.2.2.8 GST pull down assays

Glutathione Sepharose 4B beads (75 % slurry) (GE Healthcare, Munich, Germany) were prepared by washing and blocking the beads three times in bead washing and blocking buffer following the manufacturer's instructions and diluting the beads in the same buffer to make a 50 % slurry. 30 µl of the 50 % bead slurry was

then mixed with 5 µg of bait GST-fusion protein in 800 ml assay buffer and incubated in 1.5 ml tubes at RT for 1 h on an end-to-end roller (LTF Labortechnik, Wasserburg, Germany). Following centrifugation for 10 min at 500 *g*, supernatant was discarded and 5 µg of prey protein (recombinant *X.laevis* histone H3, kindly provided by Prof. Wolfgang Fischle, MPI-BPC, Göttingen) was added together with 800 ml fresh assay buffer. After incubating the mixture for 1 h at RT on an end-to-end roller, samples were washed 6 times in 1 ml fresh assay buffer. The tubes were centrifuged for 5 min at 500 *g* in between and the supernatant was discarded. After the final wash step, 30 µl SDS sample buffer were added to beads and incubated for 10 min at 95 °C with 350 rpm shaking on a thermomixer (Eppendorf, Hamburg, Germany). The samples were then briefly cooled on ice, and loaded on SDS polyacrylamide gels for the separation and visualization of proteins. The NaCl concentration of the assay buffer has been adjusted as stated (0.3 M, 0.6 M or 0.75 M) (Figure 8).

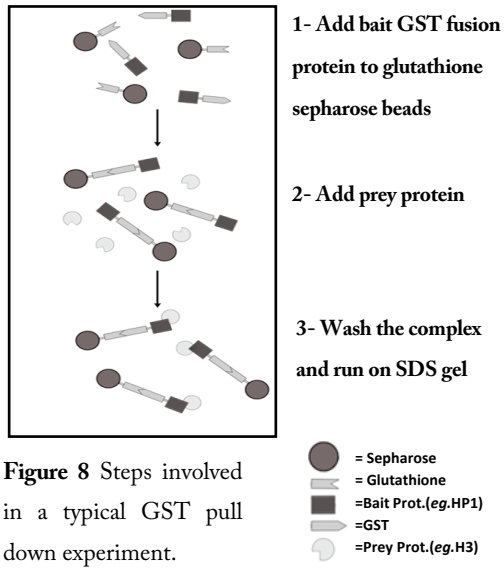

Figure 8 Steps involved in a typical GST pull down experiment.

2.2.2.9 Preparation of paraffin sections and immunohistochemistry

Mice lungs were fixed either in 4 % formalin or HOPE solution overnight and on the next day embedded in paraffin blocks with Hypercenter (Shandon, Pittsburgh, USA) using the automated program (70 % Ethanol-30 min, 70 % Ethanol-1h, 85 % Ethanol-45 min, 2X 95 % Ethanol-45 min, 2X 100 % Ethanol-45 min, 2X 100 % Xylene-2 h and 2X Paraffin-1 h). They were cut to 10 µm sections with Leica SM200R microtome (Leica Microsystems, Wetzlar, Germany). Lung sections were then stained using indirect immune-peroxidase staining. Briefly, slides were deparaffinated by 10 min incubation in xylene followed by 10 min serial incubations in 100 %, 70 % and 40 % acetone. Antigen retrieval was achieved by boiling the slides in 10 mM citric acid (pH 6.0), using a normal household pressure cooker for 2 min. After this step, the pressure cooker was immediately cooled under running cold tap water and slides were transferred to distilled water and incubated for 5 min. For the blocking of endogenous peroxidase activity, slides were then incubated in 3 % H_2O_2 in TBS for 20 min followed by 3 washes in TBS. For the reduction of background staining, slides were then incubated in Image-iT FX signal enhancer (Invitrogen, Carlsbad/CA, USA) for 30 min. Primary antibody incubation was done for 1 h followed by 30 min incubation with species specific horseradish-peroxidase coupled secondary antibodies. Primary and secondary antibodies were diluted in 10 % BSA/TBS. Finally, the PO staining was developed by incubating the slides in DAB developing solution (Sigma-Aldrich, Munich, Germany) for 10 min. The slides were counterstained with haematoxylin and coverslipped with a drop of Kaiser's glycerol gelatine.

Pictures were taken on an Olympus BX41 microscope (Olympus, Hamburg, Germany) equipped with a Nikon DS-Ri1 camera (Nikon, Surrey, UK).

2.2.2.10 Indirect immunofluorescence

MEFs grown on „superfrost plus" glass slides (R. Langenbrinck, Emmendingen, Germany) were washed twice with PBS and fixed in 2 % formaldehyde (w/v) (in PBS) solution for 10 min. Following the permeabilization in 0.25 % Triton X-100 (in PBS) for 10 min, cells were incubated 1 h with primary antibody solution (in 10 % BSA/PBS). Cells were then washed three times in PBS for 5 min and incubated 1 h with secondary antibody solution (in 10 % BSA/PBS) and coverslipped with a drop of vectashield antifade medium with DAPI (Vector laboratories, Burlingame, USA) after washing three times for 5 min in PBS. All images were taken using a Leica SP5 confocal microscope (Leica Microsystems, Wetzlar, Germany).

2.2.2.11 Preparation of chromosome spreads and indirect immunofluorescence staining

One day before the experiment, cells were passaged at a split ratio of 1:5 to achieve maximal cell division rate. On the next day, Colcemid (PAA, Pasching, Austria) was added to flasks to a final concentration of 0.1 µg/ml and incubated for 3 h. The cells at metaphase were then shaken off by hitting the bottom of the cell culture dish couple of times and the supernatant including cells at metaphase was transferred into 50 ml tubes. Following centrifugation at 1200 rpm for 10 min at 4 °C, the supernatant was discarded and the cell pellet was resuspended in 2 ml 4 °C cold PBS. After counting, cells were pelletted at 1200 rpm for 10 min at 4 °C and 4 ml 4 °C cold hypotonic buffer was added drop wise while mixing the cells gently. The cell suspension was then incubated at 37 °C for 20 min and $5x10^4$ cells were centrifuged on glass slides using a cytospin (Shandon, Pittsburgh, USA) for 5 min at 2000 rpm. Slides were then transferred immediately into KCM medium and incubated for 10 min at RT. After blocking for 30 min using ImageIT Signal Enhancer solution, primary antibody of interest in 10 % BSA/KCM was added and incubated for 1 h at RT in a humid chamber. Following 3 washes in KCM medium each for 5 min, secondary antibody solution in 10 % BSA/KCM was added and incubated for 1 h at RT in a humid chamber. The slides were then washed three times in KCM buffer and fixed in 4 % formaldehyde/KCM solution for 15 min at RT. After briefly rinsing in distilled water, slides were then coverslipped using Vectashield antifade medium with DAPI (Vector laboratories, Burlingame, USA).

2.2.2.12 Isothermal titration calorimetry (ITC)

For the determination of binding affinities, isothermal titration calorimetry was used which is the only technique that can directly measure the binding energetics of biological processes. A typical ITC instrument is a heat-flux calorimeter which measures the amount of power (µcal/s) required to maintain a constant temperature between the sample and reference cell (Figure 9). With the injection of ligand, a certain amount of macromolecule/ligand complex is formed which is accompanied by the release (exothermic reaction) or the absorption (endothermic

reaction) of heat that causes a difference in temperature between sample and reference cell which is then compensated by either lowering or raising the thermal power applied. After each injection, the system reaches equilibrium, and the temperature balance is restored, resulting in a signal in the form of a peak. The amount of heat associated with the injection is then provided by integrating the area under this curve. The heat signal

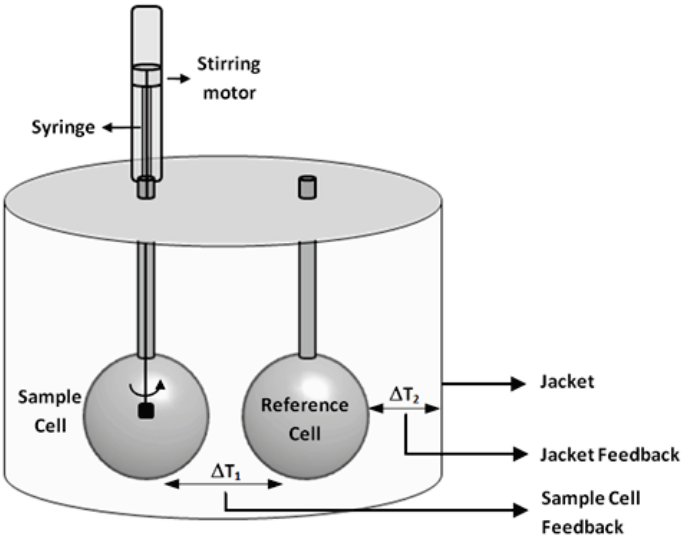

Figure 9 Schematic diagram of ITC_{200} instrument used in calorimetry experiments. This instrument uses a cell feedback network (CFN) to differentially measure and compensate for heat produced or absorbed between the sample and reference cell. A thermoelectric device measures the temperature difference between the two cells and a second device measures the temperature difference between the cells and the jacket. The temperature difference between the sample and reference cells (ΔT_1) is kept at a constant value (i.e. baseline) by the addition or removal of heat to the sample cell, as appropriate, using the CFB system. The integral of the power required to maintain ΔT_1 constant over time is a measure of total heat resulting from the process being studied (redrawn from http://www.microcal.us/technology/itc.asp).

reduces until only a background heat as the reactant becomes saturated. Thermodynamic parameters for histone H3-HP1β and H3K9me3-HP1β binding were determined using an ITC_{200} instrument ((Microcal) GE Healthcare, Munich, Germany) following manufacturer's instructions and software. His tagged recombinant mouse HP1β, its T51A, V23M, F45E, I161E mutants and recombinant *X. laevis* histone H3 (kindly provided by Prof. H. Bartunik, MPG-ASMB, Hamburg) were all excessively dialyzed against 50 mM sodium phosphate, 25 mM NaCl (pH 6.0). Lyophilized histone H3 tail peptide (Peptide Protein Research, Fareham, UK) was also dissolved in the same dialysis buffer. Histone H3 tail peptide used was H3K9me3 trimethylated at lysine 9 (ARTKQTARK^{Me3}STGGKAY) (underlining corresponds to a non native residue). The heats of binding reactions (μcal/s) were measured by 20 sequential injection of 1 mM ligand (histone H3, or H3K9me3), each 2 μl, spaced at 3-5 min intervals, into 100 μM HP1β in the cell. Binding curves were analyzed using fitting parameter "one set of sites" of instrument's software. All calculations were based on the Gibbs free energy equation:

$$\Delta G = -RT \ln K_a = \Delta H - T\Delta S$$

(ΔG is the free energy of binding, R is the gas constant, T is the absolute temperature, K_a is the association constant, ΔH is the enthalpy and ΔS is the entropy).

Based on this equation, it can be seen that two determinants of the binding affinity are enthalpy (ΔH) and entropy (ΔS). The strength of the interactions (*e.g.* hydrogen bond, van der Waals, electrostatic) between the target and the ligand is reflected by the binding enthalpy, whereas the entropy change primarily reflects two contributions: changes in solvation entropy and changes in conformational entropy. Binding of a ligand to the macromolecule results in desolvation and triggers the release of water molecules from the binding site and the ligand, which then increases the entropy of the system.

2.2.3 Cell biology

2.2.3.1 Production of primary mouse embryonic fibroblasts (MEFs)

Cbx1 knock out (-/-) primary MEFs were derived from 13.5 day old embryos generated by crossing two *Cbx1* heterozygous (+/-) mice. Following removal of head and organs, embryos were rinsed with PBS, minced and digested with Trypsin/EGTA (PAA, Pasching, Austria) for 5 min at 37 °C, using 2 ml per embryo. Trypsin was inactivated by addition of MEF culture medium. Cells from single embryos were plated in one T75 cell culture dish and incubated at 37 °C in a cell culture incubator (Thermo Fisher Scientific, Bonn, Germany).

2.2.3.2 MEF cell culture

MEFs were cultured in medium containing 87 % (v/v) DMEM (Sigma-Aldrich, Munich, Germany), 10 % (v/v) FCS (Biochrome, Berlin, Germany), 1 % (v/v) L-glutamine (Biochrome, Berlin, Germany), 1 % (v/v) Non essential amino acids 100x (PAA, Pasching, Austria) and 1 % (v/v) Penicillin/Streptomycin 100x (PAA, Pasching, Austria). For the passaging of MEFs, 85-90 % confluent cells were washed twice in PBS, detached with Trypsin/EGTA medium, pH 7.6 (TEG, see Table 3) for 5 min, centrifuged for 10 min at 1200 rpm at 4 °C and split into a new culture dish with a 1:10 ratio.

TEG	
KH_2PO_4	0.0216 % (w/v)
NaCl	0.63 % (w/v)
Na_2HPO_4	0.012 % (w/v)
KCl	0.0333 % (w/v)
D – Glucose	0.099 % (w/v)
Tris	0.27 % (w/v)
Phenol red (1%)	0.09 % (w/v)
Trypsin (10 x)	10 % (w/v)
EGTA	0.04 % (w/v)
PVA	0.01 % (w/v)

Table 3 TEG medium composition

2.2.3.3 Cell counting

Counting of cells was performed with exclusion of dead cells by trypan blue (Biochrom, Berlin, Germany). Trypan blue permeates the membrane of only dead cells, which appear blue. Working solution of trypan blue was prepared by diluting trypan blue 1:10 in 0.9 % NaCl. The cell suspension to be counted was diluted 1:10 in the working solution of trypan blue and cells were counted using a Neubauer counting chamber (Assistent, Sondheim, Germany) under an optical microscope.

2.2.3.4 3T9 assay

For the 3T9 assay, cells were maintained on a defined schedule: 9 x 10^5 cells per 60 mm diameter dish were trypsinized, counted and passaged every 3 days. Plating after disaggregation of embryo cells was considered passage 1 and the first replating three days later as passage 2.

2.2.3.5 Transient transfection of EGFP-TPP1, -POT1a and -POT1b

pCAG-EGFP-TPP1, -POT1a and -POT1b plasmids were transiently introduced into MEF cells by the transfection reagent "lipofectamine 2000" (Invitrogen, Carlsbad/CA, USA) following manufacturer's instructions. Afterwards, cells were incubated for 48 h, and indirect immunofluorescence staining of cells was done as described. These experiments were performed in collaboration with Dr. K. Okamoto (Scripps, San Diego).

2.2.4 Animal experiments

2.2.4.1 Induction of K-ras^{V12} in K-ras$^{+/V12}$;RERTn$^{+/ERT}$;Cbx1$^{+/-}$ transgenic mice

K-ras$^{+/V12}$;RERTn$^{+/ERT}$ mice were provided by Dr. C. Guerra (cnio, Madrid, Spain). *Cbx1*$^{+/-}$ mutation was introduced into these mice by crossing K-ras$^{+/V12}$;RERTn$^{+/ERT}$ with *Cbx1*$^{+/-}$ mice. Genotyping of the newborn mice was done using stated primers (see primers). Expression of Kras^{V12} oncogene in 3 weeks old mice was induced by intraperitoneal injection of 0.5 mg 4-hydroxytamoxifen (Sigma-Aldrich, Munich, Germany) in 100 µl corn oil (Sigma-Aldrich, Munich, Germany) three times a week for two weeks. Expression of K-ras^{V12} oncogene was screened by sequencing the cDNA obtained from mice with K-ras V12 for and K-ras V12 rev primers.

Chapter 3

Results

3.1 Investigation of the effect of *Cbx1* mutation on genomic stability

In order to investigate the effect of *Cbx1* disruption on genome stability in mouse, primary MEFs from the three genotypes, WT, *Cbx1*$^{+/-}$ and *Cbx1*$^{-/-}$ were cultured, in duplicates, according to a 3T9 protocol, which is an established method for measuring the growth rate and immortalization frequency of mouse cells (Kamijo *et al.*, 1997). Briefly, cells were passaged every three days, and 9x10^5 cells were plated per passage. As shown in figure 10, by passage 16 the WT cells had undergone senescence crisis and died. In contrast, cultures of *Cbx1*$^{+/-}$ and *Cbx1*$^{-/-}$ MEFs either went through the crisis and continued to proliferate or simply continued to proliferate without any sign of having been through crisis.

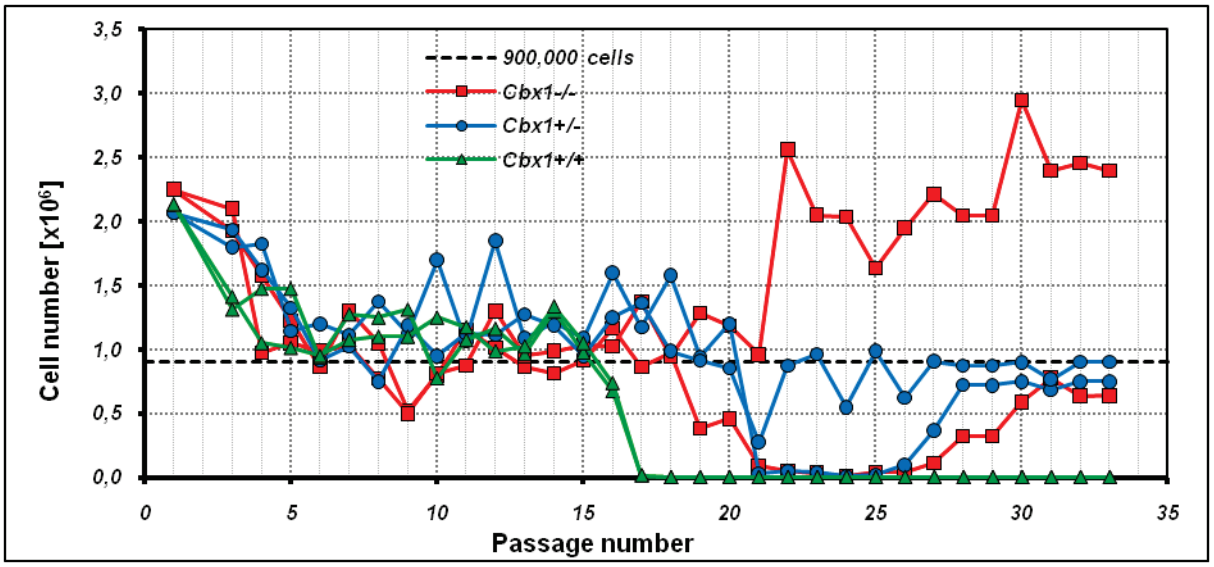

Figure 10 3T9 assay of primary MEFs showing that homo- and heterozygous deletion of *Cbx1* results in escape from senescence. WT MEFs are depicted as green lines with triangles, *Cbx1*$^{+/-}$ MEFs are depicted as blue lines with circles and *Cbx1*$^{-/-}$ MEFS are depicted as red lines with squares.

Having shown that *Cbx1*$^{-/-}$ MEFs exhibited an increased immortalization frequency, the next step was to determine the possible reasons underlying this observation. To this end, Giemsa staining and telomere FISH analysis were undertaken on metaphase chromosomes of early passage *Cbx1*$^{-/-}$ MEFs. Telomere FISH is a valuable technique that involves the hybridization of a fluorescent labelled telomeric PNA probe to the metaphase chromosomes, enabling the discrimination of individual chromosome ends. Analysis of metaphases prepared from exponentially growing early passage (passage 2-4, before senescence crisis) MEFs revealed

that there was an increase in aneuploid metaphases (Figure 11A) in *Cbx1*$^{-/-}$ cultures compared to *Cbx1*$^{+/-}$ and *Cbx1*$^{+/+}$. A variety of other chromosomal aberrations were also present including premature chromosome separations (Figure 11B) as evidenced by presence of single chromatids, which is indicative of chromosome segregation defects, telomere-telomere fusions with loss (Figure 11D) and retention (Figure 11C) of telomere signals, chromosomal translocations (Figure 11E), formation of diplochromosomes (Figure 11F) and micronucleus formation (Figure 11G).

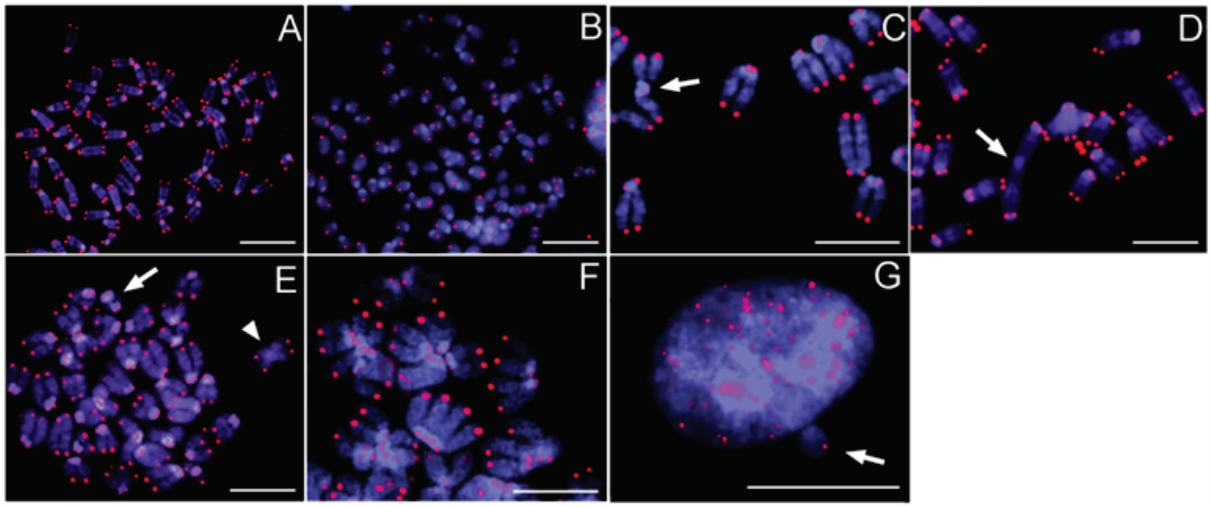

Figure 11 Telomere FISH analysis on metaphases from *Cbx1*$^{-/-}$ primary MEFs reveals a variety of karyotypic aberrations. **A.** Example of an aneuploid metaphase seen in *Cbx1*$^{-/-}$ MEFs. **B.** Some of the aneuploid *Cbx1*$^{-/-}$ metaphases exhibit premature chromosome separation. **C.** Chromosome end associations with retention of telomere signals. **D.** Telomere-telomere fusions with loss of telomere signals. **E.** Chromosomal translocations, including ring chromosomes (arrow) and inversions (arrowhead). **F.** Diplochromosomes. **G.** Micronucleus formation. Experiment was done in collaboration with Prof. T. Pandita (WUSOM, St. Louis). Scale bars: 10 μm.

Genotype	Chromosome gaps and breaks	Telomere associations	Bridges
Cbx1$^{+/+}$	5	31	7
Cbx1$^{+/-}$	6	29	10
Cbx1$^{-/-}$	24 ($p<0.001$)	88($p<0.001$)	51($p<0.001$)

Table 4 Comparison of the frequencies of chromosome aberrations (chromosome gaps and breaks, telomere associations and anaphase bridges) per 200 cells analyzed. In all three categories, *Cbx1*$^{-/-}$ cells showed significantly increased numbers of aberrations compared to wild type controls. Experiment was done in collaboration with Prof. T. Pandita (WUSOM, St. Louis).

Statistical analysis (chi-squared test with 1 degree of freedom) showed that *Cbx1*$^{-/-}$ cells exhibited significantly more aberrations compared to *Cbx1*$^{+/+}$ wild type controls ($p<0.001$). In *Cbx1*$^{-/-}$ cells, there were 5 times more chromosomal gaps and breaks, almost 3 times more telomere associations and more than 7 times more anaphase bridges than in wild type controls (Table 4).

3.2 Investigation of the effect of *Cbx1* null mutation on telomere function

3.2.1 Investigation of the effect of *Cbx1* null mutation on the telomeric "shelterin"

The presence of chromosomal translocations including telomere-telomere fusions in chromosomes derived from *Cbx1*$^{-/-}$ MEFs indicated that telomere function had been affected by the *Cbx1*$^{-/-}$ mutation. It has been shown that mammalian telomeres are protected from being sensed as DNA damage by the "shelterin" protein complex, which is a complex of 6 interacting proteins that form a protective cap at the end of mammalian chromosomes. When the shelterin complex is disrupted telomeres become "uncapped" and such uncapped telomeres elicit the DNA damage response that can trigger non-homologous end joining and consequent telomere-telomere fusions (Palm and de Lange; 2008).

To address the question of whether the telomeric fusions and end associations observed in the chromosomes of *Cbx1*$^{-/-}$ MEFs were due to a disruption of the protective shelterin complex or changes in the telomeric heterochromatin itself, **ch**romatin **i**mmuno**p**recipitation (ChIP) assay was undertaken using chromatin isolated from early passage WT and *Cbx1*$^{-/-}$ MEFs. ChIP assay is an established method for detecting the association of individual proteins with specific genomic regions. Briefly, chromatin from early passage WT and *Cbx1*$^{-/-}$ MEFs was precipitated with antibodies directed against known markers of heterochromatin, namely trimethylated lysine 9 on histone H3 (H3K9me3), dimethylated lysine 9 on histone H3 (H3K9me2), and trimethylated lysine 20 on histone H4 (H4K20me3). ChIP was also performed with TRF1 and TRF2, which are components of the "shelterin" complex. DNA from the precipitated chromatin was then dot/slot blotted on nylon membrane, probed with ^{32}P labelled telomeric probe and the signals were quantified using the Imagequant software.

Mean values with standard deviations of 3 experiments are depicted in figure 12. As shown, there were little or no differences in the levels of the heterochromatin marks H3K9me3, H3K9me2, H4K20me3 and TRF2 protein, although a slight decrease in TRF1 association with the telomeres in *Cbx1*$^{-/-}$ MEFs was observed compared to WT MEFs.

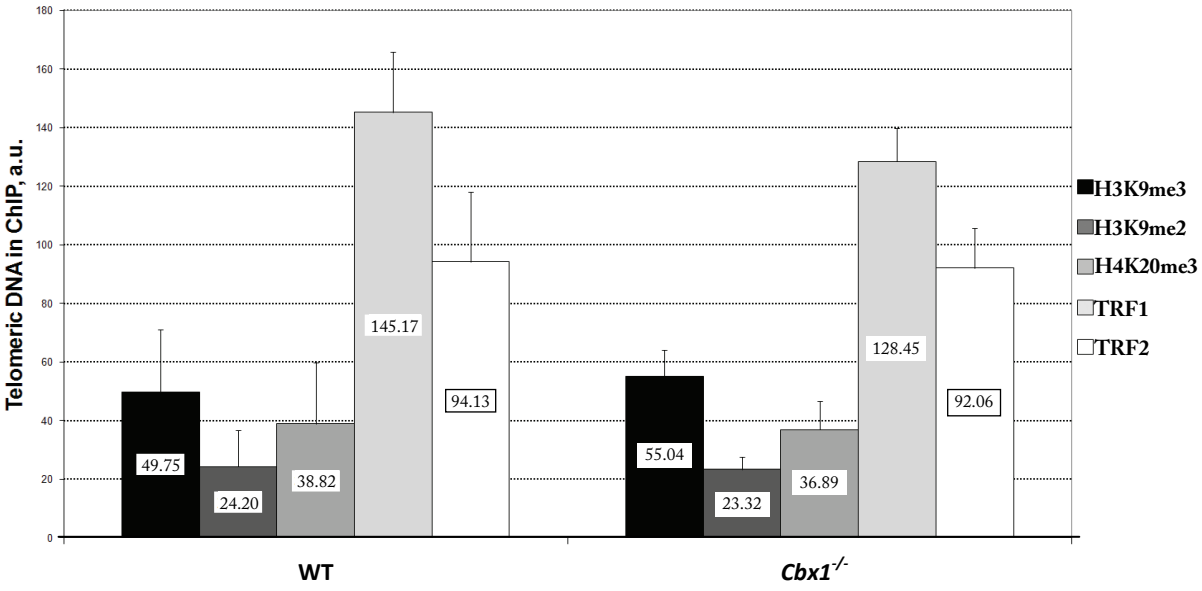

Figure 12 ChIP experiments were undertaken for the analysis of telomeric heterochromatin. Chromatin from early passage wild type and *Cbx1*$^{-/-}$ MEFs was immunoprecipitated with antibodies against several marks of heterochromatin and telomeric proteins. While there was no or very little change in the heterochromatic state of telomeres, there was a slight decrease in TRF1 found in the telomeres of *Cbx1*$^{-/-}$ cells compared to WT. Averages of three independent experiment are shown (n=3). a.u.: arbitrary units

Guided by the observation that there was a decrease in TRF1 association with *Cbx1*$^{-/-}$ telomere (Figure 12) it has been investigated whether the cellular levels of TRF1 were changed due to removal of *Cbx1* gene. To address this question, equal amounts of crude cell lysates obtained from early passage WT and *Cbx1*$^{-/-}$ MEFs were loaded on SDS polyacrylamide gels and western blotting using antibodies against HP1β, TRF1 and TRF2 was performed. As expected, HP1β was not detectable in *Cbx1*$^{-/-}$ MEFs. There was no difference in the TRF1 (and TRF2) signal intensities in *Cbx1*$^{-/-}$ MEFs compared to WT (Figure 13). It was also observed that the molecular weight of the lower TRF1 band in *Cbx1*$^{-/-}$ MEFs had a slightly lower molecular weight than compared to same band in WT cells.

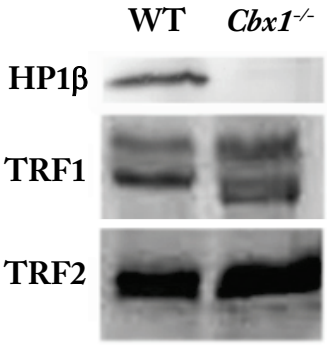

Figure 13 Equal amounts of crude cell lysates from early passage WT and *Cbx1*$^{-/-}$ MEFs were loaded on a 15 % SDS gel. Western blotting was then performed with antibodies against HP1β, TRF1 and TRF2.

3.2.2 Investigation of the effect of *Cbx1* null mutation on cellular distribution of "shelterin" proteins

In order to explore the possibility that the telomeric phenotypes observed in *Cbx1*$^{-/-}$ MEFs were due to the mis-localisation of TPP1, POT1a and POT1b proteins, WT and *Cbx1*$^{-/-}$ MEFs were transiently transfected with pCAG-EGFP-TPP1, POT1a and POT1b EGFP fusion expression plasmids and immunofluorescence staining was performed using anti-GFP primary and Alexa-fluor-488 secondary antibodies for the enhancement of the GFP signal (green). As shown in figure 14, all three proteins gave a "dotty" nuclear staining pattern.

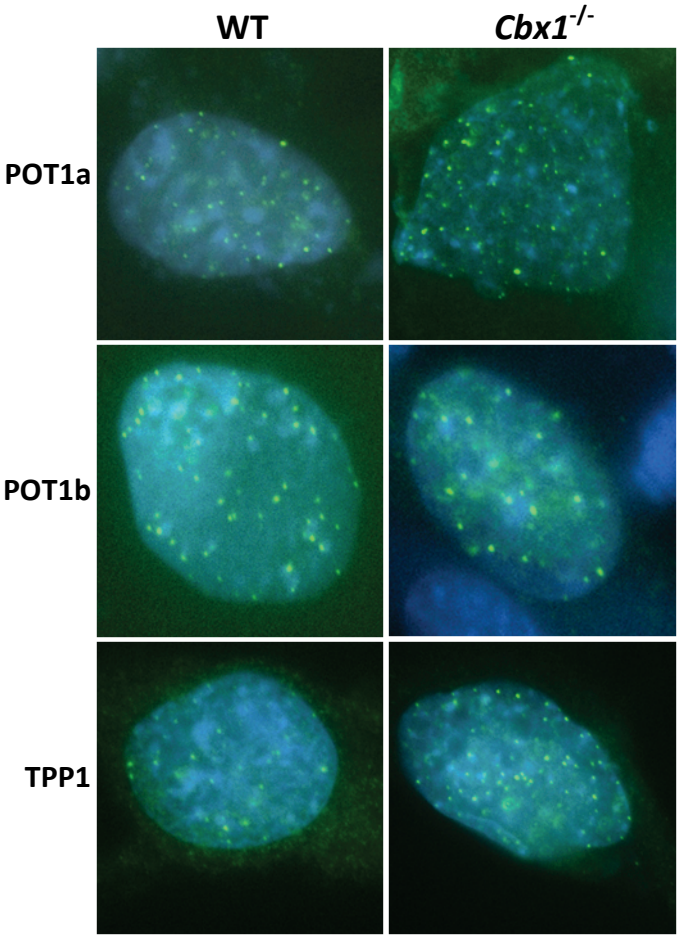

Figure 14 Intracellular localizations of telomeric proteins POT1a, POT1b and TPP1 in G1 interphase nuclei. Expression vectors encoding EGFP fusions of the proteins were transiently transfected into WT and *Cbx1*$^{-/-}$ MEFs. Following transfection, indirect immunofluorescence double staining was performed using anti-GFP(Rb) and anti-rabbit Alexa-fluor-488 antibodies in order to enhance the GFP signal (green). Cells were also counterstained with DAPI (blue) for the visualization of DNA. Note the slightly larger, more diffuse, blocks of Pot1b staining in *Cbx1*$^{-/-}$ Experiment was done in collaboration with Dr. K. Okamoto (Scripps, San Diego).

There were no differences in the pattern of TPP1, POT1a and POT1b staining in *Cbx1*$^{-/-}$ MEFs compared to WT MEFs although in some *Cbx1*$^{-/-}$ nuclei, POT1b was sometimes observed as slightly larger, more diffusely distributed dots (see the POT1b staining in the nucleus shown in figure 14).

3.2.3 Investigation of the effect of *Cbx1* null mutation on telomere length

Mammalian telomeres are enriched for HP1 proteins and the heterochromatic marks H3K9me3, H4K20me3 (Blasco, 2007). Deletion of the Suv39h1/2 and Suv4-20h1/h2 histone methyltransferases that impose the H3K9me3 and H4K20me3 marks on heterochromatin results in the loss of the histone modifications, HP1α and HP1γ with only residual amounts of HP1β remaining at the telomeres (Garcia-Cao *et al.*, 2004; Benetti *et al.*, 2007). Notably, mutation in these enzymes also results in telomere recombination and in elongated telomeres.

A critical role for HP1β in telomere physiology has been underscored by the overexpression of HP1β in human cells, which results in reduced association of human telomerase reverse transcriptase with the telomere and a higher frequency of end-to-end chromosomal fusions (Sharma *et al.*, 2003). To investigate whether the genomic instability seen in *Cbx1*$^{-/-}$ MEFs was associated with a change in telomere lengths, FLOW-FISH analysis on early and late passage WT and *Cbx1*$^{-/-}$ MEFs was undertaken. FLOW-FISH is an established method for the measurement of mean telomere length (Baerlocher *et al.*, 2006). Briefly, early passage (passages 1-3) and late passage (passages 30-35) WT and *Cbx1*$^{-/-}$ MEFs were hybridized with and without FITC-conjugated PNA probes specific for the telomeric sequences. After hybridisation, a flow cytometer was used to "gate" on G1 cells containing 2n DNA content for further analysis (Figure 15). Focussing on the 2n G1 cells, quantitative fluorescence values were obtained using the flow cytometer and mean telomere lengths of *Cbx1*$^{-/-}$ MEFs could be determined by first subtracting the autofluorescence levels obtained using unstained cells and then, second, by calculating the mean telomere length by comparison to the quantitative signals obtained from parallel analysis of cells with a known telomere length.

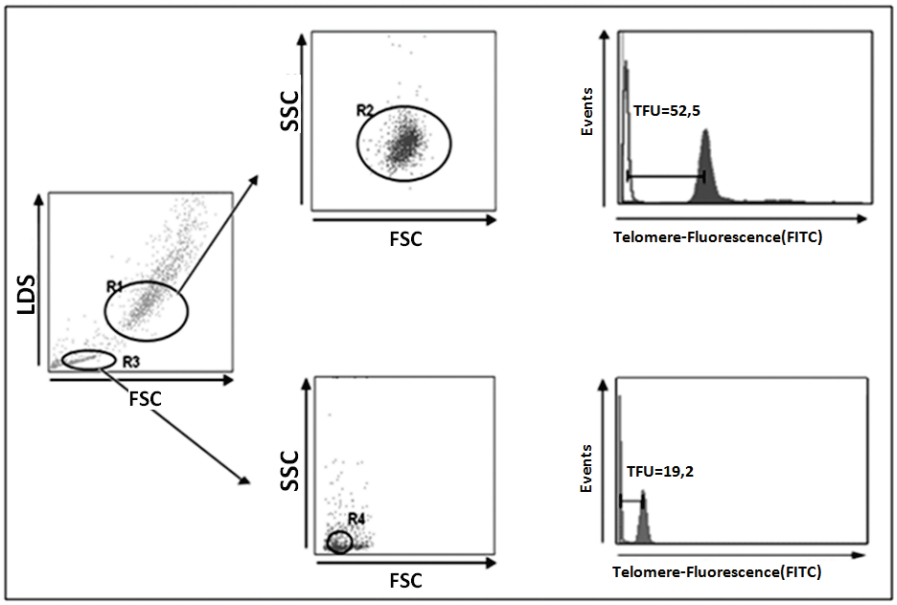

Figure 15 For measuring the lengths of telomeres, the FLOW-FISH technique was used. WT MEFs (R1) and bovine thymocytes (R3) in G1 phase, gated for the diploid content of DNA, were analysed by FACS. Quantitative fluorescence values were obtained for MEFs (R2) and bovine thymocytes (R4) respectively. Because bovine thymocytes have a known telomere length (~19.5 kb) it is possible to compare the fluorescence values obtained with the bovine thymocytes with those obtained from the MEFs and thus calculate the mean telomere length of experimental cells. Experiment was done in collaboration with Dr. U. Brassat (UKE, Hamburg).

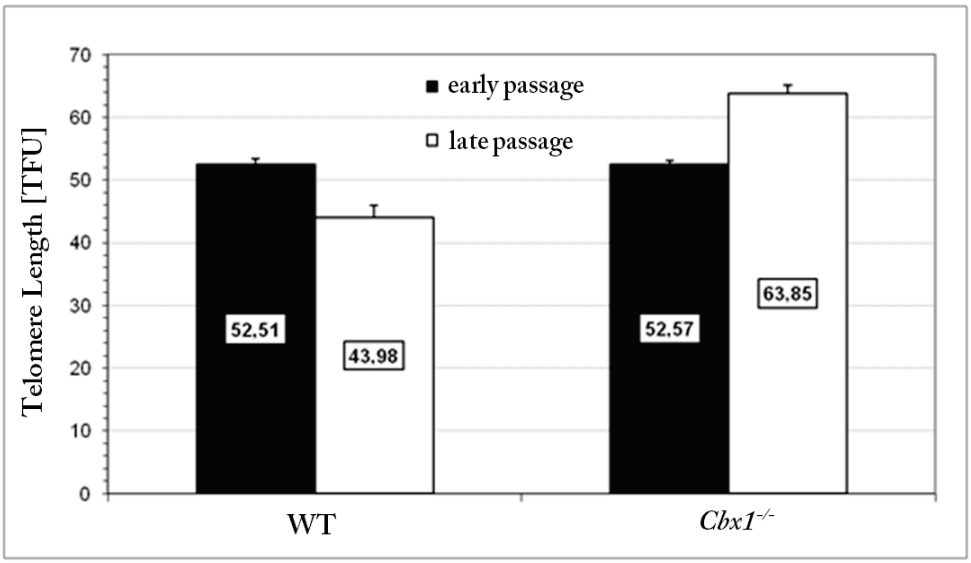

Figure 16 Mean telomere lengths of early and late passages of WT and *Cbx1*$^{-/-}$ MEFs measured by FLOW-FISH (n = 3) (1 TFU = 1 kb). Where telomeres of early passage WT and *Cbx1*$^{-/-}$ MEFs were of almost identical length, late passage *Cbx1*$^{-/-}$ MEFs had much longer telomeres (~20 kb longer) compared to WT controls. Experiment was done in collaboration with Dr. U. Brassat (UKE, Hamburg).

As shown in figure 16, there was very little or no difference found in the telomere lengths of early passage WT and *Cbx1*$^{-/-}$ cells. However, at late passage, the *Cbx1*$^{-/-}$ cells had telomeres that were longer (~20 kb) than the WT telomeres.

3.3 Investigation of the effect of *Cbx1* null mutation on sister chromatid cohesion

Considering the role of HP1 proteins on cohesion in yeast, it has been investigated whether the genomic instability seen in *Cbx1*$^{-/-}$ MEFs was associated with defects in sister chromatid cohesion and kinetochore attachment. Consequently, indirect immunofluorescence staining experiments were performed on unfixed metaphase spreads from early passage WT and *Cbx1*$^{-/-}$ MEFs. Accordingly, cells were arrested at metaphase by culturing cells in the presence of colcemid, incubated in a hypotonic medium for swelling and then centrifuged on glass objectives which resulted in the disruption of the cell membrane and enabled the visualization of metaphase chromosomes. Following this, slides were subjected to double indirect immunofluorescence staining without fixation with antibodies against SMC3, BUB1 and SGO1. Anti-CREST antibody was used in parallel for the localization of centromeres. DNA was counterstained with DAPI.

As shown in figure 17, staining of chromosomes with an anti-SMC3 antibody revealed that there were no changes in SMC3 localization in early passage WT and *Cbx1*$^{-/-}$ MEFs. In both genotypes, SMC3 signal was present in between the two centromeric signals of CREST staining. The staining of unfixed metaphase chromosomes from early passage WT and *Cbx1*$^{-/-}$ MEFs with anti-BUB1 and anti-SGO1 antibodies are shown in figures 18 and 19, respectively. BUB1 signals in figure 18 perfectly colocalized with the centromeric signals obtained by the CREST staining with no change between WT and *Cbx1*$^{-/-}$ MEFs. The staining pattern of SGO1 in figure 19 was slightly different than the pattern observed by BUB1. SGO1 seemed to partially colocalize with centromeres, while some of the protein was localized around the centromeric signals of CREST staining. Notably, there were again no differences between the staining patterns obtained from WT and *Cbx1*$^{-/-}$ MEFs when an anti-SGO1 antibody was used.

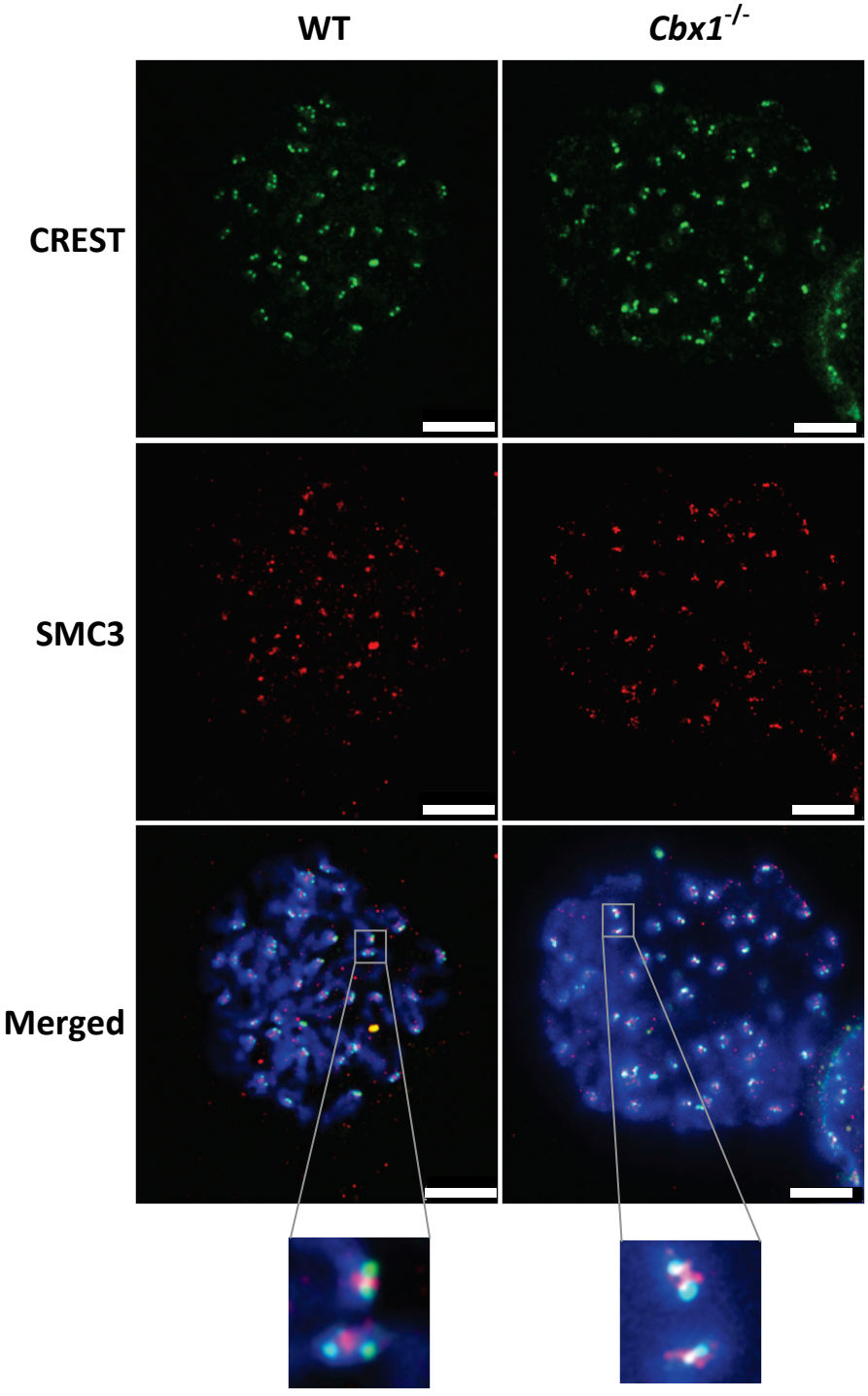

Figure 17 Localization of cohesion subunit SMC3 on WT and *Cbx1*$^{-/-}$ metaphase chromosomes. SMC3 is shown in red, CREST in green and the DNA was counterstained with DAPI. Scale bars: 10 μm

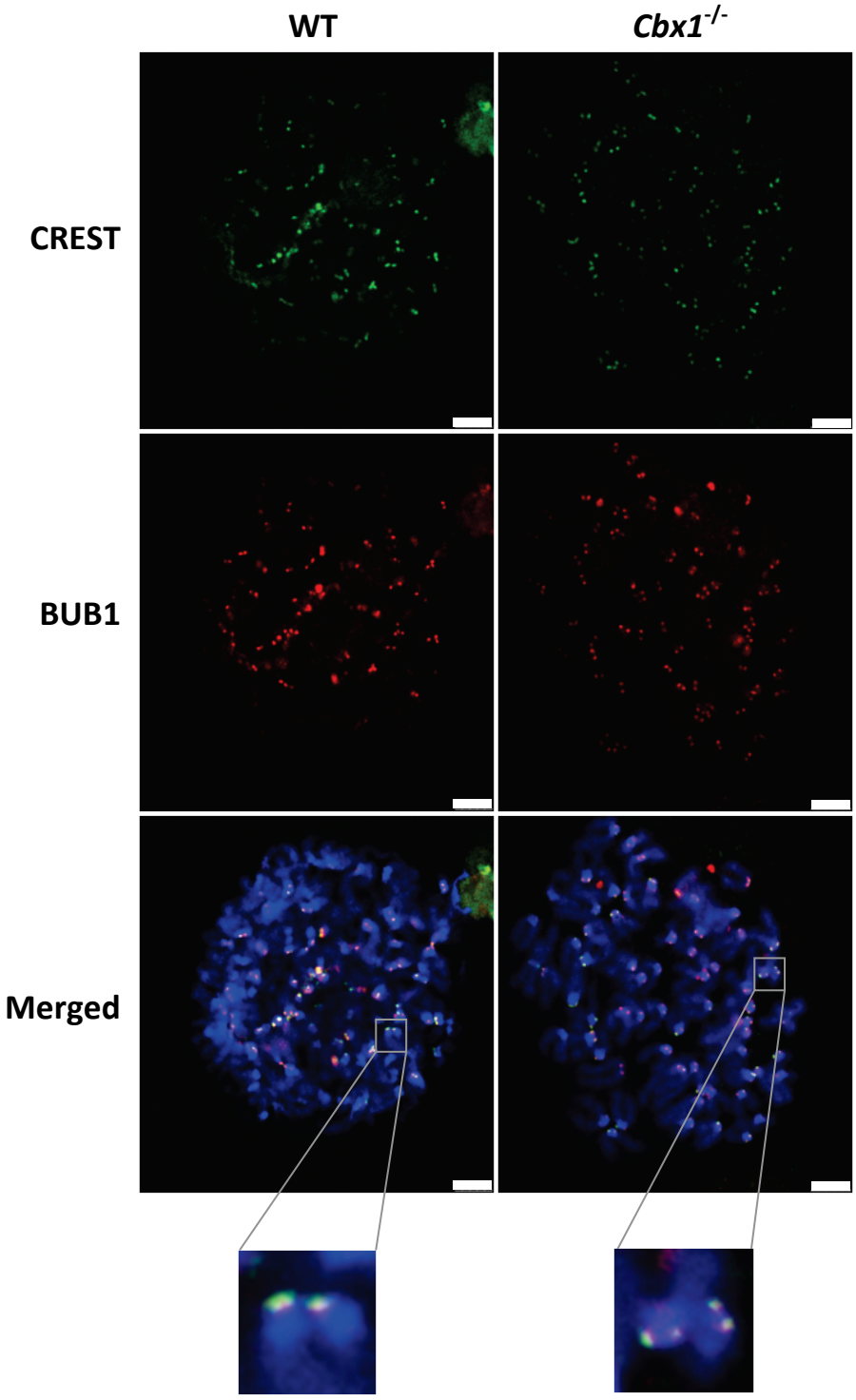

Figure 18 Localization of spindle assembly checkpoint protein BUB1 on WT and *Cbx1*$^{-/-}$ metaphase chromosomes. BUB1 is shown in red, CREST in green and the DNA was counterstained with DAPI. Scale bars: 5 μm

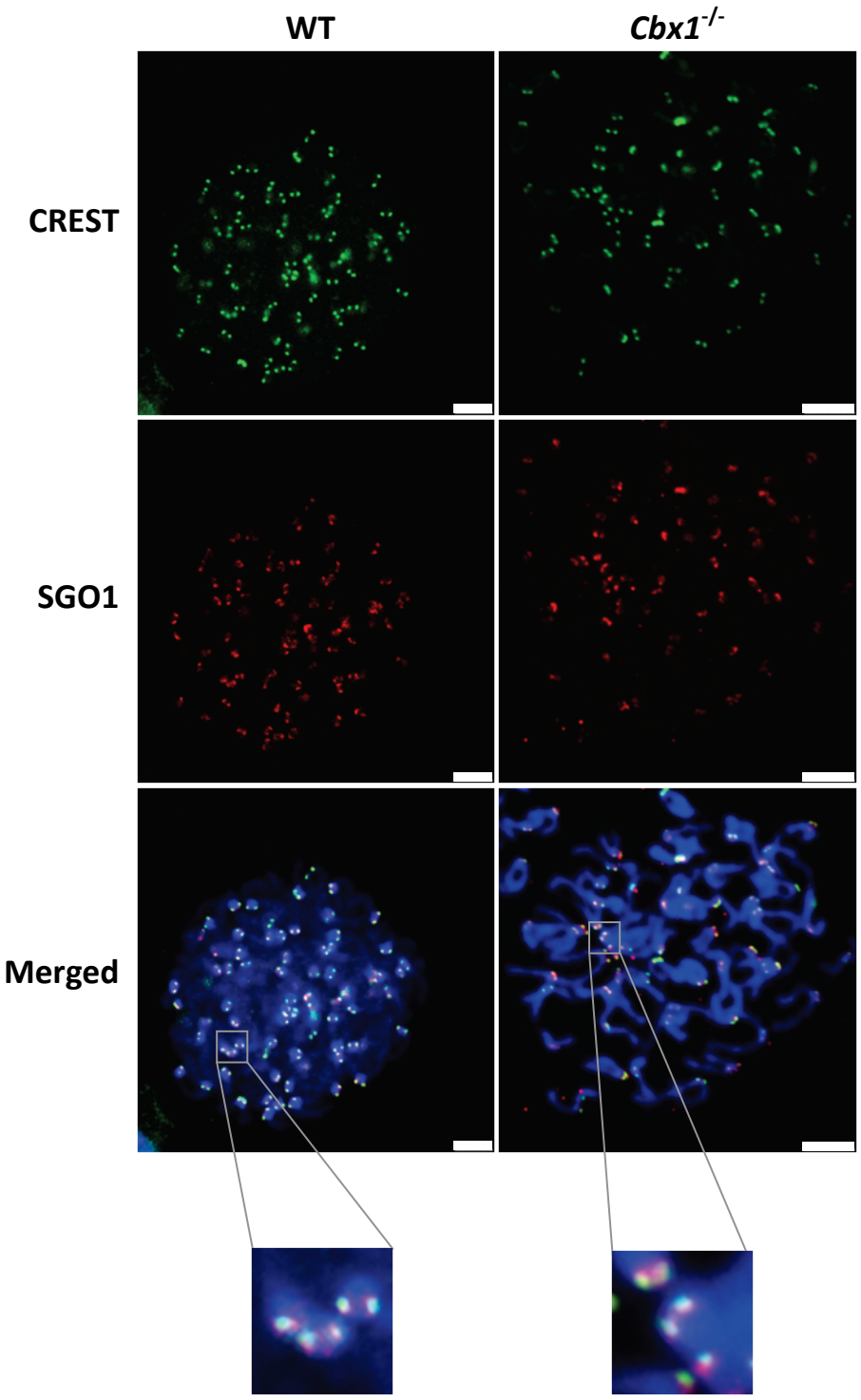

Figure 19 Localization of SGO1 protein on WT and *Cbx1*$^{-/-}$ metaphase chromosomes. SGO1 is shown in red, CREST in green and the DNA was counterstained with DAPI. Scale bars: 5 μm

3.4 Investigation of the effect of *Cbx1* mutation on oncogene-induced senescence in the K-ras$^{+/V12}$;RERTn$^{+/ERT}$ mouse model system

K-ras$^{+/V12}$;RERTn$^{+/ERT}$ transgenic mice carry the inducible K-ras^{V12} allele along with the wt allele. These mice express the oncogenic K-ras^{V12} upon 4-hydroxytamoxifen (4-OHT) *i.p.* injection, which results in the activation of the inducible Cre-ERT2 recombinase expression leading to removal of the STOP transcriptional sequences that prevent expression of the targeted K-ras^{V12} allele (Guerra *et al.*, 2003). Oncogenic K-ras protein only differs from WT K-ras in one amino acid: the glycine 12 residue (GGT) is changed into the oncogenic valine 12 (GTA). These animals have been shown to develop lung adenomas (premalignant tumours) and adenocarcinomas (malignant tumours). The premalignant adenomas exhibit characteristic features of OIS: they stain positive for SA-β-gal, p16 and DcR2 and are negative for pKi-67 staining (Collado *et al.*, 2005). In contrast, the malignant adenocarcinomas escape cellular senescence; they show a low expression of SA-β-gal, p16 and DcR2 and a concomitant increase in pKi-67 expression.

In order to investigate the effects of *Cbx1* mutation on oncogene-induced senescence, *Cbx1* heterozygous mutation was introduced into mice carrying the inducible K-ras^{V12} allele to create the strain K-ras$^{+/V12}$;RERTn$^{+/ERT}$;*Cbx1*$^{+/-}$. Mice were then injected with 4-OHT to induce expression of the K-ras^{V12} oncogene. In our hands, these mice neither died nor showed severe breathing difficulties when they were around 8 months old as described in the original reference (Guerra *et al.*, 2003); therefore they were not killed at month 8 and allowed to live longer. The experiment was eventually stopped and the mice were killed. Some of the mice were by then 22 months old. Lungs of these mice were analyzed for the expression of oncogenic K-ras^{V12} and examined for the presence of adenomas and adenocarcinomas by histopathological and immunohistochemical analysis of sections using markers for senescence (p16, DcR2) and proliferation (pKi-67). Histopathological analysis was done in collaboration with Prof. E. Vollmer (FZB). Analysis of the expression of oncogenic K-ras^{V12} was done by sequencing of RT-PCR products amplified from lung tissues with K-ras^{V12} specific primers.

As a result of this analysis, it was found that at the time the tissues were taken, K-ras^{V12} was expressed in 4 of the experimental (*Cbx1*$^{+/-}$) and 6 of the control (WT) mice (Figure 20).

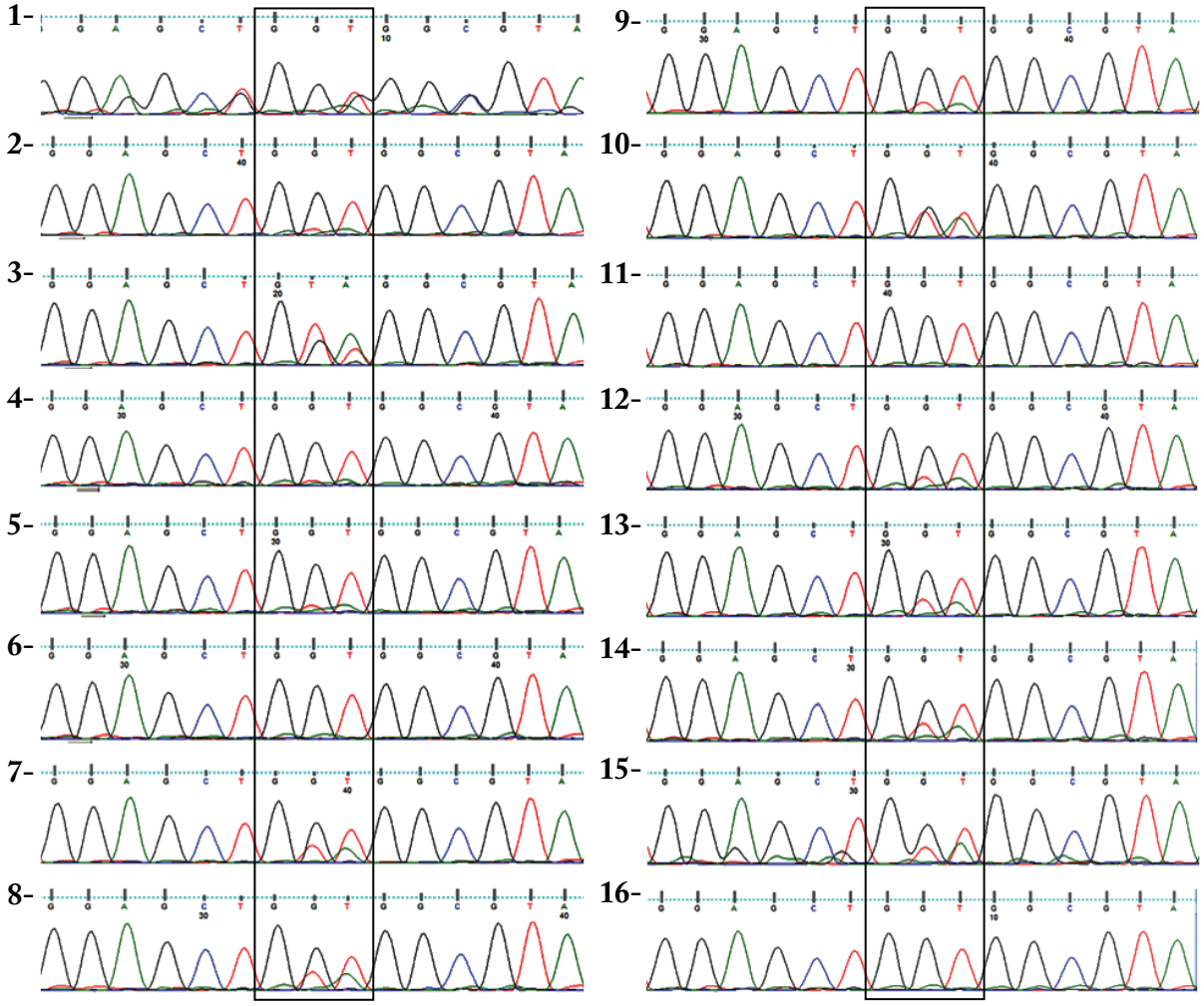

Figure 20. RT-PCR products amplified using "K-ras V12 for" and "K-ras V12 rev" primers from lung tissues of K-ras$^{+/V12}$;RERTn$^{+/ERT}$ (WT control group on the right side, numbers 9-16) and K-ras$^{+/V12}$;RERTn$^{+/ERT}$;*Cbx1*$^{+/-}$ (experimental group on the left side, numbers 1-8) mice were sequenced. Chromatographs with codons 10-14 of K-ras gene, with codon 12 in black rectangle, are shown. Valine 12 (GTA) was considered as expressed when the chromatograph peaks had at least 10 % of the size of the WT allele (GGT). This analysis has revealed that oncogenic K-ras^{V12} was expressed in 4/8 experimental and in 6/8 of WT mice (see also Table 5).

16 mice were analyzed in total in these experiments (8 experimental and 8 control). In 5 out of 8 experimental mice, histopathological analyses revealed obvious malignant adenocarcinomas whereas in control group there was only one mouse with a small region of adenocarcinoma (Figure 21, Table 5). In contrast, there were surprisingly no premalignant adenomas found in any of the lungs dissected.

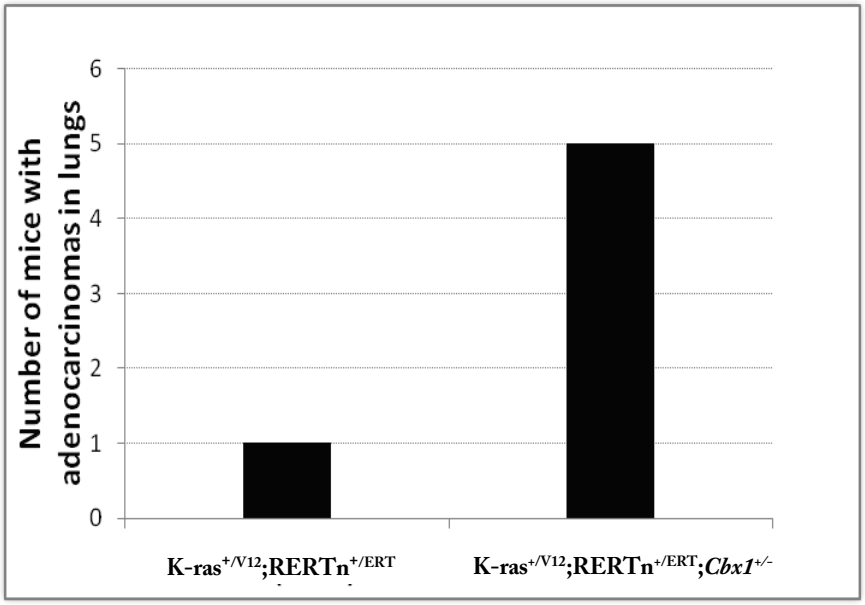

Figure 21 Number of adenocarcinomas found in K-ras$^{+/V12}$;RERTn$^{+/ERT}$;*Cbx1*$^{+/-}$ mice compared to WT (n= 8 for both genotypes). While the only adenocarcinoma from WT control mice was identified in only one of the many lung sections prepared, 5 of the experimental K-ras$^{+/V12}$;RERTn$^{+/ERT}$;*Cbx1*$^{+/-}$ mice had obvious malignant tumours with 4 of them present in multiple sections.

Mice No.	Adenocarcinoma	K-ras^{V12} expressed	Age at time of death (weeks)
K-ras$^{+/V12}$;RERTn$^{+/ERT}$;*Cbx1*$^{+/-}$			
1-	×	×	82
2-	✓	×	92
3-	✓	✓	73
4-	✓	×	65
5-	✓	✓	92
6-	×	×	86
7-	×	✓	84
8-	✓	✓	84
K-ras$^{+/V12}$;RERTn$^{+/ERT}$ (Control group)			
9-	×	✓	72
10-	×	✓	67
11-	×	×	67
12-	×	✓	66
13-	✓	✓	86
14-	×	✓	79
15-	×	✓	79
16-	×	×	56

Table 5 Analysis of lungs from WT and experimental mice. Each lung was screened for the presence of tumors and expression of oncogenic K-ras^{V12} by 4-OHT injection. Ages of mice when they were killed are also included.

Immunohistochemical analysis on lung sections possessing adenocarcinomas was done with markers of senescence and proliferation. It was only possible to stain 4 of the 5 adenocarcinomas found in K-ras$^{+/V12}$;RERTn$^{+/ERT}$;*Cbx1*$^{+/-}$ lungs as the fifth tumour was only seen in one of the sections prepared, and there were no sections left for further staining. Likewise, the staining of the only adenocarcinoma in control group lungs was also not possible due to same problem. All stainings shown in figures 22 - 27 were performed on adjacent sections of the same tumours for each mouse.

As shown in figure 22, none of the tumours were positively stained for p16, which shows that the cells were unlikely to be senescent. DcR2 staining, another cellular marker of *in vitro* oncogene-induced senescence confirmed the result with p16 (Figure 23). The tumours from K-ras$^{+/V12}$;RERTn$^{+/ERT}$;*Cbx1*$^{+/-}$ lungs were also negative for DcR2 staining.

Having shown that the tumours found in K-ras$^{+/V12}$;RERTn$^{+/ERT}$;*Cbx1*$^{+/-}$ lungs were negative for senescent markers, pKi-67 staining was performed next on the lung adenocarcinomas in order to assess the proliferation rate (Figure 24). As shown in figure 24, there was a strong positive staining for pKi-67 in all four lung sections with malignant tumours, which is indicative of strong cellular proliferation. Lung sections from WT mice were negative for pKi-67 staining.

In order to investigate the expression levels and cellular distribution of HP1 isoforms, IHC staining with HP1α, HP1β and HP1γ antibodies was performed in parallel (Figures 25-27). All three isoforms gave strong nuclear staining patterns, typical for HP1 proteins. There were no obvious differences in the staining patterns observed between K-ras$^{+/V12}$;RERTn$^{+/ERT}$ and K-ras$^{+/V12}$;RERTn$^{+/ERT}$;*Cbx1*$^{+/-}$ mice apart from HP1γ staining which was stronger in K-ras$^{+/V12}$;RERTn$^{+/ERT}$;*Cbx1*$^{+/-}$ tumour sections.

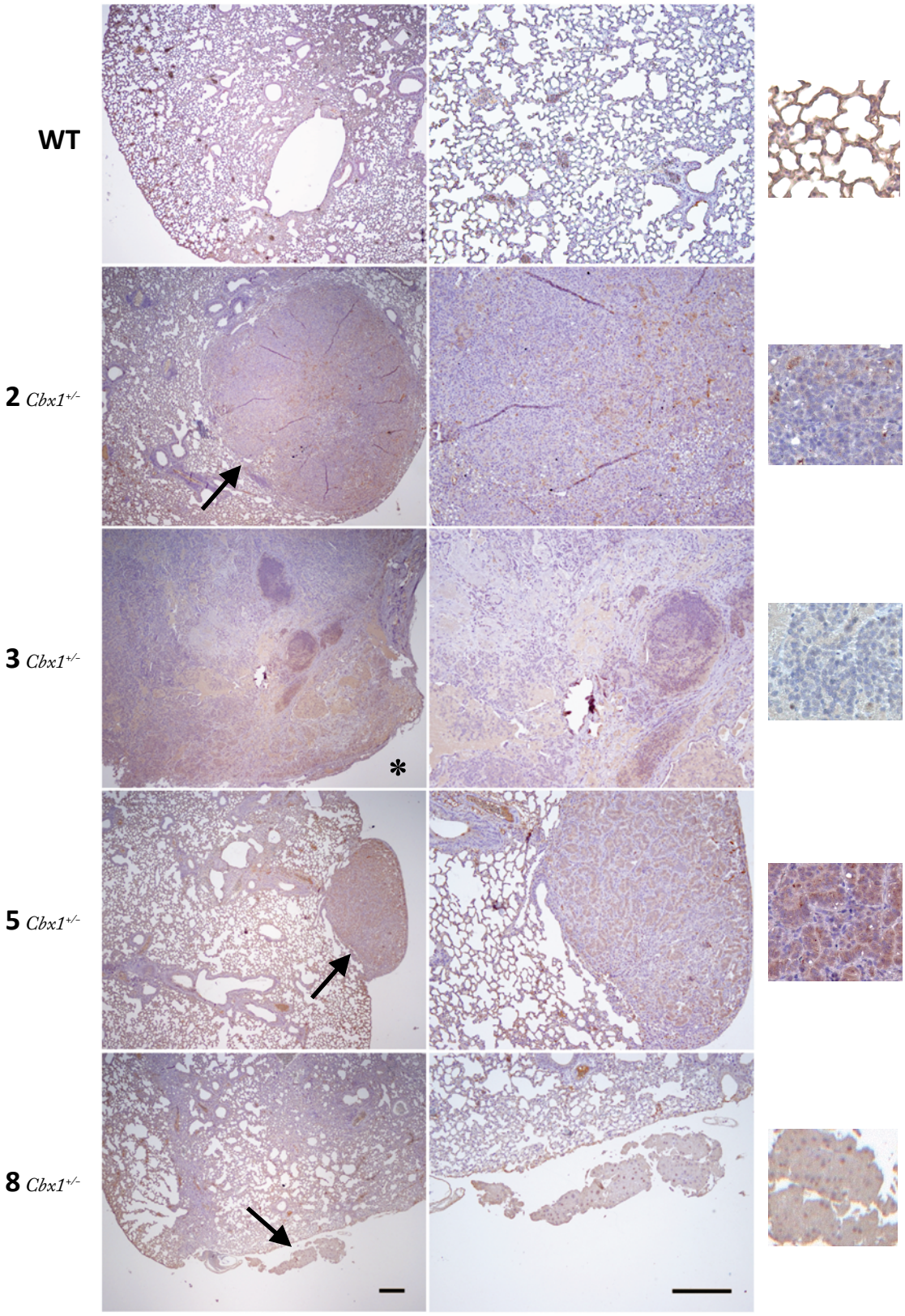

Figure 22 Immunohistochemical staining of a WT tissue and lung tumours found in K-ras$^{+/V12}$;RERTn$^{+/ERT}$;*Cbx1*$^{+/-}$ lungs with the p16 antibody. Numbers on the left side are the numbers of mice as given in table 2. Black arrows indicate regions with adenocarcinomas. In the right columns, same tumour regions with a higher magnification are shown. * indicates adenocarcinomas existed in all over the section. Blue colour: Haematoxylin, Brown colour: PO staining. Scale bars: 250 µm

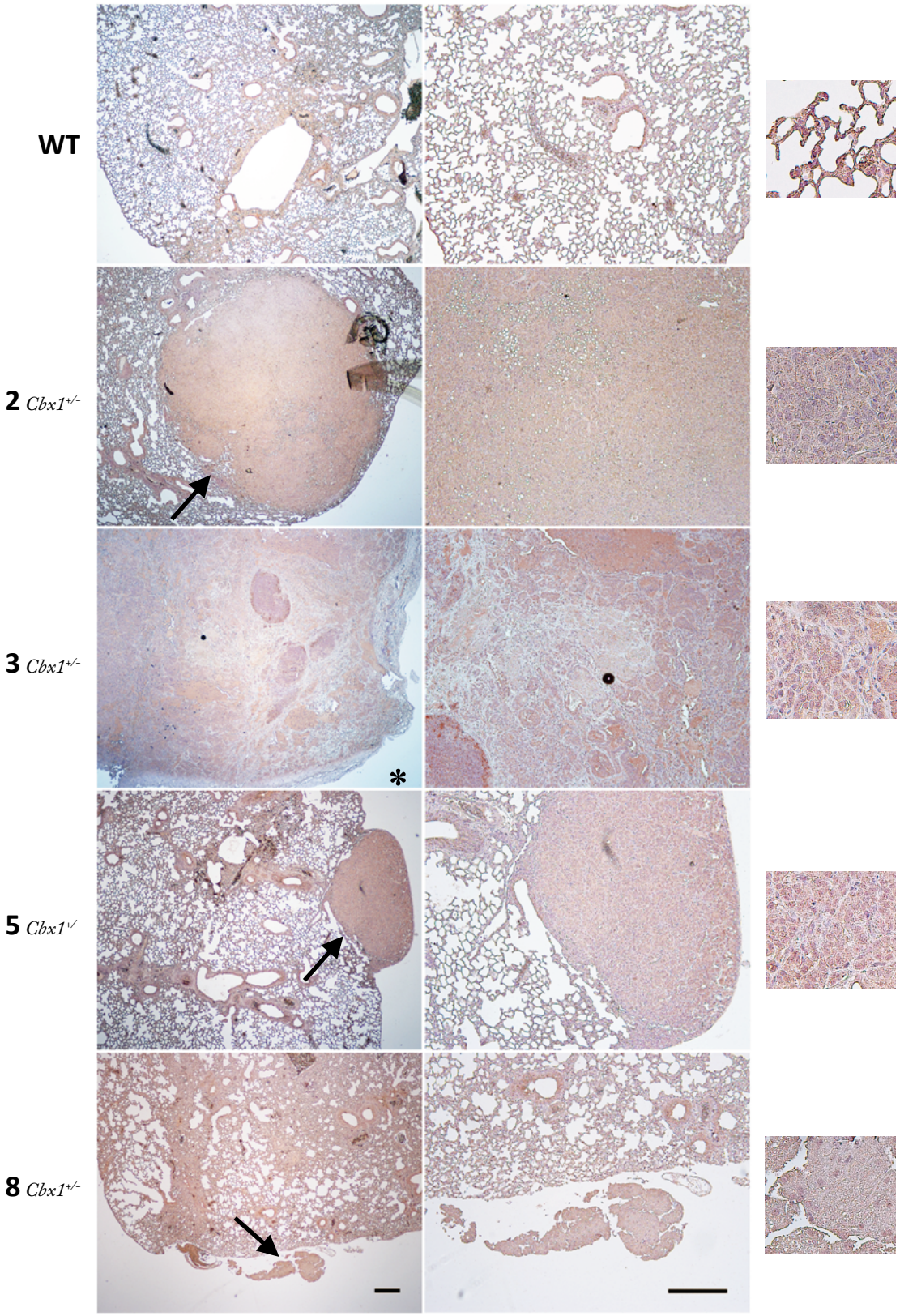

Figure 23 Immunohistochemical staining of a WT tissue and lung tumours found in K-ras$^{+/V12}$;RERTn$^{+/ERT}$;*Cbx1*$^{+/-}$ lungs with DcR2 antibody. Numbers on the left side are the numbers of mice as given in table 2. Black arrows indicate regions with adenocarcinomas. In the right columns, same tumour regions with a higher magnification are shown. * indicates adenocarcinomas existed in all over the section. Blue colour: Haematoxylin, Brown colour: PO staining. Scale bars: 250 µm

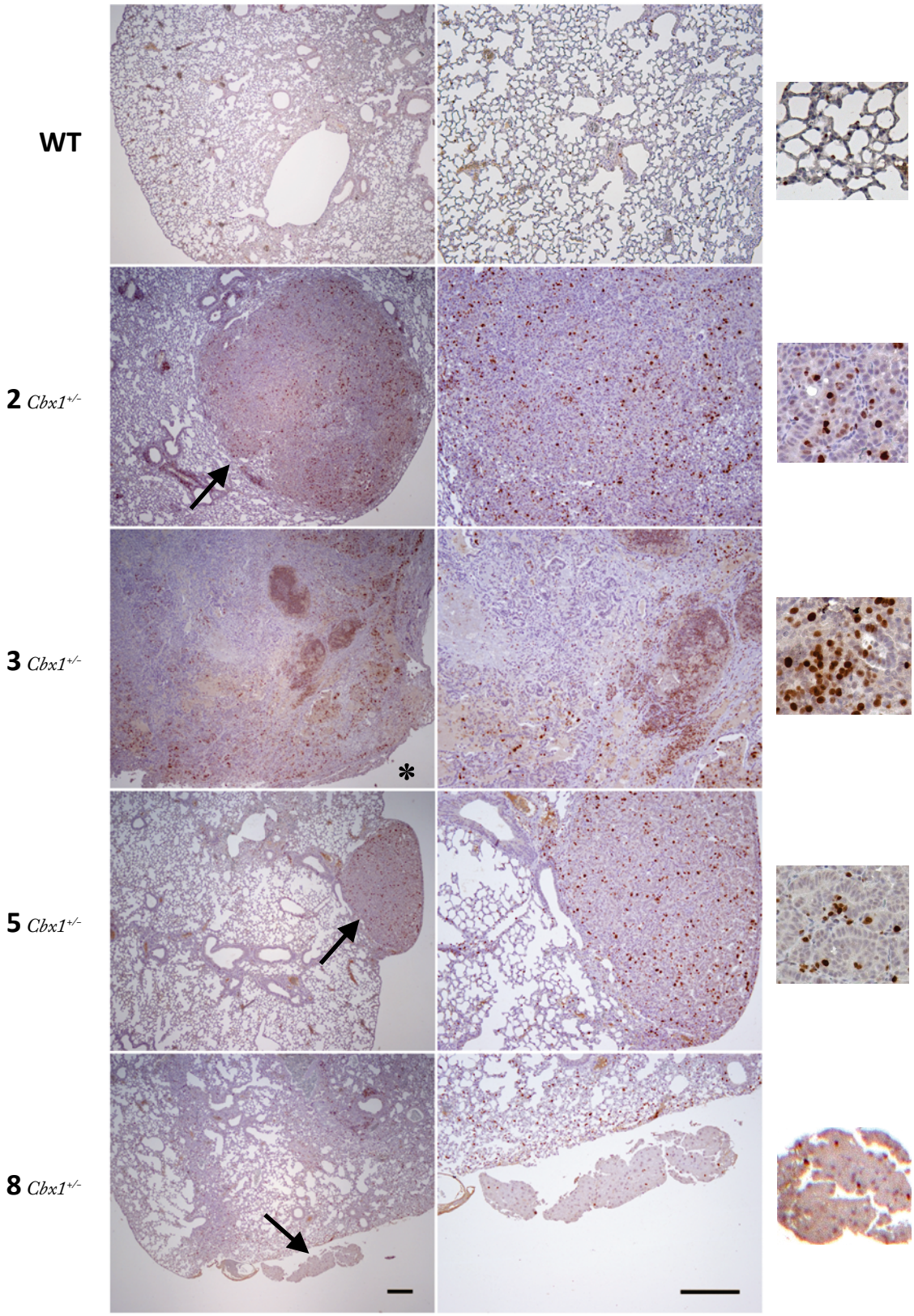

Figure 24 IHC staining of a WT lung tissue and lung tumours found in K-ras$^{+/V12}$;RERTn$^{+/ERT}$;*Cbx1*$^{+/-}$ lungs with pKi-67 antibody. Numbers on the left side are the numbers of mice as given in table 2. Black arrows indicate regions with adenocarcinomas. In the right columns, same tumour regions with a higher magnification are shown. * indicates adenocarcinomas existed in all over the section. Blue colour: Haematoxylin, Brown colour: PO staining. Scale bars: 250 µm

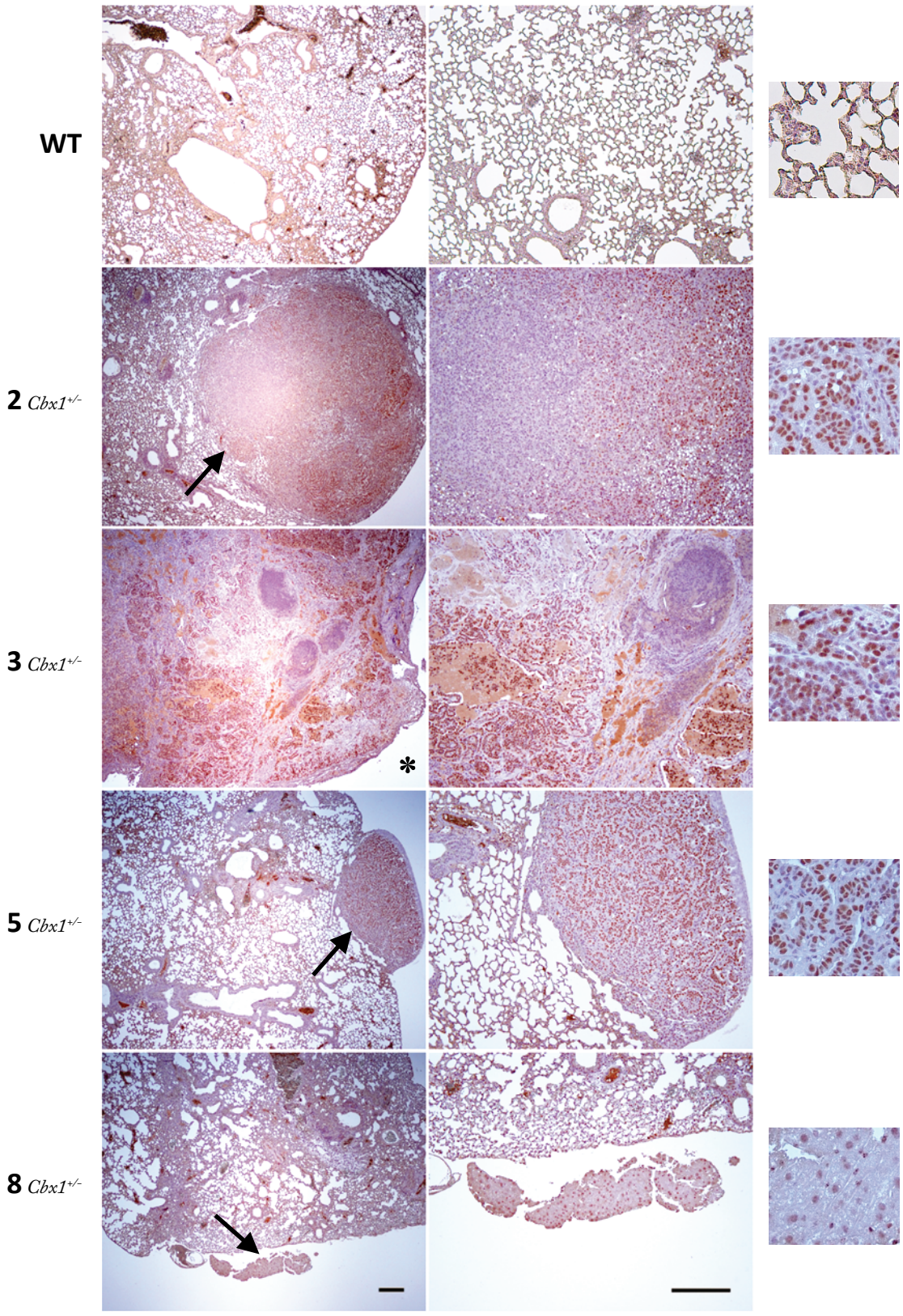

Figure 25 Immunohistochemical staining of a WT tissue and lung tumours found in K-ras$^{+/V12}$;RERTn$^{+/ERT}$;*Cbx1*$^{+/-}$ lungs with HP1α antibody. Numbers on the left side are the numbers of mice as given in table 2. Black arrows indicate regions with adenocarcinomas. In the right columns, same tumour regions with a higher magnification are shown. * indicates adenocarcinomas existed in all over the section. Blue colour: Haematoxylin, Brown colour: PO staining. Scale bars: 250 µm

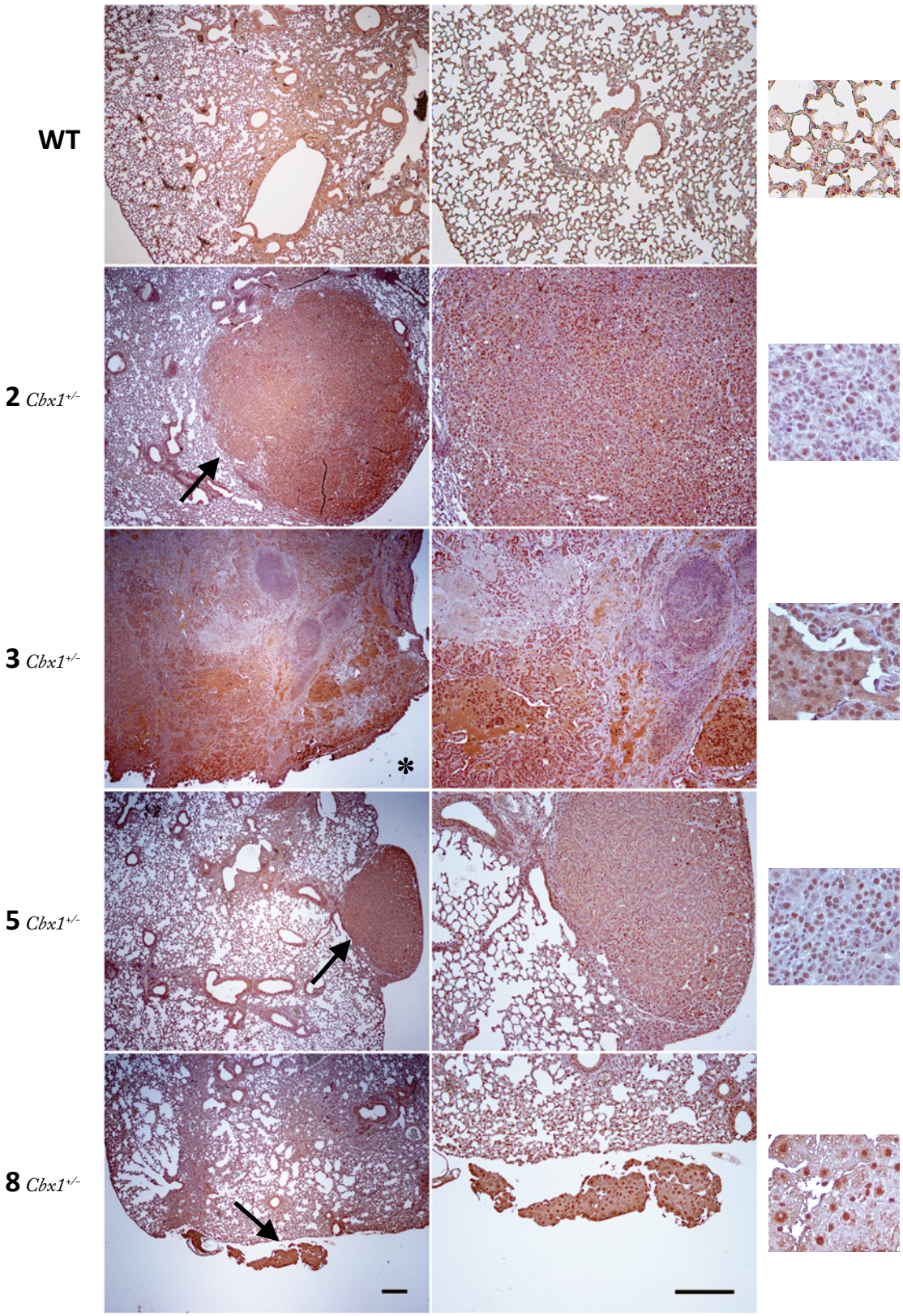

Figure 26 Immunohistochemical staining of a WT tissue and lung tumours found in K-ras$^{+/V12}$;RERTn$^{+/ERT}$;*Cbx1*$^{+/-}$ lungs with HP1β antibody. Numbers on the left side are the numbers of mice as given in table 2. Black arrows indicate regions with adenocarcinomas. In the right columns, same tumour regions with a higher magnification are shown. * indicates adenocarcinomas existed in all over the section. Blue colour: Haematoxylin, Brown colour: PO staining. Scale bars: 250 µm

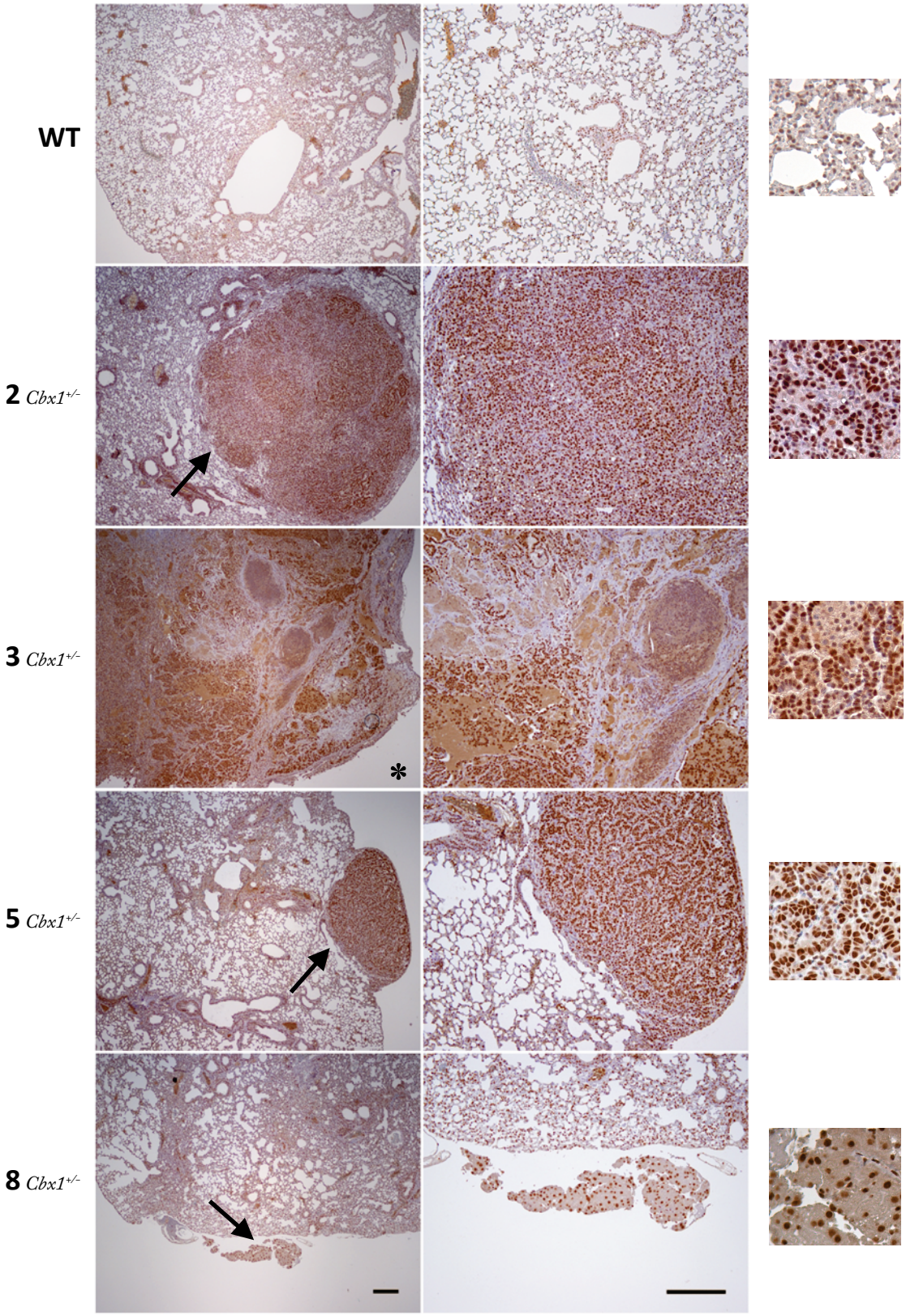

Figure 27 Immunohistochemical staining of a WT tissue and lung tumours found in K-ras$^{+/V12}$;RERTn$^{+/ERT}$;*Cbx1*$^{+/-}$ lungs with HP1γ antibody. Numbers on the left side are the numbers of mice as given in table 2. Black arrows indicate regions with adenocarcinomas. In the right columns, same tumour regions with a higher magnification are shown. * indicates adenocarcinomas existed in all over the section. Blue colour: Haematoxylin, Brown colour: PO staining. Scale bars: 250 µm

3.5 Investigation of the effect of *Cbx1* mutation on oncogene-induced senescence *in vitro*

Guided by the observation (detailed in last section) that a reduction in *Cbx1* gene dosage likely resulted in escape from senescence and increased proliferation followed by the formation of malignant adenocarcinomas in the K-ras mouse model, it has been tested whether this effect was also reproducible *in vitro* using the well established H-ras^{V12} oncogene model (Serrano *et al.*, 1997). Previously, it has been shown that cells transduced with an H-ras^{V12} expression plasmid undergo cellular senescence as evidenced by a cessation of proliferation and positivity for SA-β-gal staining. In collaboration with Dr. M. Balabanov (UKE, Hamburg), retroviral transduction experiments on WT, *Cbx1*$^{+/-}$ and *Cbx1*$^{-/-}$ MEFs were performed using an empty control vector pBabe-puro and pBabe-Ras-puro expressing an H-ras^{V12} cDNA. Upon selection with puromycin (2.5 µg/ml) for 3 days, cells were plated at low density and allowed to proliferate for 8 days while counting them on days 2, 4, 6 and 8 respectively for growth curve analysis. As seen in figure 28, WT MEFs transduced with an empty control vector (red circles with a continuous line) continued to proliferate until day 8, same cells transduced with the ras expression vector (red circles with a dotted line) showed a proliferation arrest, as previously shown (Serrano *et al.*, 1997). When *Cbx1*$^{-/-}$ MEFs were transduced with the H-ras^{V12} expression vector (blue triangles with a dotted line), there was also a growth arrest compared to *Cbx1*$^{-/-}$ MEFs transduced with empty vector (blue triangles with a continuous line), indicating that the *Cbx1*$^{-/-}$ MEFs behave similar to the WT MEFs when challenged by oncogenic virus.

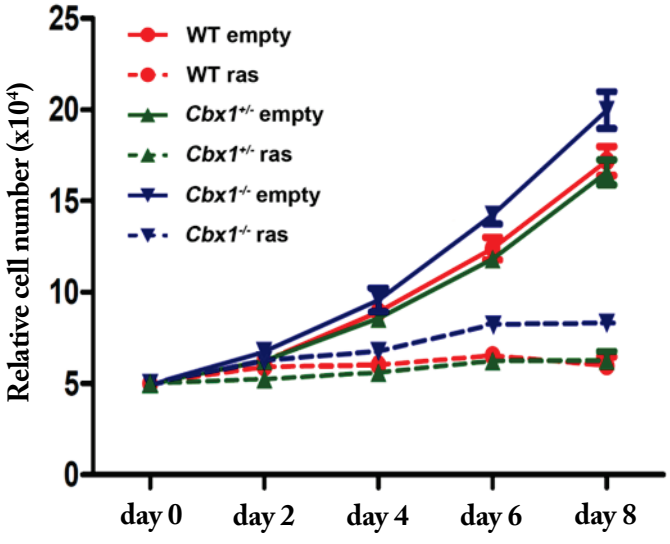

Figure 28 Growth curve analysis of the cells transduced with an empty control vector or a ras expression vector. Graph shows the averages of 3 independent experiments. Experiments were done in collaboration with Dr. M. Balabanov (UKE, Hamburg).

Next, in order to investigate whether the cells with proliferation arrest were also positive for senescent, SA-β-gal staining was performed on MEFs 7 days after transduction. 100 cells from each genotype were counted and the averages of three independent experiments were taken. As shown in figure 29, cells transduced with the empty control vector were not senescent, while cells transduced with oncogenic ras expressing pBabe-ras-puro were stained positive for SA-β-gal. WT, *Cbx1*$^{+/-}$ and *Cbx1*$^{-/-}$ MEFs were stained positively 91 %, 94 % and 80 %, respectively. The percentages of positively stained cells correlated well with the growth curve analysis of the individual genotypes shown in figure 18.

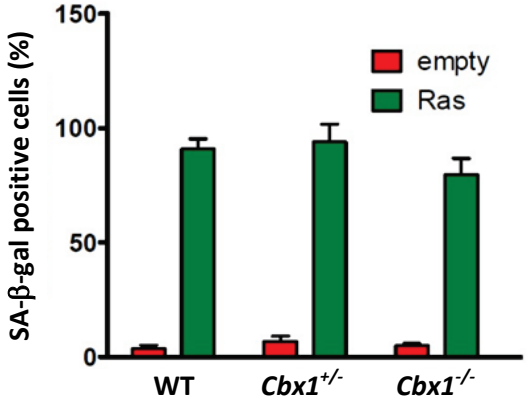

Figure 29 WT, *Cbx1*$^{+/-}$ *and Cbx1*$^{-/-}$ MEFs were transduced either with an empty vector or a ras expression vector. 7 days after transduction, cells were then exposed to SA-β-gal staining and positively stained cells for each genotype were counted. 100 cells for each genotype were analyzed and averages of three independent experiments are shown. Experiments were done in collaboration with Dr. M. Balabanov (UKE, Hamburg).

3.6 Investigation of the binding of HP1β to Histone H3

The binding of HP1β to trimethylated lysine 9 of histone H3 and SUV39H1 histone methyltransferase is thought to be the key interaction of HP1β (Lachner *et al.*, 2001 and Bannister *et al.*, 2001). However, in the light of rapidly increasing evidence, originally stemming from biophysical studies, a more complex picture has emerged which cannot easily be explained by a simple binary H3K9me3-HP1β interaction (Festenstein *et al.*, 2003; Cheutin *et al.*, 2003; Schmiedeberg *et al.*, 2004 and Dialynas *et al.*, 2007; see introduction). Notably, the striking fact that *Suv39h1/h2* knock out animals live whereas *Cbx1* knock out animals die, suggests that the essential function of HP1β must lie outside the Suv39h1/h2 dependent heterochromatic H3K9me3-HP1β interaction. One key candidate for this interaction is HP1β binding to the histone H3 histone-fold, which has been studied in some detail (Nielsen *et al.*, 2001 and Dialynas *et al.*, 2006). A few HP1β residues have been tested for their affinities to H3K9me3 peptide and histone H3.

However, it remains to be identified whether there are specific residues that may play a role in the interaction of HP1β with histone H3.

In order to investigate the interaction of HP1β with histone H3 *in vitro*, GST pull down experiments with recombinant, unmethylated histone H3 were undertaken. Recombinant WT mouse HP1β was expressed as a GST fusion protein along with several mutant forms harbouring mutations in the chromo and chromoshadow domains (Figure 30). The type of mutation was decided upon from a review of the literature and aimed at addressing the interaction of HP1β with recombinant, unmethylated histone H3. The rationale for the experiments was to incubate WT and mutant GST-HP1β proteins with histone H3 in increasing NaCl concentrations so that the affinity of the interaction could be gauged.

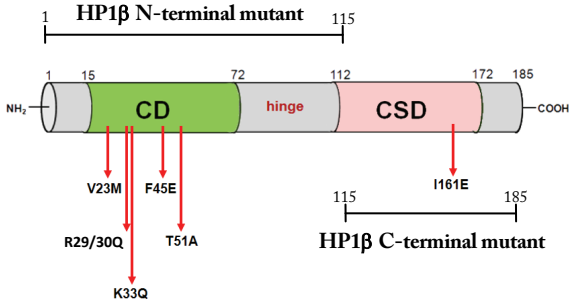

Figure 30 An overview of mutations and recombinant HP1β proteins used in pull down experiments is shown. Single letter codes of the substituted amino acids are shown and their position in the mouse HP1β sequence was drawn to scale. CD and CSD depict to chromo domain and chromoshadow domain, respectively.

The results obtained in GST pull down experiments are shown in figure 31 and table 6. All full length recombinant HP1β mutant proteins (Figure 31, left and right section) tested were able to pull down recombinant histone H3 at all NaCl concentrations except for the I161E mutant which lost its binding to histone H3 at 0.6 M and 0.75 M NaCl. In case of N-terminal HP1β mutants lacking amino acids 115-185 (Figure 31, middle section), the WT N-terminal HP1β and N-terminal T51A, V23M and K33Q mutants all lost binding to histone H3 at 0.6 M and 0.75 M NaCl. This binding was surprisingly rescued at 0.6 M in F45E mutant and at both 0.6/0.75 M in R29/30Q mutant. C-terminal HP1β lacking amino acids 1-115 was also able to pull down histone H3 in all three NaCl concentrations tested.

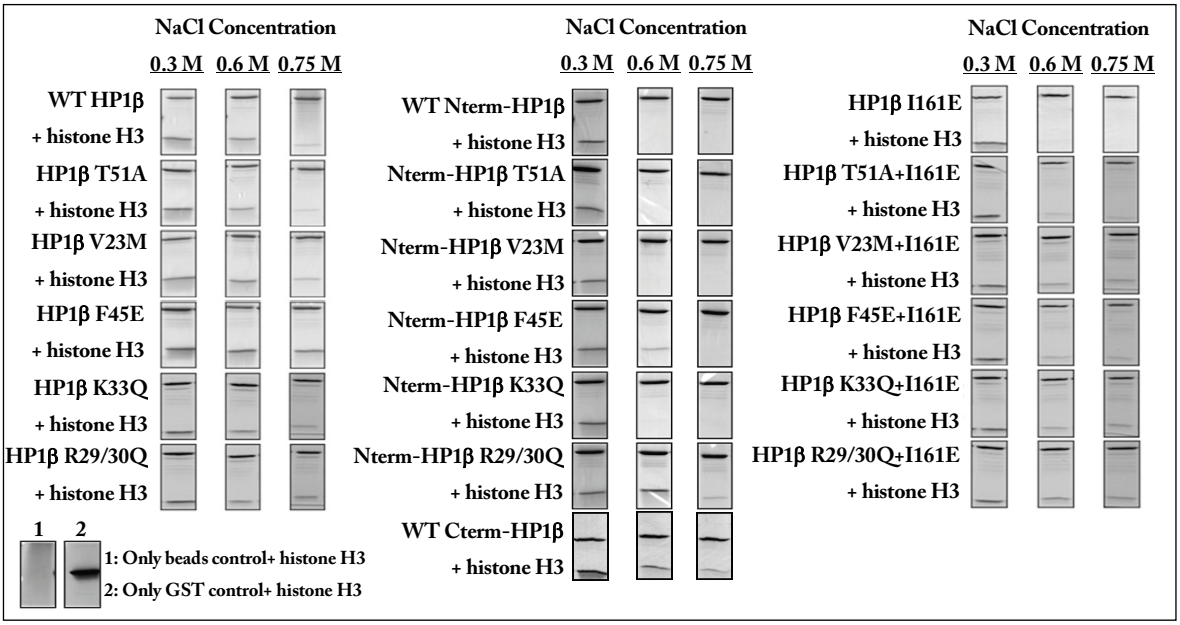

Figure 31 Coomassie stained SDS gels, showing the results of GST pull down experiments done with several HP1β mutants and histone H3. The higher band seen in each gel is HP1β and the lower band is histone H3. Experiments using the same proteins were repeated in increasing NaCl concentration (three rows in each section). In the left section, pull down experiments are shown in which full length recombinant HP1β mutants were used. In the middle section, proteins used were either N-terminal HP1β mutants expressing amino acids 1-115, or C-terminal HP1β expressing amino acids 115-185. In the right section, full length recombinant HP1β mutants with an additional I161E mutation are shown. In each experiment histone H3 was also incubated with glutathione sepharose beads only and GST protein without fusion partner (left, bottom corner) as controls.

Proteins	Histone H3 binding			Proteins	Histone H3 binding		
	0.3 M	0.6 M	0.75 M		0.3 M	0.6 M	0.75 M
HP1α	✓	✓	✓	HP1β F45E	✓	✓	✓
HP1β	✓	✓	✓	HP1β N-terminal F45E	✓	✓	×
HP1γ	✓	✓	✓	HP1β T51A	✓	✓	✓
HP1β C-terminal (115-185)	✓	✓	✓	HP1β N-terminal T51A	✓	×	×
HP1β N-terminal (1-115)	✓	×	×	HP1β I161E	✓	×	×
HP1β V23M	✓	✓	✓	HP1β I161E+V23M	✓	✓	✓
HP1β N-terminal V23M	✓	×	×	HP1β I161E+K33Q	✓	✓	✓
HP1β K33Q	✓	✓	✓	HP1β I161E+F45E	✓	✓	✓
HP1β N-terminal K33Q	✓	×	×	HP1β I161E+T51A	✓	✓	✓
HP1β R29/30Q	✓	✓	✓	HP1β I161E+R29/30Q	✓	✓	✓
HP1β N-terminal R29/30Q	✓	✓	✓				

Table 6 An overview of the results of the GST pull down experiments performed. Several HP1β mutants were tested for their binding affinities to histone H3 at increasing NaCl concentrations. An observed binding was depicted as a tick, whereas a lost in binding was depicted as an X.

3.7 Investigation of the binding affinity of HP1β to histone H3 and H3K9me3

Having shown the *in vitro* binding of HP1β and several mutants with histone H3 in high salt concentrations, the strength of this interaction was then measured quantitatively. Isothermal titration calorimetry was the method of choice as it is the only method that can measure biomolecular interactions through the simultaneous determination of all binding parameters (n, K_D, ΔH and ΔS) in a single experiment. To compare the affinities and to determine which mutants retain the ability to bind to histone H3 but not to H3K9me3 (or vice versa), binding of HP1β to H3K9me3 tail peptide was also included in this analysis. Full length recombinant mouse HP1β and V23M, F45E, T51A and I161E mutant proteins, were expressed in bacteria as His-tag fusion proteins and affinity purified using Ni-NTA beads. HP1β proteins (and mutants thereof) were put in the sample cell and either recombinant *X. laevis* histone H3 or H3K9me3 tail peptide were then injected into the sample cell using the automated syringe (see Figure 9 in Materials & Methods). These experiments were performed both at 25 °C and 37 °C.

While binding of HP1β to H3K9me3 was always an exothermic (negative ΔH value, peaks of the reaction downwards) reaction, binding to histone H3 was endothermic (positive ΔH value, peaks of the reaction upwards). The binding affinities of all reactions (Table 7) were calculated by the software of the instrument in terms of a K_a value (association constant), and this was converted manually into a K_D value (dissociation constant, μM) where the affinity of the reaction (K_a) and the K_D value were inversely proportional (*e.g.* higher the K_D value, lower the affinity). All calculations were based on the Gibbs free energy equation: $\Delta G = -RT \ln K_a = \Delta H - T\Delta S$ (ΔG is the free energy of binding, R is the gas constant, T is the absolute temperature, K_a is the association constant, ΔH is the enthalpy and ΔS is the entropy).

As shown in table 7, figures 32 and 33, it was found that the binding affinity of wild type HP1β to histone H3 was approximately 4 times higher than for the trimethylated lysine 9 tail peptide (H3K9me3) at both 25 °C and 37 °C. In the HP1β T51A mutant, the binding to histone H3 was slightly stronger than for the H3K9me3 peptide (Table 7, Figures 34 and 35). On the other hand, HP1β V23M mutant had a very low affinity for H3K9me3, in line with

published data, while still having a high affinity for histone H3 (Table 7, Figures 36 and 37). In case of HP1β F45E mutant, data obtained at 25 ˚C with Histone H3 was not accurate as confirmed by an unstable baseline (Figure 39). However, a direct comparison could be made at 37 ˚C, which gave reproducible results; at 37 ˚C HP1β F45E mutant has lost its affinity for the H3K9me3 peptide but retained its high affinity for the recombinant histone H3 (Figures 38 and 39). The binding affinity of HP1β I161E mutant for histone H3 was almost two times higher than its affinity for H3K9me3 peptide, both at 25 ˚C and 37 ˚C (Table 7, Figures 40 and 41). On the other hand, compared to WT protein, this mutant showed a higher (ca. 2 times higher) affinity for the trimethylated lysine 9 peptide at both tested temperatures.

		Histone H3				H3K9me3			
		K_D	N	ΔH	ΔS	K_D	N	ΔH	ΔS
25 °C	HP1β	**7.6**	0.679	2838	32.9	**30**	1.32	-9152	-9.99
	HP1β T51A	**24.5**	0.758	7471	46.2	**31.9**	1.22	-9859	-12.5
	HP1β V23M	**7.5**	0.834	10500	58.7	**189**	0.0324	-97550	-310
	HP1β F45E	**77.5***	0.678*	3943*	32*	**179.5**	0.0358	-234600	-769
	HP1β I161E	**7.7**	1.72	911.7	26.5	**14.3**	1.21	-8634	-6.8
37 °C	HP1β	**16.4**	0.564	14510	68.7	**59.5**	0.69	-23100	-55.3
	HP1β T51A	**n.d.**	n.d.	n.d.	n.d.	**63.3**	1	-18760	-41.3
	HP1β V23M	**n.d.**	n.d.	n.d.	n.d.	**182.5**	0.00387	-1568000	-5040
	HP1β F45E	**15**	0.451	16030	73.7	**344.9**	0.173	-66110	-197
	HP1β I161E	**19**	1.05	10680	56	**35**	1.31	-10480	-13.4

Table 7 An overview of thermodynamic parameters obtained from the ITC experiments performed. *: data not accurate due to unstable baseline, n.d.: experiment not done. K_D: dissociation constant (μM), N: number of binding sites, ΔH: the heat of binding (enthalpy change, cal/mol), ΔS: entropy change (cal/mol/deg)

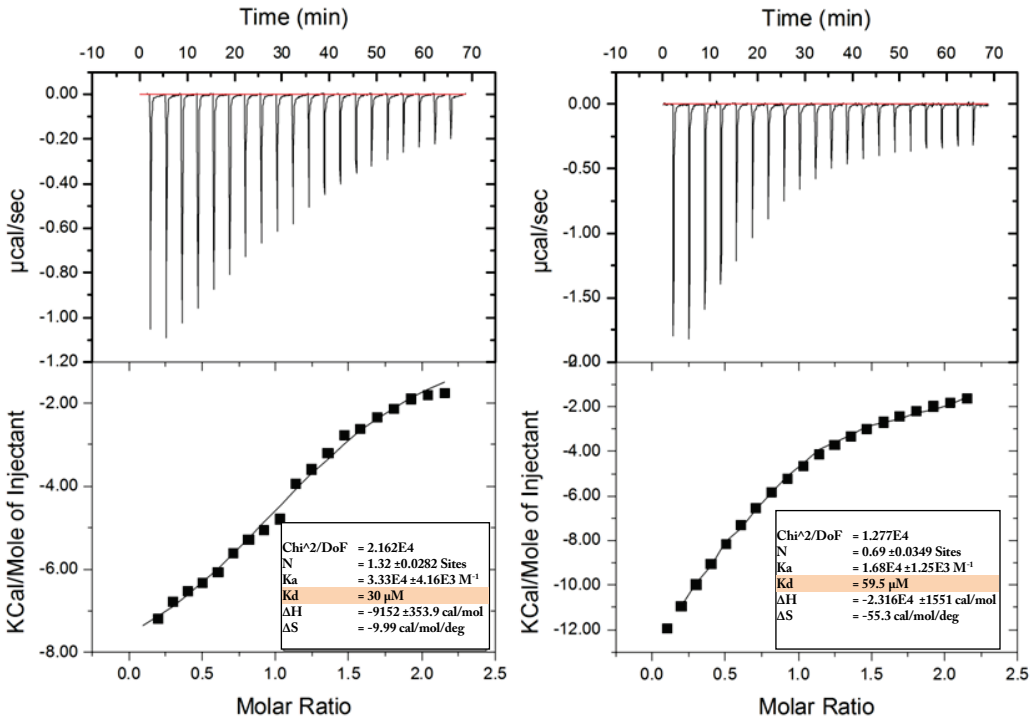

Figure 32 Binding of wild type HP1β to H3K9me3 tail peptide as measured by isothermal titration calorimetry at 25°C (figure on the left) and 37°C (figure on the right). Raw data (upper parts of both figures) and integrated heats of injections (lower parts of both figures), with the solid line corresponding to the best fit of the data using "one set of sites" parameter of instruments software are shown.

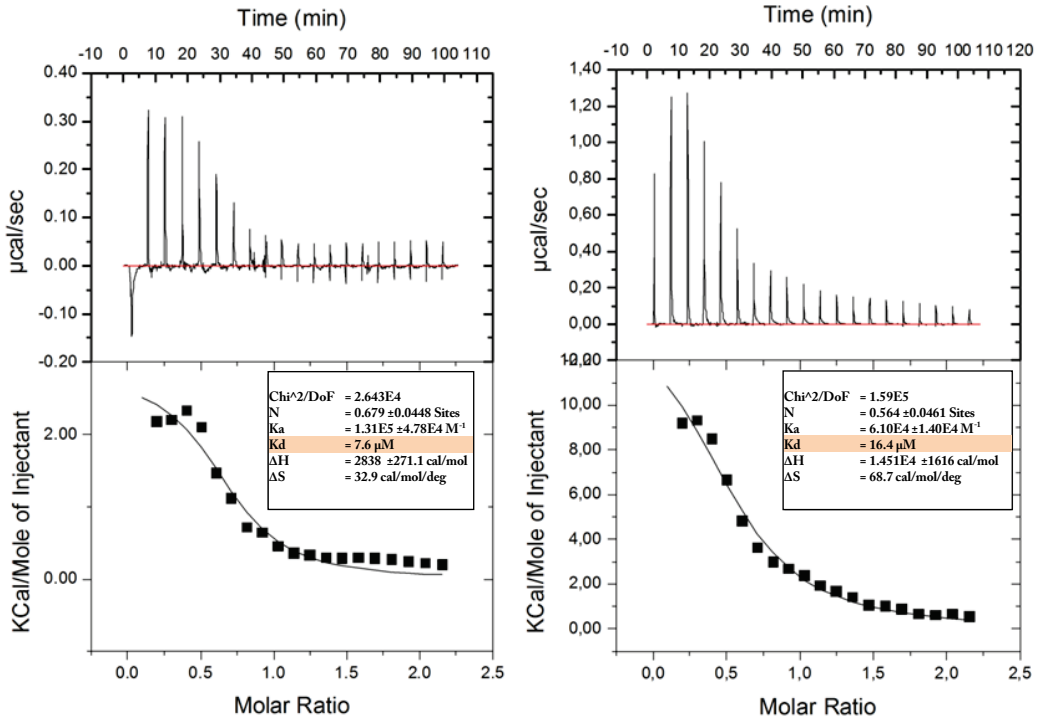

Figure 33 Binding of wild type HP1β to histone H3 as measured by isothermal titration calorimetry at 25°C (figure on the left) and 37°C (figure on the right). Raw data (upper parts of both figures) and integrated heats of injections (lower parts of both figures), with the solid line corresponding to the best fit of the data using "one set of sites" parameter of instruments software are shown.

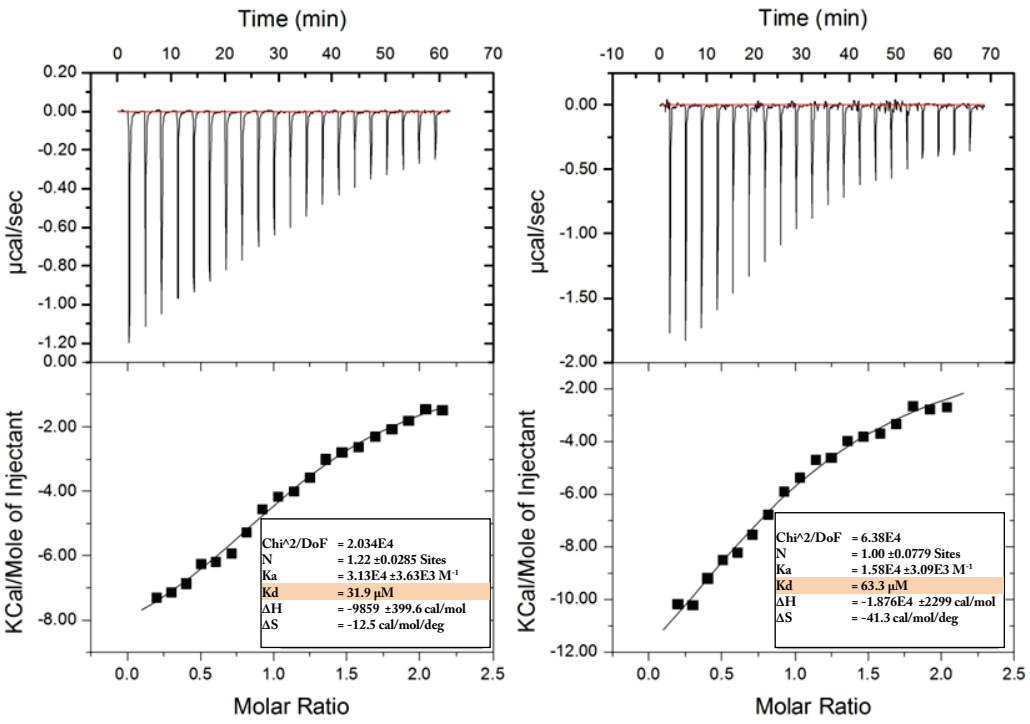

Figure 34 Binding of HP1β T51A mutant to H3K9me3 tail peptide as measured by isothermal titration calorimetry at 25°C (figure on the left) and 37°C (figure on the right). Raw data (upper parts of both figures) and integrated heats of injections (lower parts of both figures), with the solid line corresponding to the best fit of the data using "one set of sites" parameter of instruments software are shown.

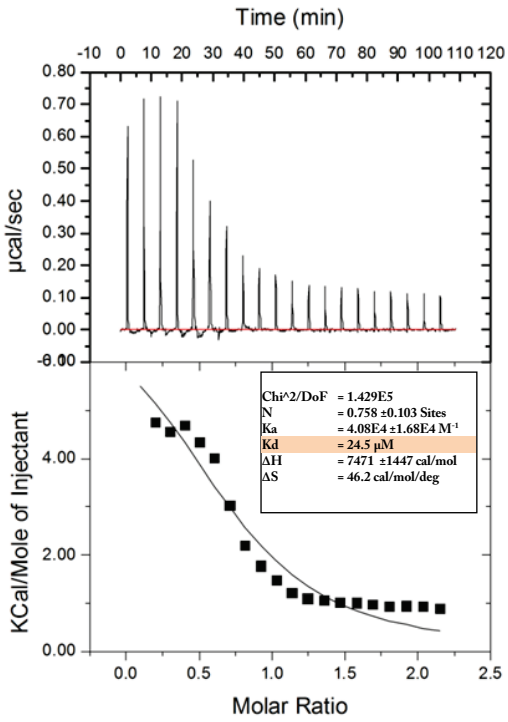

Figure 35 Binding of HP1β T51A mutant to histone H3 as measured by isothermal titration calorimetry at 25°C (figure on the left). Raw data (upper part of figure) and integrated heats of injections (lower part of figure), with the solid line corresponding to the best fit of the data using "one set of sites" parameter of instruments software are shown.

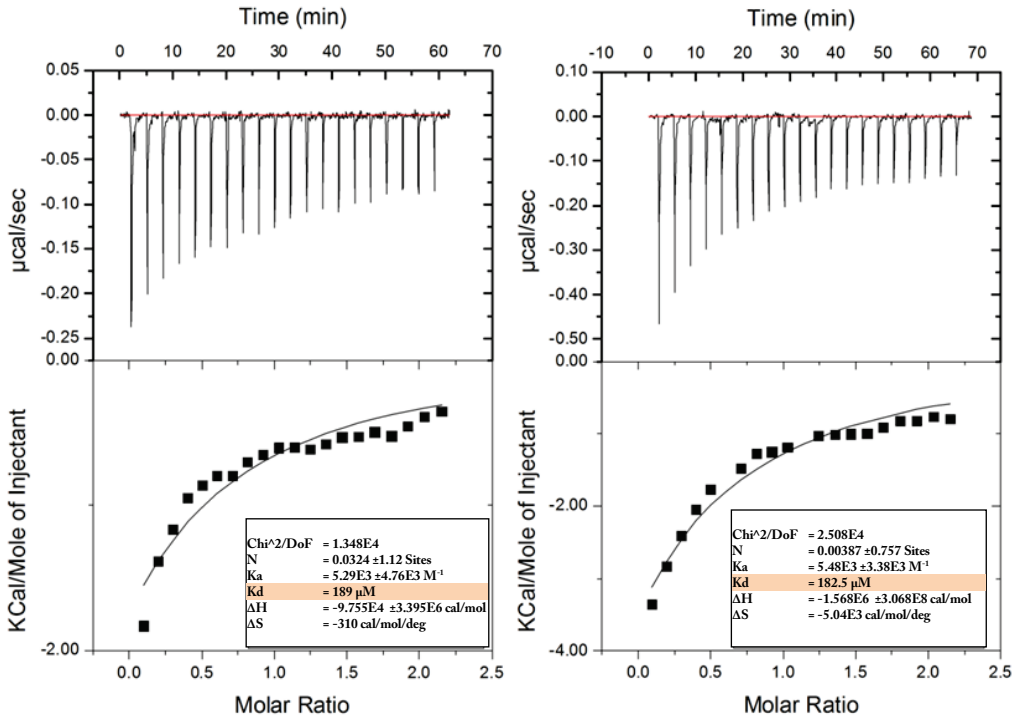

Figure 36 Binding of HP1β V23M mutant to H3K9me3 tail peptide as measured by isothermal titration calorimetry at 25°C (figure on the left) and 37°C (figure on the right). Raw data (upper parts of both figures) and integrated heats of injections (lower parts of both figures), with the solid line corresponding to the best fit of the data using "one set of sites" parameter of instruments software are shown.

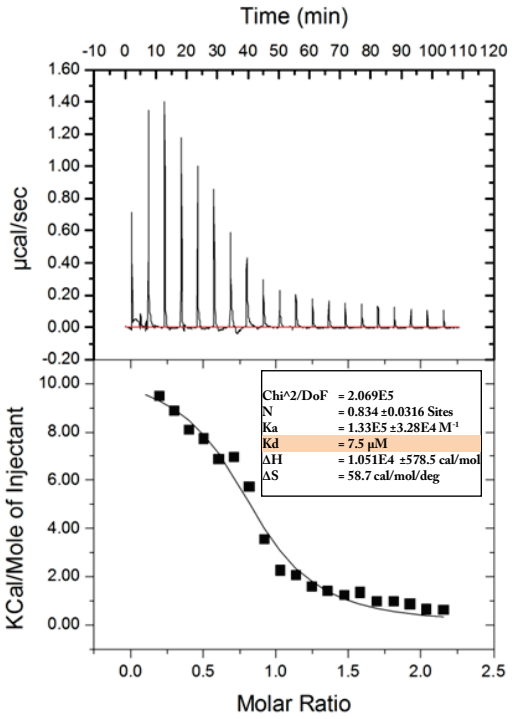

Figure 37 Binding of HP1β T51A mutant to histone H3 as measured by isothermal titration calorimetry at 25°C (figure on the left). Raw data (upper part of figure) and integrated heats of injections (lower part of figure), with the solid line corresponding to the best fit of the data using "one set of sites" parameter of instruments software are shown.

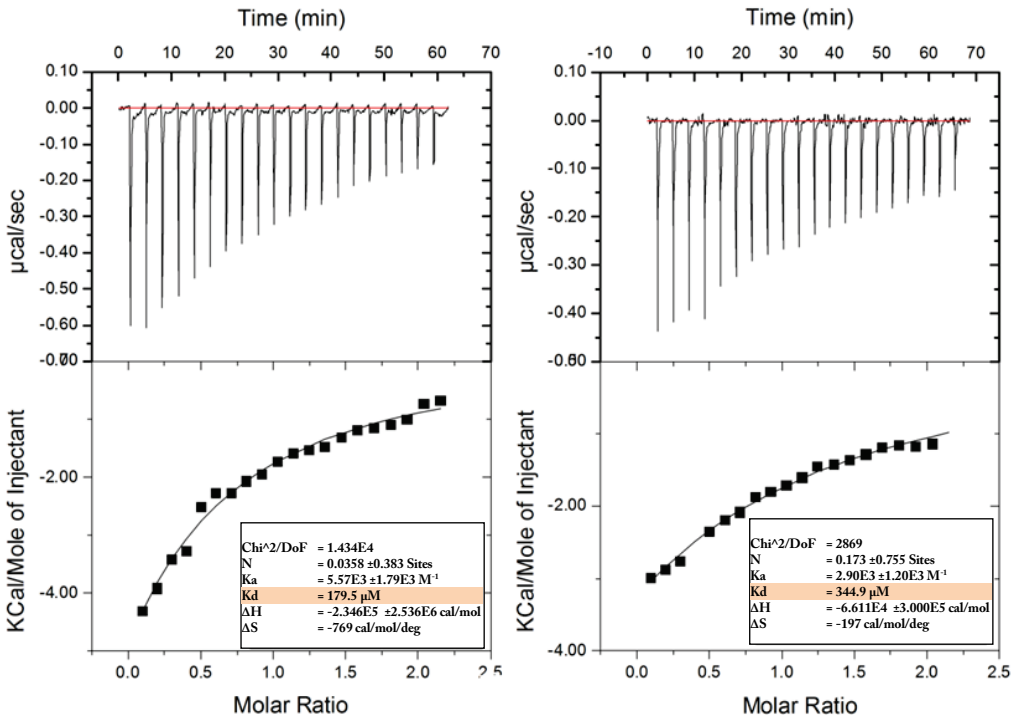

Figure 38 Binding of HP1β F45E mutant to H3K9me3 tail peptide as measured by isothermal titration calorimetry at 25°C (figure on the left) and 37°C (figure on the right). Raw data (upper parts of both figures) and integrated heats of injections (lower parts of both figures), with the solid line corresponding to the best fit of the data using "one set of sites" parameter of instruments software are shown.

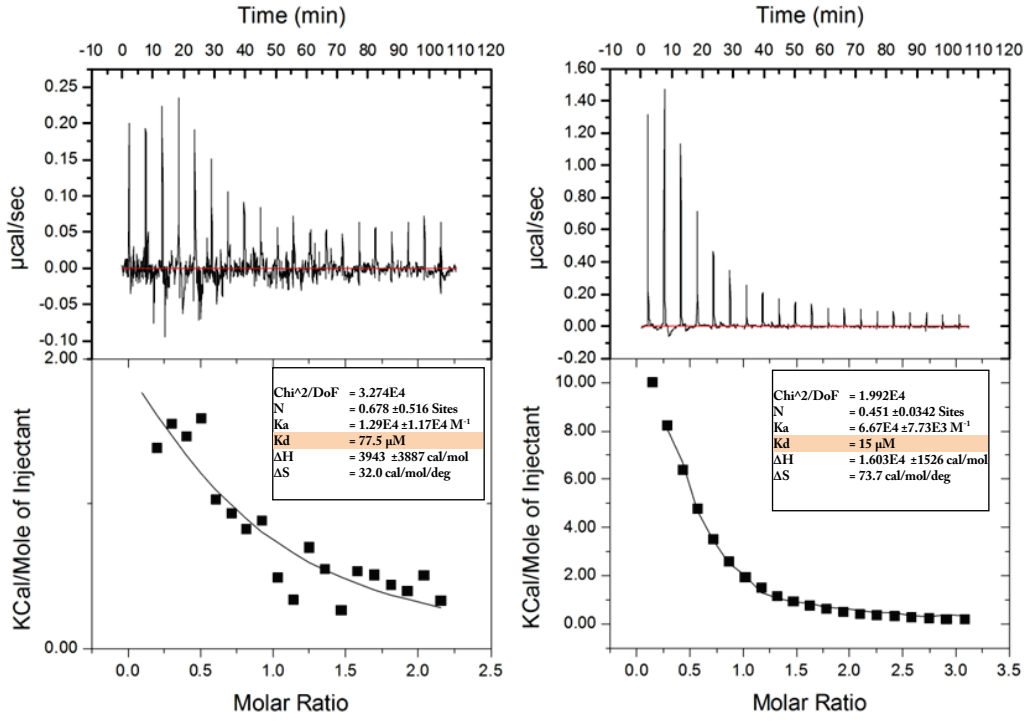

Figure 39 Binding of HP1β F45E mutant to histone H3 as measured by isothermal titration calorimetry at 25°C (figure on the left) and 37°C (figure on the right). Raw data (upper parts of both figures) and integrated heats of injections (lower parts of both figures), with the solid line corresponding to the best fit of the data using "one set of sites" parameter of instruments software are shown.

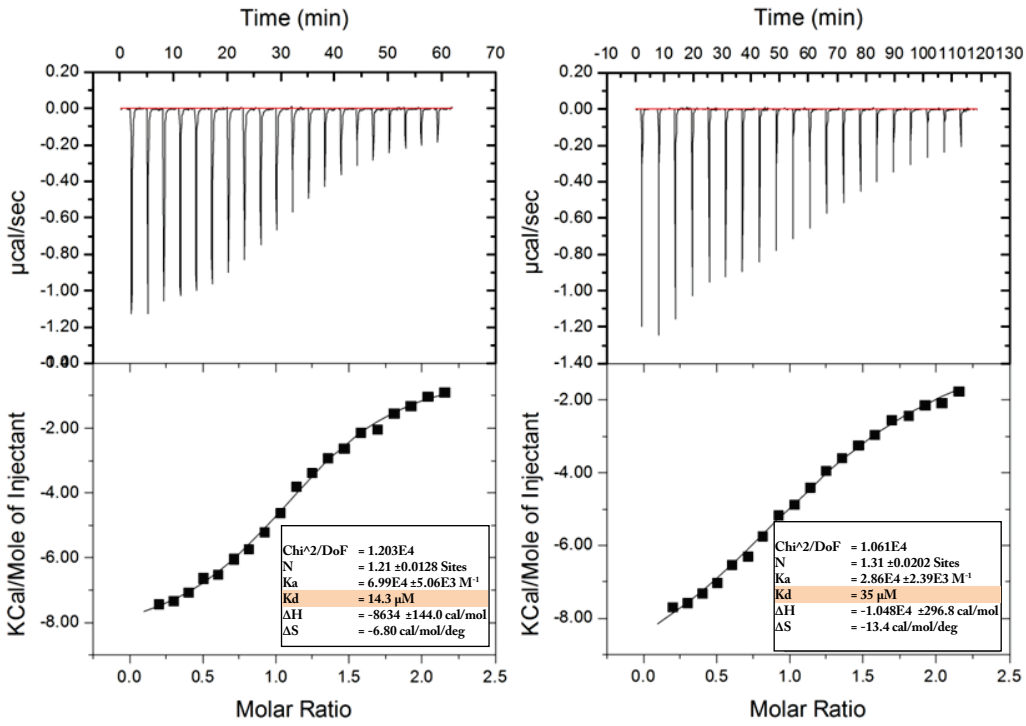

Figure 40 Binding of HP1β I161E mutant to H3K9me3 tail peptide as measured by isothermal titration calorimetry at 25°C (figure on the left) and 37°C (figure on the right). Raw data (upper parts of both figures) and integrated heats of injections (lower parts of both figures), with the solid line corresponding to the best fit of the data using "one set of sites" parameter of instruments software are shown.

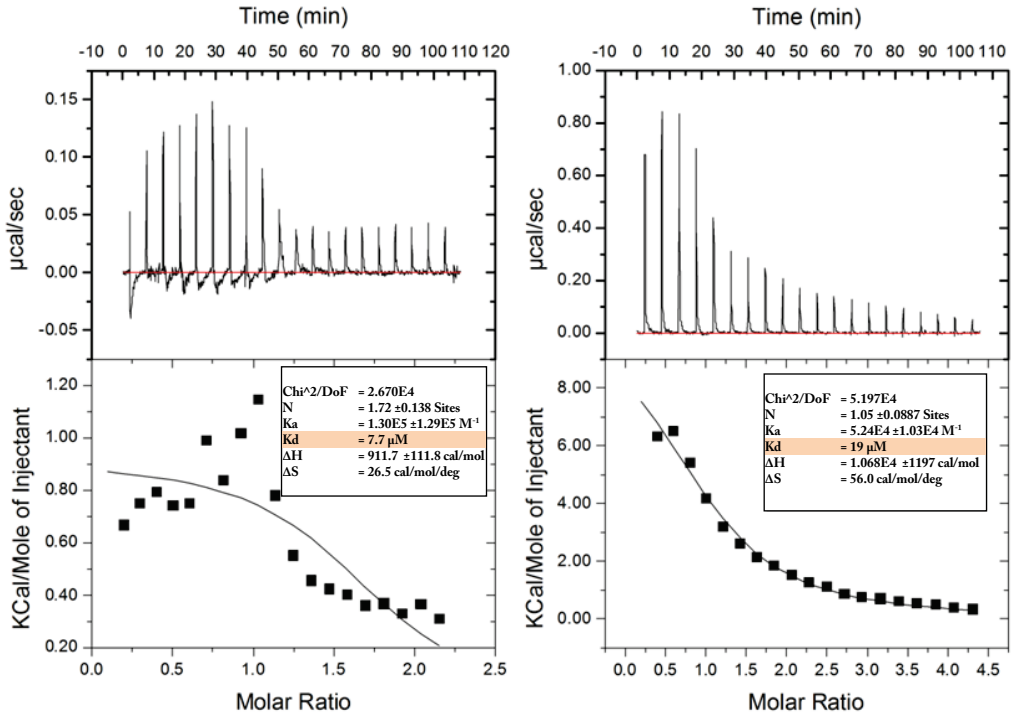

Figure 41 Binding of HP1β I161E mutant to histone H3 as measured by isothermal titration calorimetry at 25°C (figure on the left) and 37°C (figure on the right). Raw data (upper parts of both figures) and integrated heats of injections (lower parts of both figures), with the solid line corresponding to the best fit of the data using "one set of sites" parameter of instruments software are shown.

Chapter 4

Discussion

HP1 proteins are thought to be modulators of chromatin organization in all mammals, yet their exact physiological function remains unknown. In a first attempt to elucidate the function of HP1β in vivo, the murine *Cbx1* gene encoding HP1β was disrupted recently (Aucott *et al.*, 2008). The *Cbx1* null mutation results in perinatal lethality. The proximate cause of death is that the mice cannot breathe due to the defective development of neuromuscular junctions within the endplate of the diaphragm; in the absence of contraction of the diaphragm the lungs do not expand. Study of other neuronal structures revealed that *Cbx1* null mice exhibit aberrant development of the cerebral cortex and cytological examination of neurospheres cultured *in vitro* from *Cbx1* null brains revealed a striking genomic instability. It is toward understanding, in concrete cellular and molecular terms, the role of *Cbx1* gene product, HP1β, in regulating genome stability that is the major focus of this thesis. As explained (see Introduction) genomic instability is found in many cancers and is associated with the uncontrolled proliferation of cells. To that end, the effects of *Cbx1* null mutation on telomere function and sister chromatid cohesion have been investigated first. Next, based on the known role of HP1 proteins in cellular senescence (see Introduction), the effects of the *Cbx1* mutation in a sensitized cancer model with the express aim to understand the role of HP1β in OIS have been investigated. Finally, alternative ways in which HP1β binds to histone H3 have been characterized by measuring the affinity of the different interactions of HP1β with histone H3. In this way, it was aimed to define the critical interaction whose loss likely results in the *Cbx1* null lethal phenotype.

4.1 The *Cbx1* gene and the regulation of genomic stability

In order to characterise the chromosomal instabilities that were initially observed in *Cbx1*$^{-/-}$ neurospheres cultures, a model system was set up, namely the 3T9 assay (Figure 10). This allowed us to obtain enough material to characterise the instabilities in more detail; neurosphere cultures provide only limited amounts of material for analysis. Accordingly, culture of primary MEFs from three genotypes, WT, *Cbx1*$^{+/-}$ and *Cbx1*$^{-/-}$, according to a 3T9 protocol showed that by passage 16 the WT cells had undergone senescence crisis, while in stark contrast, *Cbx1*$^{+/-}$ and *Cbx1*$^{-/-}$ MEFs either went through the crisis and continued to proliferate or simply continued to proliferate without any sign of having been through crisis.

Cytological analysis of early passage cells showed that the instabilities were of several different types, including an increased number of telomere-telomere fusions and also premature chromosome separations (Figure 11, Table 4). In this thesis the molecular bases of these two types of defect were studied further (see below).

4.2 Investigation of the effect of *Cbx1* null mutation on telomere function

The presence of telomere-telomere fusions in low passage *Cbx1*$^{-/-}$ cells strongly indicated that the absence of the *Cbx1* gene product, HP1β, compromises telomere function. To explore the molecular basis of these aberrant fusions further, the H3K9me3-HP1-H4K20me3 epigenetic pathway was investigated first. The pathway from H3K9me3 to H4K20me3 via HP1 is thought to be important for the assembly of HP1-containing constitutive heterochromatin at both centromeres and telomeres (Kourmouli *et al.*, 2004; 2005; Schotta *et al.*, 2004). Disruption of this pathway in cells deficient in Suv39h1/h2 HMTases showed decreased levels of H3K9 trimethylation at telomeres, concomitant with a reduction in binding of HP1 proteins and aberrant telomere elongation (Garcia-Cao *et al.*, 2004). Using ChIP assays, no change in the levels of H3K9me3, H3K9me2 and H4K20me3 at telomeric heterochromatin was observed indicating that the H3K9me3-HP1-H4K20me3 epigenetic pathway is unlikely to be disrupted in *Cbx1* null cells (Figure 12). Given that the telomeric levels of H3K9me3 remain the same, the interaction site for HP1 proteins is intact. Thus, the remaining two HP1 isoforms, HP1α and HP1γ, might bind and compensate for the loss of HP1β. Because both HP1α and HP1γ can also bind the H4K20 methyltransferases Suv4-20h1/2, they can in turn recruit these methyltransferases and thus maintain trimethylation of lysine 20 on histone H4.

To address the question of whether the telomeric fusions and end associations observed in the chromosomes of *Cbx1*$^{-/-}$ MEFs were due to a disruption of the protective shelterin complex, immunofluorescence and ChIP assays were undertaken which allowed the investigation of specific changes in members of the shelterin complex. As explained (see Introduction) mammalian telomeres are protected from being sensed as DNA damage by the "shelterin" protein complex, which is a complex of 6 interacting proteins that form a protective cap at the end of mammalian chromosomes. Disruption of this protective protein complex results in the

"uncapping" of telomeres and triggers DNA damage response accompanied by non-homologous end joining and consequent telomere-telomere fusions (de Lange, 2005). The six shelterin subunits include TRF1, TRF2, TIN2, RAP1, TPP1 and POT1. Among these proteins, POT1 and TPP1 play important roles in the protection of chromosome ends (Baumann and Price, 2010). POT1 binds to single stranded TTAGGG repeats present at the 3' overhang and in the D-loop of the so-called T-loop configuration. In the mouse there are two paralogues of POT1: POT1a and POT1b. Disruption of either gene in mouse embryonic fibroblasts results in reduced proliferation, a severe telomeric DNA damage response (TIFs or **t**elomere dysfunction-**i**nduced **f**oci), chromosome reduplication, increased sister telomere recombination and resection of the telomeric C-strand to give long G-overhangs (Hockemeyer *et al.*, 2006 and Wu *et al.*, 2006). TPP1 connects POT1 with TIN2 through its centrally-located POT1 interaction domain and depletion of TPP1 leads to removal of all detectable POT1 from telomeres. Notably, impaired TPP1 function leads to unprotected telomeres and telomere length phenotypes as seen in POT1-deficient cells (Hockemeyer *et al.*, 2007, Lazzerini and de Lange, 2007, Liu *et al.*, 2004, Xin *et al.*, 2007 and Ye *et al.*, 2004).

Investigation of possible mis-localisation of TPP1, POT1a and POT1b proteins in *Cbx1* null cells showed that there was little difference in the localizations of these proteins in G1 interphase nuclei taken from *Cbx1*$^{-/-}$ MEFs compared to WT (Figure 14). While it is not possible to draw concrete conclusions simply by inspection of the (macro) cellular distributions of these two shelterin proteins, ChIP grade antibodies that can be reliably used to look at the biochemical interaction of these proteins with telomeric chromatin were, as yet, unavailable. Because of the availability of good ChIP grade antibodies, two other members of the shelterin complex, TRF1 and TRF2, were studied using ChIP assay. TRF1 and TRF2 are constitutively present at telomeres and the proportion of TRF1 and TRF2 loaded on telomeres is important for telomere length regulation. Notably, mouse HP1β has been shown to interact with SALL1 and TRF1 protein (Netzer *et al.*, 2001). Extensive cell-based *in vitro* studies using overexpression of TRF1 alleles have suggested a role for TRF1 as a negative regulator of telomere length (van Steensel and de Lange, 1997; Smogorzewska *et al.*, 2000; Ancelin *et al.*, 2002). TRF1 has other functions apart from being involved in telomere physiology because the

blastocyst stage lethality found in TRF1 null mice is not the result of any changes in telomere length or telomere capping (Karlseder *et al.*, 2003). In tissue culture cells, TRF1 deficiency has also been shown to lead to telomere aberrations including fusions and multitelomeric signals in cultured ES cells (Okamoto *et al.*, 2008). TRF1$^{-/-}$ MEFs also show abundant telomere fusions, particularly, sister telomere fusions, as well as the occurrence of multi-telomeric signals (Martínez *et al.*, 2009). In the ChIP assays performed, no change was found in the amount of TRF2 at the telomeres and but there was a reduction of TRF1 binding to *Cbx1*$^{-/-}$ telomeres. This reduction in TRF1 protein at the telomere might explain the effect of the *Cbx1*$^{-/-}$ mutation on telomere length, which will be discussed next.

It has been known for some time that a minimum length of TTAGGG repeats is required for the proper telomere function (Capper *et al.*, 2007). Telomere length is maintained by telomerase, a reverse transcriptase that adds telomeric repeats *de novo* after each cell division, counteracting the end-replication problem in those cell types in which it is expressed (Chan and Blackburn, 2002; Collins and Mitchell, 2002). The physical association of telomerase to the telomere can be affected by the overexpression of HP1β in human cells, which results in reduced association of human telomerase reverse transcriptase with the telomere and a higher frequency of end-to-end chromosomal fusions (Sharma *et al.*, 2003). These data indicate a critical role for HP1β in maintaining mammalian telomeric heterochromatin. This also appears to be true for HP1 homologues from other species. In fission yeast, various mutations that alleviate telomeric silencing and heterochromatin formation have no or limited effects on telomere length, including the inactivation of genes encoding Swi6 (HP1 homologue), Clr4 (Suv39h homologue) and other components of the RNAi machinery (Ueno *et al.*, 2004; Ekwall *et al.*, 1996; Hall *et al.*, 2003). In fruit fly, on the contrary, HP1 proteins have been shown to negatively regulate the transposition-based mechanism of telomere elongation (Perrini *et al.*, 2004). In mice, cells lacking Suv39h1/h2 HMTases show decreased levels of H3K9 trimethylation at telomeres, concomitant with aberrant telomere elongation (Garcia-Cao *et al.*, 2004). Telomere length is also similarly deregulated in cells that lack all three members of the pRb family (García-Cao *et al.*, 2002).

In order to determine whether depletion of HP1β in mouse cells has an effect on the telomere length, FLOW-FISH analysis on early and late passage WT and *Cbx1*$^{-/-}$ MEFs was undertaken. This analysis revealed that there was very little or no difference in the telomere lengths of early passage WT and *Cbx1*$^{-/-}$ cells. However, at late passage, the *Cbx1*$^{-/-}$ cells had telomeres that were much longer (~20 kb) than the WT telomeres (Figure 16). The fact that the telomeres were longer in late passage *Cbx1*$^{-/-}$ cells (and not in early passage ones) is indicative of a likely increase in telomere length in response to the *Cbx1* deficiency with each cell cycle. As for the molecular mechanism, the observation that TRF1 protein levels in early passage *Cbx1*$^{-/-}$ MEFs were decreased (Figure 12), taken together with the published result that TRF1 is a known negative regulator of telomere length (van Steensel and de Lange, 2000), leads to a model where the lack of HP1β results in reduction in TRF1 and a concomitant increased access of telomerase to telomeric sequences, resulting in an increased telomere length. Future experiments would include a more detailed analysis of the passage number at which telomeres of *Cbx1*$^{-/-}$ cells start to increase in length. The fact that *Cbx1*$^{-/-}$ MEFs escape senescence around passage 16 is suggestive of a critical stage that might trigger telomere elongation. These experiments could be combined with DNAse I hypersensitivity assays to determine whether telomere elongation in *Cbx1*$^{-/-}$ cells is accompanied by greater accessibility of the telomeric sequences.

4.3 The *Cbx1* null mutation and sister chromatid cohesion

Sister chromatid cohesion is required during mitosis in order to align the chromosomes at the spindle equator at metaphase and thereby enable segregation to precede normally with equal distribution of sister chromatids to the daughter nuclei. In the absence of cohesion, segregation is aberrant, leading to premature separation of chromosomes and concomitant aneuploidy in daughter cells (Bernard *et al.*, 2001). Sister chromatid cohesion is mediated by a set of evolutionarily conserved proteins that form a complex known as cohesin (Onn *et al.*, 2008). This complex consists of 4 proteins, SMC1, SCC1, SCC3 and SMC3. The timely release of cohesion from duplicated chromosomes is required for accurate chromosome segregation during mitosis. This release is tightly regulated by the **s**pindle **a**ssembly **c**heckpoint (SAC) that prevents progression to anaphase if chromosomes remain unattached to mitotic spindles.

A critical, conserved component of SAC is BUB1; BUB1 is required for targeting other SAC proteins to the kinetochore. Another key protein that is important for proper chromosome segregation is the shugoshin (SGO1) protein that prevents the removal of centromeric cohesin during mitotic prophase and ensures sister chromatid cohesion is maintained before bidirectional attachment to the mitotic spindle (Kitajima *et al.*, 2005).

There has been conflicting data in the literature regarding the role of HP1 proteins in maintaining sister chromatid cohesion. Initial reports in *S. pombe* showed that Swi6 (HP1 homologue) not only functions in pericentromeric heterochromatin silencing, but also recruits cohesin, which is important for centromeric sister chromatid cohesion and kinetochore biorientation (Bernard *et al.*, 2001; Nonaka *et al.*, 2002). Swi6 was also shown to interact with Psc3 (an SCC3 homolog) by both co-immunoprecipitation and yeast two hybrid assays (Nonaka *et al.*, 2002). There are also other reports which state that it is the cohesin loading factor SCC2, rather than cohesin, which interacts with HP1 (Fischer *et al.*, 2009; Serrano *et al.*, 2009; Lechner *et al.*, 2005; Zeng *et al.*, 2009). Human HP1α and *S. pombe* Swi6 were also found to interact with SGO1 and this interaction was shown to be important for SGO1 localization at centromeres in early mitosis, where it plays a role in cohesin retention and sister chromatid cohesion (Yamagishi *et al.*, 2008). In human cells treated with an siRNA against HP1α, SGO1 localization was abolished and the centromeric cohesion was largely dissociated in the SGO1-lacking chromosomes (Yamagishi *et al.*, 2008). Besides SGO1 has also been shown to directly interact with GST-tagged HP1α, HP1β and HP1γ indicating a role for HP1 proteins in the localization of SGO1 (Serrano *et al.*, 2009).

By contrast in *Suv39h1/h2* double-knockout mouse embryonic fibroblasts (Koch *et al.*, 2008), where both H3K9 trimethylation and HP1 proteins are much reduced, no reduction in cohesin association at centromeres was observed. Furthermore, in another study, depletion of HP1 proteins in human cells by siRNA has been shown to have no effect on cohesin recruitment (Serrano *et al.*, 2009).

Using *Cbx1*$^{-/-}$ MEFs, it was investigated whether the defects in sister chromatid cohesion seen in the chromosome spreads from *Cbx1*$^{-/-}$ MEFs show a difference in distribution of the

proteins involved in cohesion, kinetochore attachment and spindle assembly checkpoint (SAC). Accordingly, unfixed metaphase spreads from early passage WT and *Cbx1*$^{-/-}$ MEFs were stained for SMC3, BUB1 and SGO1 (Figures 17-19). This analysis has revealed that there were no changes in SMC3, BUB1 and SGO1 localization in early passage *Cbx1*$^{-/-}$ cells compared to WT MEFs indicating that either HP1β is unlikely to be involved in the recruitment of these kinetochore/cohesion components to the centromeres of mouse cells or that its function is redundant, being compensated by the two other HP1 isotypes.

Although HP1β seems unlikely to be involved in cohesion recruitment to mouse centromeres, there is some evidence that the HP1 isotype, human HP1γ, can recruit cohesin, albeit to specific chromosomal sites outside of the centromere. At the D4Z4 chromosomal site (D4Z4 is a 3.3 kb long macrosatellite repeat sequence) binding of HP1γ, in an H3K9me3 dependent manner, in turn recruits the cohesion complex (Zeng *et al.*, 2009). Thus, the possibility remains that the recruitment of cohesin to mammalian centromeres might require an isotype-specific interaction with either of the other two HP1 isotypes other than HP1β.

4.4 Investigation of the effect of *Cbx1* mutation on oncogene-induced senescence (OIS)

The 3T9 assay also showed that *Cbx1* null fibroblasts escape the typical senescence crisis that is seen when culturing primary mouse fibroblasts (Figure 10). This result is consistent with observations that HP1 proteins are involved in regulating the exit of cells from the cell cycle during the progression towards cellular senescence. HP1 proteins interact with the tumour repressor pRb, which is a key regulator of the p16^{INK4A}/pRb senescence pathway that has been shown to be crucial for SAHF formation (Gil and Peters, 2006; Kim and Sharpless, 2006). Notably, loss of pRb function gives rise to phenotypes similar to those found in *Cbx1*$^{-/-}$ tissue culture cells. Embryos lacking pRb function exhibit a genomic instability that is consistent with defects in DNA replication and abnormal segregation of chromosomes during mitosis (Kennedy *et al.*, 2000; Foijer *et al.*, 2005; Eguchi *et al.*, 2007). In mouse embryonic stem cells the deletion of both pRb alleles results in increased chromosomal alterations (Zheng *et al.*, 2002). In MEFs, the inactivation of pRb leads to polyploidy (Srinivasan *et al.*, 2007). In mouse hepatocytes, loss of pRb function promotes aneuploidy (Mayhew *et al.*, 2005). Similarly, knockdown of pRb in human primary cells

has been shown to promote aneuploidy via micronuclei formation (Amato *et al.*, 2009). The resemblance of these pRb phenotypes to those observed in *Cbx1*$^{-/-}$ MEFs opens up the possibility that the loss of *Cbx1* gene function results in defects downstream from the cellular functions of pRb. However, this is, at least for the moment, speculation and remains to be proved.

Related to cellular senescence that occurs during organismal and cellular ageing, senescence can also be induced in response to a variety of stresses (Serrano and Blasco, 2001). One of these is OIS, which is a tumour suppressor mechanism in primary cells. OIS is mediated by two main pathways: the p19^{ARF}/p53 and/or the p16^{INK4A}/pRb (Gil and Peters, 2006; Kim and Sharpless, 2006). It is characterised by the acquisition of senescence markers in response to oncogenic stress. Typically, OIS has been observed in a variety of mouse and human premalignant tumours and these observations have been interpreted as *in vivo* evidence for OIS acting as a barrier to tumorigenesis (Braig *et al.*, 2005; Chen *et al.*, 2005; Collado *et al.*, 2005; Lazzerini-Denchi *et al.*, 2005; Michaloglou *et al.*, 2005).

In this study, a K-ras model of OIS established by Collado and colleagues was utilised (Collado *et al.*, 2005). These colleagues were able to show that the expression of oncogenic K-ras (K-ras^{V12}) triggered senescence during the early premalignant stages of tumorigenesis that results from oncogene expression. As explained, (see Introduction) premalignant (adenomas) as well as malignant tumours (adenocarcinomas) were identified in the lungs of these mice and, most strikingly, the premalignant lesions in the lung contained abundant senescent cells positive for OIS markers (SA-β-gal, p15, p16, Dec1, DcR2 and HP1γ) (Collado *et al.*, 2005). Using this model, *Cbx1*$^{+/-}$ mutation was introduced to investigate whether senescence might be bypassed leading to an increased numbers of malignant tumours. Accordingly, K-ras$^{+/V12}$;RERTn$^{+/ERT}$; *Cbx1*$^{+/-}$ mice were generated that are heterozygous for the *Cbx1* null allele and also possesses the inducible K-ras^{V12} oncogene. These mice were then injected with 4-OHT to induce the expression of the K-ras^{V12} oncogene. In the original reference, these mice have been shown to develop severe breathing difficulties and die at around 8 months after birth (Guerra *et al.*, 2003). However, in this study, it was found that these mice did not develop a severe breathing difficulty after eight months. The experiment was therefore continued and mice were allowed

to live longer. The experiment was eventually stopped when some of these mice already had reached 22 months of age (see Table 5). There was no difference found in the death rates between K-ras$^{+/V12}$;RERTn$^{+/ERT}$ (WT control) and K-ras$^{+/V12}$;RERTn$^{+/ERT}$;*Cbx1*$^{+/-}$ mice (data not shown). The lungs of these mice were then analyzed for the expression of oncogenic K-ras^{V12} as well as for the presence of premalignant adenomas and/or malignant adenocarcinomas. Sequencing of RT-PCR products amplified from lung tissues revealed that, K-ras^{V12} was expressed in 4 of the experimental and 6 of the control mice at the time the tissues were taken (Figure 20). K-ras$^{+/V12}$;RERTn$^{+/ERT}$ mice induce the expression of oncogenic K-ras^{V12} (upon 4-OHT injection) in only one allele along with the wt allele. In the original report, the expression efficiency of K-ras^{V12} using this inducible system has been shown to be 5 % to 15 % in most of the tissues examined and this level of expression was sufficient to cause the malignancies observed in the lungs of K-ras$^{+/V12}$;RERTn$^{+/ERT}$ mice (Guerra *et al.*, 2003). The fact that the K-ras^{V12} oncogene could not be detected in some of the lungs analyzed might probably be due to the insensitivity of the sequencing method used for a quantitative analysis or that the expression was stronger earlier, soon after induction, and after many months the expression might then have been extinguished.

Histopathological analysis of lung sections was then carried out on the H&E stained lung sections. This analysis has revealed malignant adenocarcinomas in the five lungs heterozygous for the *Cbx1* mutation in which the oncogenic K-ras^{V12} had been induced, while only one WT mouse possessed a very small region of malignant tumour. Analysis of the lung tumours found in K-ras$^{+/V12}$;RERTn$^{+/ERT}$;*Cbx1*$^{+/-}$ mice were negative for senescence markers (p16, DcR2) but positive for the proliferation marker, pKi-67. The absence of premalignant tumours might be due to the genetic background of mice (mixed 129 x Bl/6) or at the time at which the mice were killed, they had passed through the premalignant stage and only full-blown tumours survived. These data indicate that there may be a limited role for the *Cbx1* gene in OIS but rather that it acts as a tumour suppressor. This view is supported by the *in vitro* work, to be described next.

In order to explore further the role of HP1β in OIS, a well established H-ras^{V12} oncogene *in vitro* model was utilised (Serrano *et al.*, 1997). In this model, mouse embryonic fibroblasts transduced with an H-ras^{V12} expression plasmid undergo OIS as evidenced by a cessation of proliferation and positivity for SA-β-gal staining.

In this current study, *Cbx1*$^{-/-}$ MEFs transduced with the H-ras^{V12} expression vector were shown to undergo a proliferation arrest similar to seen in WT MEFs transduced with the same vector (Figure 28). Subsequent positive SA-β-gal staining on MEFs 7 days after transduction with the H-ras^{V12} expression vector has also shown that these cells were senescent indeed, which indicates that the *Cbx1* gene product, HP1β, is unlikely to be involved in the OIS response (Figure 29).

It is known that OIS in primary cells is mediated by the two main tumour suppressor pathways: the p19^{ARF}/p53 and/or the p16^{INK4A}/pRb (Gil and Peters, 2006; Kim and Sharpless, 2006). The p16^{INK4A}/pRb pathway is crucial for the formation of SAHF, which are highly condensed regions of chromatin that develop in cells that will exit the cell cycle and become senescent. SAHF are characterised by the accumulation of histone H3 trimethylated at lysine 9 and heterochromatin proteins, including heterochromatin protein 1 (HP1), high-mobility group A (HMGA) proteins and macroH2A (Narita *et al.*, 2003; Narita *et al.*, 2006; Zhang *et al.*, 2005). *In vivo* and *in vitro* data described above indicate that HP1β is unlikely to be an important marker of OIS. Instead it is likely to be a tumour suppressor that may act downstream of the pRB pathway. Very similar lung tumours to those obtained in K-ras$^{+/V12}$;RERTn$^{+/ERT}$;*Cbx1*$^{+/-}$ mice have also been observed in pRb/p130 conditional mutant mice carrying a conditional oncogenic K-ras allele, whose controlled expression results in the development of high-grade lung adenocarcinomas (Ho *et al.*, 2009). Although there are currently no known human diseases that are associated with mutations in the *Cbx1* gene, changes in its level of expression have been reported for many cancers (Dialynas *et al.*, 2008). It has also been demonstrated that decreased HP1β expression, correlates with invasive potential in five human melanoma cell lines suggesting that HP1β acts as a tumour suppressor in melanoma oncogenesis (Nishimura *et al.*, 2006).

There is some support for the HP1γ isoform in mediating OIS, probably in SAHF formation. Collado *et al.* have shown that the premalignant adenomas that were formed by the induced expression of K-ras^{V12} oncogene were all positive for HP1γ staining whereas adenocarcinomas were negative. In another study, senescent prostatic intraepithelial neoplasia found in the AKT1 transgenic mice were also shown to have an increased HP1γ staining, in support of the idea that HP1γ is a marker of OIS (Majumder *et al.*, 2008). However, in a contradictory study where various human malignant tumours were screened, HP1γ was found to be expressed uniformly in the cell nucleus of all cancers examined, including lung adenocarcinomas. Furthermore, these same workers were able to demonstrate that siRNA knockdown of HP1γ sufficiently stopped the growth of colon cancer cells (Takanashi *et al.*, 2009). In the present study, strong HP1γ staining was observed in adenocarcinomas found in the lungs of K-ras$^{+/V12}$;RERTn$^{+/ERT}$**;***Cbx1*$^{+/-}$ mice (Figure 27), arguing against a role for HP1γ in OIS, and rather in favour of role as a marker of proliferating cells.

4.5 The binding of HP1β to histone H3

A large body of work in various organisms has shown that the presence of HP1 structural proteins and trimethylated lysine 9 of histone H3 (H3K9me3) represent the characteristic hallmarks of heterochromatin. Similarly, the binding of HP1β to H3K9me3 and Suv39h1 histone methyltransferase is thought to be the key interaction of HP1β leading to spreading of repressive heterochromatic domains (Lachner *et al.*, 2001 and Bannister *et al.*, 2001). In favour of this idea, it has been shown that HP1β is mislocalized in cells taken from *Suv39h1/h2* double null (dn) animals. Rather than being concentrated within constitutive heterochromatin, HP1β is found uniformly throughout euchromatic and heterochromatic regions in these *Suv39h1/h2* dn cells (Bannister *et al.*, 2001). However, in the light of recent evidence from biophysical studies a more complex picture has emerged which cannot easily be explained by a simple binary H3K9me3-HP1β interaction (Festenstein *et al.*, 2003, Cheutin *et al.*, 2003, Schmiedeberg *et al.*, 2004 and Dialynas *et al.*, 2007). Another key interaction of HP1β, which has been studied in some detail, is the binding to the histone H3 histone-fold domain (Nielsen *et al.*, 2001 and Dialynas *et al.*, 2006). However, the essential physiological function of this HP1β-H3 fold interaction still remains to be solved.

In the present study, the *in vitro* interaction of HP1β (and its mutants) with histone H3 has been investigated first by GST pull down experiments. Several single/multiple amino acid substitutions have been introduced into GST tagged murine HP1β, which were decided upon from a review of the literature and aimed at addressing the interaction of HP1β with recombinant, unmethylated histone H3. The rationale for the experiments was to incubate WT and mutant GST-HP1β proteins with histone H3 in increasing NaCl concentrations so that the affinity of the interaction of the mutants with recombinant histone H3 could be measured. The mutations introduced into HP1β were valine 23 to methionine (V23M), arginine 29 and 30 to glutamine (R29/30Q), lysine 33 to glutamine (K33Q), phenylalanine 45 to glutamic acid (F45E), threonine 51 to alanine (T51A) and isoleucine 161 to glutamic acid (I161E). Valine 23 is thought to be required for binding of the HP1β CD to the H3K9me3 peptide (Nielsen *et al.*, 2002). In HP1α the V22M mutation (which corresponds to V23M in HP1β) has been shown to be required for histone H3 binding as well (Nielsen *et al.*, 2001). Similarly, the V26M mutation in *D. melanogaster* HP1 (which corresponds to V23M in HP1β) was also shown to result in a dramatic loss of binding to methylated H3K9 peptide (Jacobs *et al.*, 2001). The reason for choosing R29/30Q and K33Q mutations were to reduce the overall basic charge of the protein in this evolutionarily conserved region of the protein and to use them as controls. The R28/29Q substitutions in HP1α (which correspond to R29/30Q in HP1β) have been shown to have no effect on interaction with purified calf thymus histone H3 (Nielsen *et al.*, 2001); the corresponding mutations of R29/30Q and K33Q in *D. melanogaster* HP1 have also been shown to have no effect on PEV (Platero *et al.*, 1995). F45 is one of the three evolutionarily conserved aromatic residues (Y21, W42 and F45) that form the notional aromatic "cage", into which the positively charged methylammonium functional moiety of H3K9me3 fits (Jacobs and Khorasanizadeh, 2002; Nielsen *et al.*, 2002). T51 has been shown to be phosphorylated upon DNA damage and play a role in the rapid mobilisation of HP1β in euchromatin and heterochromatin (Ayoub *et al.*, 2008). T51 is also known to play a role in the interaction with H3K9me3, by the formation of a network of hydrogen bonds between the side chains of E53, T51 and W42 of the human HP1β chromodomain. This network of hydrogen bonds is disrupted in the T51A mutant (Ayoub *et al.*, 2008, Figure 42). Isoleucine 161 residue is important in the formation of HP1β dimers; I161E mutation has been shown to

inhibit dimerisation of the two CSDs with each other, and disrupt the formation of functional HP1β dimers (Brasher *et al.*, 2000).

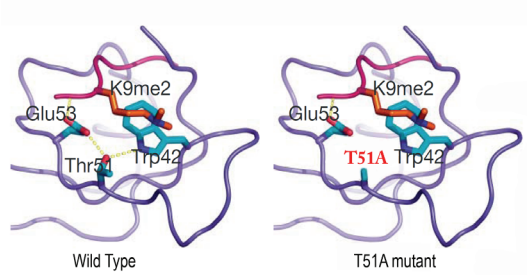

Figure 42 A model for the interaction of the wild type human HP1β chromodomain bound to dimethylated K9 of histone H3 (H3K9me2), based on the PDB coordinates 1KNA, compared with its T51A mutant. A network of hydrogen bonds between the side chains of E53, T51 and W42 of the human HP1β chromodomain, marked as yellow dashed lines, is disrupted in the T51A mutant. Figure modified from Ayoub *et al.*, 2008.

This analysis has revealed that together with WT HP1β, all full length recombinant HP1β mutants tested were able to pull recombinant histone H3 down in all NaCl concentrations, except from I161E mutant which has lost its binding to histone H3 at 0.6 M and 0.75 M NaCl (Figure 32, left and right section). This indicates that the CSD is the important module for binding to recombinant histone H3, through as a dimer (HP1β dimerisation is disrupted by the I161E mutation), although this conclusion may need to be qualified in light of the isothermal titration calorimetry results discussed below. The importance of the CSD in H3 binding was supported by two further observations. First, that an HP1β mutant that lacks the CD (named C-terminal HP1β) was capable of binding to histone H3 in all NaCl concentrations and, second, that an HP1β mutant lacking the conserved CSD (named N-terminal HP1β) failed to bind to histone H3 at 0.6 M and 0.75 M salt concentrations. Taken together these data showed that the CSD has a strong affinity (greater than the CD) for the recombinant histone H3. However, the influence of the CD in binding of the intact protein to recombinant H3 cannot be ignored because specific CD mutations in combination with the I161E mutation rescue binding at 0.6 M (F45E) and at both 0.6/0.75 M salt (R29/30Q).

Other pull-down experiments gave results which show that mutations in CD residues do not affect binding to recombinant H3 histone. Previously, V22M mutation in HP1α has been shown to inhibit histone H3 binding (Nielsen *et al.*, 2001), however, the corresponding V23M mutation in HP1β seems to have no effect on binding to histone H3. Similarly, T51A mutation in HP1β has been thought to disrupt the binding of His-tagged HP1β to H3K9me3 and histone H3 (Ayoub *et al.*, 2008) (Figure 42). The present study, however, clearly

has shown that the HP1β T51A mutant remains capable of binding to histone H3 even at higher salt concentrations.

To support and extend the data obtained from GST pull down experiments, the strength of HP1β-histone H3 interaction was also determined quantitatively by the isothermal titration calorimetry (ITC) technique which enabled the quantitative determination of biomolecular interactions and all binding parameters in a single experiment. The binding affinity of HP1β to H3K9me3 tail peptide was also measured in parallel as a comparison. The ITC analysis has revealed that the binding affinity of wild type HP1β to histone H3 was approximately 4 times higher than for the trimethylated lysine 9 tail peptide (H3K9me3) at both 25 °C and 37 °C indicating a more critical role for HP1β-histone H3 interaction than its canonical interaction with the H3K9me3 determinant of the histone code (Figures 32-33).

In support of the previous result obtained in the pull down experiments, the binding of the HP1β T51A mutant to both histone H3 and H3K9me3 could be proven and the binding affinity to histone H3 has been shown to be greater than for the H3K9me3 peptide (Table 7, Figures 34 and 35). As expected, HP1β V23M mutant had a very low affinity for H3K9me3, in line with published data, while still retaining a high affinity for histone H3 (Table 7, Figures 36 and 37). In case of HP1β F45E mutant, it was not possible to accurately measure its affinity to histone H3 at 25 °C as a result of an unstable baseline due to an unknown reason (Figure 39). However, a direct comparison could be made at 37 °C, which gave reproducible results; at 37 °C HP1β F45E mutant has lost its affinity for the H3K9me3 peptide as expected but retained its high affinity for the recombinant histone H3 (Figures 38 and 39). The binding affinity of HP1β I161E mutant for histone H3 was almost two times higher than its affinity for H3K9me3 peptide, both at 25 °C and 37 °C (Table 7, Figures 40 and 41). Interestingly, compared to WT protein, this mutant showed a higher (ca. 2 times higher) affinity for the trimethylated lysine 9 peptide at both tested temperatures. Considering the previous result obtained from GST pull down experiments, it is also surprising that the His-HP1β I161E protein had a similarly high affinity to histone H3 as WT HP1β which implicates a negligible role for dimerisation of HP1β in its binding to histone H3 in this particular technique used. It has been shown that GST tagged fusion

proteins are found in homodimers and tend to aggregate, which might have impeded the interaction of GST-HP1β I161E mutant with histone H3 in higher salt concentrations (Kaplan *et al.*, 1997).

Taken together, the GST pull down and ITC experiments give a picture of a high affinity binding of HP1β to histone H3 histone-fold domain likely through its CSD, which puts emphasis on an interaction that has previously received little attention. In contrast, the binding of HP1β CD to H3K9me3 determinant of the histone code has been widely accepted as the essential function of HP1β in the assembly of heterochromatin domain in the genome. Despite its elegant simplicity, the accepted view that the H3K9me3–HP1β interaction is the key one for heterochromatin assembly and organismal survival needs modification. Recent dynamics studies have revealed a more complex picture that is not readily explained by a simple binary H3K9me3–HP1β interaction. Fluorescence recovery after photo-bleaching (FRAP) studies in mammalian cells showed that HP1β is a dynamic protein with recovery half-lives ($t_{1/2}$) of 0.5 s – 10 s for euchromatin and 2.5 s – 50 s for heterochromatin (Festenstein *et al.*, 2003; Cheutin *et al.*, 2003). Further studies showed that a small fraction (4 % – 7 %) of very slow-moving HP1 molecules in constitutive heterochromatin could take >1 hour to recover after photo-bleaching, a property indicative of tight binding to chromatin (Schmiedeberg *et al.*, 2004; Dialynas *et al.*, 2007). Moreover, the existence of several kinetically distinct HP1β species in the nucleus has been confirmed by the observation that the nuclear distribution of HP1β varied upon cell type examined, micro-environmental conditions and the cellular differentiation state (*e.g.* ES cells possess hyperdynamic HP1 molecules compared with differentiated cells) (Meshorer and Misteli, 2006; Ritou *et al.*, 2007; Dialynas *et al.*, 2007). As a consequence of these data and supported by genetic studies made in the mouse and in *D. melanogaster*, it is clear that a new conceptual framework is needed to understand the chromatin dynamics of HP1β and that any such framework must now extend beyond the canonical H3K9me3–HP1β interaction. The fact that *Suv39h1/h2*$^{-/-}$ mice live and *Cbx1*$^{-/-}$ die clearly shows that the essential function of HP1β must lie outside the Suv39h1/h2-dependent heterochromatic H3K9me3–HP1β interaction (Lachner *et al.*, 2001; Aucott *et al.*, 2008). The same situation appears to occur in *D. melanogaster*: flies lacking HP1 (*Su(var)2-5*^{05} homozygotes) die at the third larval instar stage

with no escapers, whereas flies lacking dKMT1A (*Su(var)3-9*^{06} homozygotes) are viable (Eissenberg *et al.*, 1992; Tschiersch *et al.*, 1994). Therefore, the essential function of HP1β proteins cannot be readily explained by their role on reading the H3K9me3 determinant of the histone code. It might be the high affinity binding of HP1β to the histone H3 histone-fold domain that is required for organismal survival. Putting emphasis on this mostly neglected interaction would also explain the survival of mice hypomorphic for *Cbx1* which have only 10 % of WT HP1β protein levels (Dr. Thorsten Bangsow, JWGU, Frankfurt am Main, unpublished). It is only if the mouse completely lacks HP1β that it dies at around birth with an associated genomic instability characterised by severe chromosomal abnormalities that are indicative of pericentric constitutive heterochromatin dysfunction (Aucott *et al.*, 2008). Placing physiological importance on the HP1β-H3 histone-fold interaction instead of the H3K9me3–HP1β interaction might also provide an alternative explanation for the recent contradictory observation which shows that HP1β is recruited to sites of DNA damage independently of the H3K9me3 (Ayoub *et al.*, 2008; Luijsterburg *et al.*, 2009; Zarebski *et al.*, 2009; Billur *et al.*, 2010). It is possible that this recruitment is via the HP1β-histone H3 histone-fold interaction. The small number of studies to date indicates that HP1 recruitment could be one of the earliest molecular events in the DNA damage response (Ball and Yokomori, 2009); however it remains too early to speculate upon the molecular mechanism(s) of how mammalian HP1 proteins aid repair at sites of DNA damage, which is the subject for future research.

Chapter 5

References

Aagaard L, Laible G, Selenko P, Schmid M, Dorn R, Schotta G, Kuhfittig S, Wolf A, Lebersorger A, Singh PB, Reuter G, Jenuwein T. **1999** Functional mammalian homologues of the Drosophila PEV-modifier Su(var)3-9 encode centromere-associated proteins which complex with the heterochromatin component M31. EMBO J. Apr 1;18(7):1923-38.

Aasland R, Stewart AF. **1995** The chromo shadow domain, a second chromo domain in heterochromatin-binding protein 1, HP1. Nucleic Acids Res. Aug 25;23(16):3168-73.

Allshire RC, Javerzat JP, Redhead NJ, Cranston G. **1994** Position effect variegation at fission yeast centromeres. Cell. Jan 14;76(1):157-69.

Allshire RC, Karpen GH. **2008** Epigenetic regulation of centromeric chromatin: old dogs, new tricks? Nat Rev Genet. Dec;9(12):923-37.

Ancelin K, Brunori M, Bauwens S, Koering CE, Brun C, Ricoul M, Pommier JP, Sabatier L, Gilson E. **2002** Targeting assay to study the cis functions of human telomeric proteins: evidence for inhibition of telomerase by TRF1 and for activation of telomere degradation by TRF2. Mol Cell Biol. May;22(10):3474-87.

Aucott R, Bullwinkel J, Yu Y, Shi W, Billur M, Brown JP, Menzel U, Kioussis D, Wang G, Reisert I, Weimer J, Pandita RK, Sharma GG, Pandita TK, Fundele R, Singh PB. **2008** HP1-beta is required for development of the cerebral neocortex and neuromuscular junctions. J Cell Biol. Nov 17;183(4):597-606.

Ayoub N, Jeyasekharan AD, Bernal JA, Venkitaraman AR. **2008** HP1-beta mobilization promotes chromatin changes that initiate the DNA damage response. Nature. May 29;453(7195):682-6.

Ayyanathan K, Lechner MS, Bell P, Maul GG, Schultz DC, Yamada Y, Tanaka K, Torigoe K, Rauscher FJ **2003** Regulated recruitment of HP1 to a euchromatic gene induces mitotically heritable, epigenetic gene silencing: a mammalian cell culture model of gene variegation. Genes Dev. Aug 1;17(15):1855-69.

Bae NS, Baumann P. **2007** A RAP1/TRF2 complex inhibits nonhomologous end-joining at human telomeric DNA ends. Mol Cell. May 11;26(3):323-34.

Baerlocher GM, Vulto I, de Jong G, Lansdorp PM. **2006** Flow cytometry and FISH to measure the average length of telomeres (flow FISH). Nat Protoc.;1(5):2365-76.

Ball AR Jr, Yokomori K. **2009** Revisiting the role of heterochromatin protein 1 in DNA repair. J Cell Biol. May 18;185(4):573-5.

Ball LJ, Murzina NV, Broadhurst RW, Raine AR, Archer SJ, Stott FJ, Murzin AG, Singh PB, Domaille PJ, Laue ED. **1997** Structure of the chromatin binding (chromo) domain from mouse modifier protein 1. EMBO J. May 1;16(9):2473-81.

Bannister AJ, Zegerman P, Partridge JF, Miska EA, Thomas JO, Allshire RC, Kouzarides T. **2001** Selective recognition of methylated lysine 9 on histone H3 by the HP1 chromo domain. Nature. Mar 1;410(6824):120-4.

Baumann P, Price C. **2010** Pot1 and telomere maintenance. FEBS Lett. May 21.

Benetti R, Gonzalo S, Jaco I, Schotta G, Klatt P, Jenuwein T, Blasco MA. **2007** *Suv4-20h* deficiency results in telomere elongation and derepression of telomere recombination. J Cell Biol. Sep 10;178(6):925-36.

Bernard P, Maure JF, Partridge JF, Genier S, Javerzat JP, Allshire RC. **2001** Requirement of heterochromatin for cohesion at centromeres. Science. Dec 21;294(5551):2539-42

Bérubé NG, Smith JR, Pereira-Smith OM. **1998** The genetics of cellular senescence. Am J Hum Genet. May;62(5):1015-9.

Bhaumik SR, Smith E, Shilatifard A. **2007** Covalent modifications of histones during development and disease pathogenesis. Nat Struct Mol Biol. Nov;14(11):1008-16.

Billur M, Bartunik HD, Singh PB. **2010** The essential function of HP1 beta: a case of the tail wagging the dog? Trends Biochem Sci. Feb;35(2):115-23.

Bird A. **2002** DNA methylation patterns and epigenetic memory. Genes Dev. Jan 1;16(1):6-21.

Bird AP. **1986** CpG-rich islands and the function of DNA methylation. Nature. May 15-21;321(6067):209-13.

Blasco MA. **2007** The epigenetic regulation of mammalian telomeres. Nat Rev Genet. Apr;8(4):299-309.

Blower MD, Sullivan BA, Karpen GH. **2002** Conserved organization of centromeric chromatin in flies and humans. Dev Cell. Mar;2(3):319-30.

Braig M, Lee S, Loddenkemper C, Rudolph C, Peters AH, Schlegelberger B, Stein H, Dörken B, Jenuwein T, Schmitt CA. **2005** Oncogene-induced senescence as an initial barrier in lymphoma development. Nature. Aug 4;436(7051):660-5.

Brasher SV, Smith BO, Fogh RH, Nietlispach D, Thiru A, Nielsen PR, Broadhurst RW, Ball LJ, Murzina NV, Laue ED. **2000** The structure of mouse HP1 suggests a unique mode of single peptide recognition by the shadow chromo domain dimer. EMBO J. Apr 3;19(7):1587-97.

Bringold F, Serrano M. **2000** Tumor suppressors and oncogenes in cellular senescence. Exp Gerontol. May;35(3):317-29.

Brown SW. **1966** Heterochromatin. Science. Jan 28;151(709):417-25.

Bullwinkel J, Baron-Lühr B, Lüdemann A, Wohlenberg C, Gerdes J, Scholzen T. **2006** Ki-67 protein is associated with ribosomal RNA transcription in quiescent and proliferating cells. J Cell Physiol. Mar;206(3):624-35.

Cairns BR. **2009** The logic of chromatin architecture and remodelling at promoters. Nature. Sep 10;461(7261):193-8.

Capper R, Britt-Compton B, Tankimanova M, Rowson J, Letsolo B, Man S, Haughton M, Baird DM. **2007** The nature of telomere fusion and a definition of the critical telomere length in human cells. Genes Dev. Oct 1;21(19):2495-508.

Chan SR, Blackburn EH. **2004** Telomeres and telomerase. Philos Trans R Soc Lond B Biol Sci. Jan 29;359(1441):109-21.

Chan SW, Blackburn EH. **2002** New ways not to make ends meet: telomerase, DNA damage proteins and heterochromatin. Oncogene. Jan 21;21(4):553-63.

Chen Z, Trotman LC, Shaffer D, Lin HK, Dotan ZA, Niki M, Koutcher JA, Scher HI, Ludwig T, Gerald W, Cordon-Cardo C, Pandolfi PP. **2005** Crucial role of p53-dependent cellular senescence in suppression of Pten-deficient tumorigenesis. Nature. Aug 4;436(7051):725-30.

Cheutin T, McNairn AJ, Jenuwein T, Gilbert DM, Singh PB, Misteli T. **2003** Maintenance of stable heterochromatin domains by dynamic HP1 binding. Science. Jan 31;299(5607):721-5.

Collado M, Gil J, Efeyan A, Guerra C, Schuhmacher AJ, Barradas M, Benguría A, Zaballos A, Flores JM, Barbacid M, Beach D, Serrano M. **2005** Tumour biology: senescence in premalignant tumours. Nature. Aug 4;436(7051):642.

Collado M, Serrano M. **2010** Senescence in tumours: evidence from mice and humans. Nat Rev Cancer. Jan;10(1):51-7.

Collins K, Mitchell JR. **2002** Telomerase in the human organism. Oncogene. Jan 21;21(4):564-79.

Dai J, Sullivan BA, Higgins JM. **2006** Regulation of mitotic chromosome cohesion by Haspin and Aurora B. Dev Cell. Nov;11(5):741-50.

de Lange T, Shiue L, Myers RM, Cox DR, Naylor SL, Killery AM, Varmus HE. **1990** Structure and variability of human chromosome ends. Mol Cell Biol. Feb;10(2):518-27.

de Lange T. **2005** Shelterin: the protein complex that shapes and safeguards human telomeres. Genes Dev. Sep 15;19(18):2100-10.

de Lange T. **2004** T-loops and the origin of telomeres. Nat Rev Mol Cell Biol. Apr;5(4):323-9.

Demerec M, Slizynska H. Mottled White 258-18 of Drosophila Melanogaster. Genetics. 1937 Nov;22(6):641-9.

Denchi EL, de Lange T. **2007** Protection of telomeres through independent control of ATM and ATR by TRF2 and POT1. Nature. Aug 30;448(7157):1068-71.

Dialynas GK, Makatsori D, Kourmouli N, Theodoropoulos PA, McLean K, Terjung S, Singh PB, Georgatos SD. **2006** Methylation-independent binding to histone H3 and cell cycle-dependent incorporation of HP1beta into heterochromatin. J Biol Chem. May 19;281(20):14350-60.

Dialynas GK, Terjung S, Brown JP, Aucott RL, Baron-Luhr B, Singh PB, Georgatos SD. **2007** Plasticity of HP1 proteins in mammalian cells. J Cell Sci. Oct 1;120(Pt 19):3415-24.

Dialynas GK, Vitalini MW, Wallrath LL. **2008** Linking Heterochromatin Protein 1 (HP1) to cancer progression. Mutat Res. Dec 1;647(1-2):13-20.

Dimova DK, Dyson NJ. **2005** The E2F transcriptional network: old acquaintances with new faces. Oncogene. Apr 18;24(17):2810-26.

Dimri GP, Lee X, Basile G, Acosta M, Scott G, Roskelley C, Medrano EE, Linskens M, Rubelj I, Pereira-Smith O. **1995** A biomarker that identifies senescent human cells in culture and in ageing skin in vivo. Proc Natl Acad Sci U S A. Sep 26;92(20):9363-7.

Dougherty DA. **2007** Cation-pi interactions involving aromatic amino acids. J Nutr. Jun;137(6 Suppl 1):1504S-1508S; discussion 1516S-1517S.

Dunham MA, Neumann AA, Fasching CL, Reddel RR. **2000** Telomere maintenance by recombination in human cells. Nat Genet. Dec;26(4):447-50.

Eguchi T, Takaki T, Itadani H, Kotani H. **2007** RB silencing compromises the DNA damage-induced G2/M checkpoint and causes deregulated expression of the ECT2 oncogene. Oncogene. Jan 25;26(4):509-20.

Eissenberg JC, Elgin SC. **2000** The HP1 protein family: getting a grip on chromatin. Curr Opin Genet Dev. Apr;10(2):204-10.

Eissenberg JC, James TC, Foster-Hartnett DM, Hartnett T, Ngan V, Elgin SC. **1990** Mutation in a heterochromatin-specific chromosomal protein is associated with suppression of position-effect variegation in Drosophila melanogaster. Proc Natl Acad Sci U S A. Dec;87(24):9923-7.

Eissenberg JC, Morris GD, Reuter G, Hartnett T. **1992** The heterochromatin-associated protein HP-1 is an essential protein in Drosophila with dosage-dependent effects on position-effect variegation. Genetics. Jun;131(2):345-52.

Ekwall K, Javerzat JP, Lorentz A, Schmidt H, Cranston G, Allshire R. **1995** The chromodomain protein Swi6: a key component at fission yeast centromeres. Science. Sep 8;269(5229):1429-31.

Ekwall K, Nimmo ER, Javerzat JP, Borgstrøm B, Egel R, Cranston G, Allshire R. **1996** Mutations in the fission yeast silencing factors clr4+ and rik1+ disrupt the localisation of the chromo domain protein Swi6p and impair centromere function. J Cell Sci. Nov;109 (Pt 11):2637-48.

Fanti L, Berloco M, Piacentini L, Pimpinelli S. **2003** Chromosomal distribution of heterochromatin protein 1 (HP1) in Drosophila: a cytological map of euchromatic HP1 binding sites. Genetica. Mar;117(2-3):135-47.

Fanti L, Giovinazzo G, Berloco M, Pimpinelli S. **1998** The heterochromatin protein 1 prevents telomere fusions in Drosophila. Mol Cell. Nov;2(5):527-38.

Festenstein R, Pagakis SN, Hiragami K, Lyon D, Verreault A, Sekkali B, Kioussis D. **2003** Modulation of heterochromatin protein 1 dynamics in primary Mammalian cells. Science. Jan 31;299(5607):719-21.

Fischer T, Cui B, Dhakshnamoorthy J, Zhou M, Rubin C, Zofall M, Veenstra TD, Grewal SI. **2009** Diverse roles of HP1 proteins in heterochromatin assembly and functions in fission yeast. Proc Natl Acad Sci U S A. Jun 2;106(22):8998-9003.

Fischle W, Tseng BS, Dormann HL, Ueberheide BM, Garcia BA, Shabanowitz J, Hunt DF, Funabiki H, Allis CD. **2005** Regulation of HP1-chromatin binding by histone H3 methylation and phosphorylation. Nature. Dec 22;438(7071):1116-22.

Flemming F. **1880** Beitrag zur Kenntnis der Zelle und ihrer Lebenserscheinungen, Teil II. Archiv Mikrosk Anat 18: 151-259

Foijer F, Wolthuis RM, Doodeman V, Medema RH, te Riele H. **2005** Mitogen requirement for cell cycle progression in the absence of pocket protein activity. Cancer Cell. Dec;8(6):455-66.

Fridman AL, Tainsky MA. **2008** Critical pathways in cellular senescence and immortalization revealed by gene expression profiling. Oncogene. Oct 9;27(46):5975-87.

García-Cao M, Gonzalo S, Dean D, Blasco MA. **2002** A role for the Rb family of proteins in controlling telomere length. Nat Genet. Nov;32(3):415-9.

Garcia-Cao M, O'Sullivan R, Peters AH, Jenuwein T, Blasco MA. **2004** Epigenetic regulation of telomere length in mammalian cells by the Suv39h1 and Suv39h2 histone methyltransferases. Nat Genet. Jan;36(1):94-9.

Gelato KA, Fischle W. **2008** Role of histone modifications in defining chromatin structure and function. Biol Chem. Apr;389(4):353-63.

Gil J, Peters G. **2006** Regulation of the INK4b-ARF-INK4a tumour suppressor locus: all for one or one for all. Nat Rev Mol Cell Biol. Sep;7(9):667-77.

Gilbert N, Allan J. **2001** Distinctive higher-order chromatin structure at mammalian centromeres. Proc Natl Acad Sci U S A. Oct 9;98(21):11949-54.

Gilbert N, Boyle S, Sutherland H, de Las Heras J, Allan J, Jenuwein T, Bickmore WA. **2003** Formation of facultative heterochromatin in the absence of HP1. EMBO J. Oct 15;22(20):5540-50.

Gonzalez C, Casal Jimenez J, Ripoll P, Sunkel CE. **1991** The spindle is required for the process of sister chromatid separation in Drosophila neuroblasts. Exp Cell Res. Jan;192(1):10-5.

Gonzalo S, Blasco MA. **2005** Role of Rb family in the epigenetic definition of chromatin. Cell Cycle. Jun;4(6):752-5.

Gonzalo S, García-Cao M, Fraga MF, Schotta G, Peters AH, Cotter SE, Eguía R, Dean DC, Esteller M, Jenuwein T, Blasco MA. **2005** Role of the RB1 family in stabilizing histone methylation at constitutive heterochromatin. Nat Cell Biol. Apr;7(4):420-8.

Grewal SI, Moazed D. **2003** Heterochromatin and epigenetic control of gene expression. Science. Aug 8;301(5634):798-802.

Grewal SI. **2010** RNAi-dependent formation of heterochromatin and its diverse functions. Curr Opin Genet Dev. Apr;20(2):134-41.

Griffith JD, Comeau L, Rosenfield S, Stansel RM, Bianchi A, Moss H, de Lange T. **1999** Mammalian telomeres end in a large duplex loop. Cell. May 14;97(4):503-14.

Guenatri M, Bailly D, Maison C, Almouzni G. **2004** Mouse centric and pericentric satellite repeats form distinct functional heterochromatin. J Cell Biol. Aug 16;166(4):493-505.

Guerra C, Mijimolle N, Dhawahir A, Dubus P, Barradas M, Serrano M, Campuzano V, Barbacid M. **2003** Tumor induction by an endogenous K-ras oncogene is highly dependent on cellular context. Cancer Cell. Aug;4(2):111-20.

Hall IM, Noma K, Grewal SI. **2003** RNA interference machinery regulates chromosome dynamics during mitosis and meiosis in fission yeast. Proc Natl Acad Sci U S A. Jan 7;100(1):193-8.

Hall IM, Shankaranarayana GD, Noma K, Ayoub N, Cohen A, Grewal SI. **2002** Establishment and maintenance of a heterochromatin domain. Science. Sep 27;297(5590):2232-7.

Hastie ND, Dempster M, Dunlop MG, Thompson AM, Green DK, Allshire RC. **1990** Telomere reduction in human colorectal carcinoma and with ageing. Nature. Aug 30;346(6287):866-8.

Hayflick L, Moorhead PS. **1961** The serial cultivation of human diploid cell strains. Exp Cell Res. Dec;25:585-621.

Heitz, E. **1928** Das heterochromatin der moose. I Jahrb Wiss Botanik 69, 762–818 (in German).

Hirota T, Lipp JJ, Toh BH, Peters JM. **2005** Histone H3 serine 10 phosphorylation by Aurora B causes HP1 dissociation from heterochromatin. Nature. Dec 22;438(7071):1176-80.

Ho L, Crabtree GR. **2010** Chromatin remodelling during development. Nature. Jan 28;463(7280):474-84

Ho VM, Schaffer BE, Karnezis AN, Park KS, Sage J. **2009** The retinoblastoma gene Rb and its family member p130 suppress lung adenocarcinoma induced by oncogenic K-Ras. Oncogene. Mar 12;28(10):1393-9.

Hockemeyer D, Daniels JP, Takai H, de Lange T. **2006** Recent expansion of the telomeric complex in rodents: Two distinct POT1 proteins protect mouse telomeres. Cell. Jul 14;126(1):63-77.

Hockemeyer D, Palm W, Else T, Daniels JP, Takai KK, Ye JZ, Keegan CE, de Lange T, Hammer GD. **2007** Telomere protection by mammalian Pot1 requires interaction with Tpp1. Nat Struct Mol Biol. Aug;14(8):754-61.

Holliday R, Pugh JE. **1975** DNA modification mechanisms and gene activity during development. Science. Jan 24;187(4173):226-32.

Huang Y, Myers MP, Xu RM. **2006** Crystal structure of the HP1-EMSY complex reveals an unusual mode of HP1 binding. Structure. Apr;14(4):703-12.

Hughes SE, Hawley RS. **2009** Heterochromatin: a rapidly evolving species barrier. PLoS Biol. Oct;7(10):e1000233.

Itahana K, Zou Y, Itahana Y, Martinez JL, Beausejour C, Jacobs JJ, Van Lohuizen M, Band V, Campisi J, Dimri GP. **2003** Control of the replicative life span of human fibroblasts by p16 and the polycomb protein Bmi-1. Mol Cell Biol. Jan;23(1):389-401.

Jacobs SA, Khorasanizadeh S. **2002** Structure of HP1 chromodomain bound to a lysine 9-methylated histone H3 tail. Science. Mar 15;295(5562):2080-3.

Jacobs SA, Taverna SD, Zhang Y, Briggs SD, Li J, Eissenberg JC, Allis CD, Khorasanizadeh S. **2001** Specificity of the HP1 chromo domain for the methylated N-terminus of histone H3. EMBO J. Sep 17;20(18):5232-41.

James TC, Eissenberg JC, Craig C, Dietrich V, Hobson A, Elgin SC. **1989** Distribution patterns of HP1, a heterochromatin-associated nonhistone chromosomal protein of Drosophila. Eur J Cell Biol. Oct;50(1):170-80.

James TC, Elgin SC. **1986** Identification of a nonhistone chromosomal protein associated with heterochromatin in Drosophila melanogaster and its gene. Mol Cell Biol. Nov;6(11):3862-72.

Javerzat JP. **2010** Molecular biology. Directing the centromere guardian. Science. Jan 8;327(5962):150-1.

Jones DO, Cowell IG, Singh PB. **2000** Mammalian chromodomain proteins: their role in genome organisation and expression. Bioessays. Feb;22(2):124-37.

Kamijo T, Zindy F, Roussel MF, Quelle DE, Downing JR, Ashmun RA, Grosveld G, Sherr CJ. **1997** Tumor suppression at the mouse INK4a locus mediated by the alternative reading frame product p19ARF. Cell. Nov 28;91(5):649-59.

Kaplan W, Hüsler P, Klump H, Erhardt J, Sluis-Cremer N, Dirr H. **1997** Conformational stability of pGEX-expressed Schistosoma japonicum glutathione S-transferase: a detoxification enzyme and fusion-protein affinity tag. Protein Sci. Feb;6(2):399-406.

Karlseder J, Kachatrian L, Takai H, Mercer K, Hingorani S, Jacks T, de Lange T. **2003** Targeted deletion reveals an essential function for the telomere length regulator Trf1. Mol Cell Biol. Sep;23(18):6533-41.

Kawashima SA, Yamagishi Y, Honda T, Ishiguro K, Watanabe Y. **2010** Phosphorylation of H2A by Bub1 prevents chromosomal instability through localizing shugoshin. Science. Jan 8;327(5962):172-7.

Kennedy BK, Barbie DA, Classon M, Dyson N, Harlow E. **2000** Nuclear organization of DNA replication in primary mammalian cells. Genes Dev. Nov 15;14(22):2855-68.

Kerrebrock AW, Moore DP, Wu JS, Orr-Weaver TL. **1995** Mei-S332, a Drosophila protein required for sister-chromatid cohesion, can localize to meiotic centromere regions. Cell. Oct 20;83(2):247-56.

Kim WY, Sharpless NE. **2006** The regulation of INK4/ARF in cancer and ageing. Cell. Oct 20;127(2):265-75.

Kipling D, Cooke HJ. **1990** Hypervariable ultra-long telomeres in mice. Nature. Sep 27;347(6291):400-2.

Kitajima TS, Hauf S, Ohsugi M, Yamamoto T, Watanabe Y. **2005** Human Bub1 defines the persistent cohesion site along the mitotic chromosome by affecting Shugoshin localization. Curr Biol. Feb 22;15(4):353-9.

Kitajima TS, Sakuno T, Ishiguro K, Iemura S, Natsume T, Kawashima SA, Watanabe Y. **2006** Shugoshin collaborates with protein phosphatase 2A to protect cohesin. Nature. May 4;441(7089):46-52.

Kitajima TS, Yokobayashi S, Yamamoto M, Watanabe Y. **2003** Distinct cohesin complexes organize meiotic chromosome domains. Science. May 16;300(5622):1152-5.

Koch B, Kueng S, Ruckenbauer C, Wendt KS, Peters JM. **2008** The Suv39h-HP1 histone methylation pathway is dispensable for enrichment and protection of cohesin at centromeres in mammalian cells. Chromosoma. Apr;117(2):199-210.

Kourmouli N, Jeppesen P, Mahadevhaiah S, Burgoyne P, Wu R, Gilbert DM, Bongiorni S, Prantera G, Fanti L, Pimpinelli S, Shi W, Fundele R, Singh PB. **2004** Heterochromatin and tri-methylated lysine 20 of histone H4 in animals. J Cell Sci. May 15;117(Pt 12):2491-501.

Kourmouli N, Sun YM, van der Sar S, Singh PB, Brown JP. **2005** Epigenetic regulation of mammalian pericentric heterochromatin in vivo by HP1. Biochem Biophys Res Commun. Nov 25;337(3):901-7.

Lachner M, O'Carroll D, Rea S, Mechtler K, Jenuwein T. **2001** Methylation of histone H3 lysine 9 creates a binding site for HP1 proteins. Nature. Mar 1;410(6824):116-20.

Lam AL, Boivin CD, Bonney CF, Rudd MK, Sullivan BA. **2006** Human centromeric chromatin is a dynamic chromosomal domain that can spread over noncentromeric DNA. Proc Natl Acad Sci U S A. Mar 14;103(11):4186-91.

Lazzerini Denchi E, Attwooll C, Pasini D, Helin K. **2005** Deregulated E2F activity induces hyperplasia and senescence-like features in the mouse pituitary gland. Mol Cell Biol. Apr;25(7):2660-72.

Lechner MS, Schultz DC, Negorev D, Maul GG, Rauscher FJ 3rd. **2005** The mammalian heterochromatin protein 1 binds diverse nuclear proteins through a common motif that targets the chromoshadow domain. Biochem Biophys Res Commun. Jun 17;331(4):929-37.

Lee JY, Orr-Weaver TL. **2001**The molecular basis of sister-chromatid cohesion. Annu Rev Cell Dev Biol.;17:753-77.

Lejnine S, Makarov VL, Langmore JP. **1995** Conserved nucleoprotein structure at the ends of vertebrate and invertebrate chromosomes. Proc Natl Acad Sci U S A. Mar 14;92(6):2393-7.

Li Y, Danzer JR, Alvarez P, Belmont AS, Wallrath LL. **2003** Effects of tethering HP1 to euchromatic regions of the Drosophila genome. Development. May;130(9):1817-24.

Liu D, Safari A, O'Connor MS, Chan DW, Laegeler A, Qin J, Songyang Z. **2004** PTOP interacts with POT1 and regulates its localization to telomeres. Nat Cell Biol. Jul;6(7):673-80.

Lomberk G, Bensi D, Fernandez-Zapico ME, Urrutia R. **2006** Evidence for the existence of an HP1-mediated subcode within the histone code. Nat Cell Biol. Apr;8(4):407-15.

Losada A, Hirano M, Hirano T. **2002** Cohesin release is required for sister chromatid resolution, but not for condensin-mediated compaction, at the onset of mitosis. Genes Dev. Dec 1;16(23):3004-16.

Lowry OH, Rosebrough NJ, Farr AL, Randall RJ. **1951** Protein measurement with the Folin phenol reagent. J Biol Chem. Nov;193(1):265-75.

Lue NF. **2004** Adding to the ends: what makes telomerase processive and how important is it? Bioessays. Sep;26(9):955-62.

Luger K, Mäder AW, Richmond RK, Sargent DF, Richmond TJ. **1997** Crystal structure of the nucleosome core particle at 2.8 A resolution. Nature. Sep 18;389(6648):251-60.

Luijsterburg MS, Dinant C, Lans H, Stap J, Wiernasz E, Lagerwerf S, Warmerdam DO, Lindh M, Brink MC, Dobrucki JW, Aten JA, Fousteri MI, Jansen G, Dantuma NP, Vermeulen W, Mullenders LH, Houtsmuller AB, Verschure PJ, van Driel R. **2009** Heterochromatin protein 1 is recruited to various types of DNA damage. J Cell Biol. May 18;185(4):577-86.

Lundberg AS, Hahn WC, Gupta P, Weinberg RA. **2000** Genes involved in senescence and immortalization. Curr Opin Cell Biol. Dec;12(6):705-9.

Majumder PK, Grisanzio C, O'Connell F, Barry M, Brito JM, Xu Q, Guney I, Berger R, Herman P, Bikoff R, Fedele G, Baek WK, Wang S, Ellwood-Yen K, Wu H, Sawyers CL, Signoretti S, Hahn WC, Loda M, Sellers WR. **2008** A prostatic intraepithelial neoplasia-dependent p27 Kip1 checkpoint induces senescence and inhibits cell proliferation and cancer progression. Cancer Cell. Aug 12;14(2):146-55.

Makarov VL, Lejnine S, Bedoyan J, Langmore JP. **1993** Nucleosomal organization of telomere-specific chromatin in rat. Cell. May 21;73(4):775-87.

Martínez P, Thanasoula M, Muñoz P, Liao C, Tejera A, McNees C, Flores JM, Fernández-Capetillo O, Tarsounas M, Blasco MA. **2009** Increased telomere fragility and fusions resulting from TRF1 deficiency lead to degenerative pathologies and increased cancer in mice. Genes Dev. Sep 1;23(17):2060-75.

Mayhew CN, Bosco EE, Fox SR, Okaya T, Tarapore P, Schwemberger SJ, Babcock GF, Lentsch AB, Fukasawa K, Knudsen ES. **2005** Liver-specific pRB loss results in ectopic cell cycle entry and aberrant ploidy. Cancer Res. Jun 1;65(11):4568-77.

McGuinness BE, Hirota T, Kudo NR, Peters JM, Nasmyth K. **2005** Shugoshin prevents dissociation of cohesin from centromeres during mitosis in vertebrate cells. PLoS Biol. Mar;3(3):e86.

Meshorer E, Misteli T. **2006** Chromatin in pluripotent embryonic stem cells and differentiation. Nat Rev Mol Cell Biol. Jul;7(7):540-6.

Michaloglou C, Vredeveld LC, Soengas MS, Denoyelle C, Kuilman T, van der Horst CM, Majoor DM, Shay JW, Mooi WJ, Peeper DS. **2005** BRAFE600-associated senescence-like cell cycle arrest of human naevi. Nature. Aug 4;436(7051):720-4.

Minc E, Allory Y, Worman HJ, Courvalin JC, Buendia B. **1999** Localization and phosphorylation of HP1 proteins during the cell cycle in mammalian cells. Chromosoma. Aug;108(4):220-34.

Minc E, Courvalin JC, Buendia B. **2000**HP1gamma associates with euchromatin and heterochromatin in mammalian nuclei and chromosomes. Cytogenet Cell Genet.;90(3-4):279-84.

Mizuguchi G, Shen X, Landry J, Wu WH, Sen S, Wu C. **2004** ATP-driven exchange of histone H2AZ variant catalyzed by SWR1 chromatin remodeling complex. Science. Jan 16;303(5656):343-8.

Muller HJ. **1930** Types of visible variations induced by X-rays in Drosophila. J. Genet. 22, 299–334.

Muntoni A, Reddel RR. **2005** The first molecular details of ALT in human tumor cells. Hum Mol Genet. Oct 15;14 Spec No. 2:R191-6.

Murzina N, Verreault A, Laue E, Stillman B. **1999** Heterochromatin dynamics in mouse cells: interaction between chromatin assembly factor 1 and HP1 proteins. Mol Cell. Oct;4(4):529-40.

Nakayama J, Klar AJ, Grewal SI. **2000** A chromodomain protein, Swi6, performs imprinting functions in fission yeast during mitosis and meiosis. Cell. Apr 28;101(3):307-17.

Narita M, Narita M, Krizhanovsky V, Nuñez S, Chicas A, Hearn SA, Myers MP, Lowe SW. **2006** A novel role for high-mobility group a proteins in cellular senescence and heterochromatin formation. Cell. Aug 11;126(3):503-14.

Narita M, Nũnez S, Heard E, Narita M, Lin AW, Hearn SA, Spector DL, Hannon GJ, Lowe SW. **2003** Rb-mediated heterochromatin formation and silencing of E2F target genes during cellular senescence. Cell. Jun 13;113(6):703-16.

Netzer C, Rieger L, Brero A, Zhang CD, Hinzke M, Kohlhase J, Bohlander SK. **2001** SALL1, the gene mutated in Townes-Brocks syndrome, encodes a transcriptional repressor which interacts with TRF1/PIN2 and localizes to pericentromeric heterochromatin. Hum Mol Genet. Dec 15;10(26):3017-24.

Neumeister P, Albanese C, Balent B, Greally J, Pestell RG. **2002** Senescence and epigenetic dysregulation in cancer. Int J Biochem Cell Biol. Nov;34(11):1475-90.

Nielsen AL, Ortiz JA, You J, Oulad-Abdelghani M, Khechumian R, Gansmuller A, Chambon P, Losson R. **1999** Interaction with members of the heterochromatin protein 1 (HP1) family and histone deacetylation are differentially involved in transcriptional silencing by members of the TIF1 family. EMBO J. Nov 15;18(22):6385-95.

Nielsen AL, Oulad-Abdelghani M, Ortiz JA, Remboutsika E, Chambon P, Losson R. **2001** Heterochromatin formation in mammalian cells: interaction between histones and HP1 proteins. Mol Cell. Apr;7(4):729-39.

Nielsen PR, Nietlispach D, Mott HR, Callaghan J, Bannister A, Kouzarides T, Murzin AG, Murzina NV, Laue ED. **2002** Structure of the HP1 chromodomain bound to histone H3 methylated at lysine 9. Nature. Mar 7;416(6876):103-7.

Nielsen SJ, Schneider R, Bauer UM, Bannister AJ, Morrison A, O'Carroll D, Firestein R, Cleary M, Jenuwein T, Herrera RE, Kouzarides T. **2001** Rb targets histone H3 methylation and HP1 to promoters. Nature. Aug 2;412(6846):561-5.

Nishimura K, Hirokawa YS, Mizutani H, Shiraishi T. **2006** Reduced heterochromatin protein 1-beta (HP1beta) expression is correlated with increased invasive activity in human melanoma cells. Anticancer Res. Nov Dec;26(6B):4349-56.

Noma K, Allis CD, Grewal SI. **2001** Transitions in distinct histone H3 methylation patterns at the heterochromatin domain boundaries. Science. Aug 10;293(5532):1150-5.

Nonaka N, Kitajima T, Yokobayashi S, Xiao G, Yamamoto M, Grewal SI, Watanabe Y. **2002** Recruitment of cohesin to heterochromatic regions by Swi6/HP1 in fission yeast. Nat Cell Biol. Jan;4(1):89-93.

Okamoto K, Iwano T, Tachibana M, Shinkai Y. **2008** Distinct roles of TRF1 in the regulation of telomere structure and lengthening. J Biol Chem. Aug 29;283(35):23981-8.

Onn I, Heidinger-Pauli JM, Guacci V, Unal E, Koshland DE. **2008**Sister chromatid cohesion: a simple concept with a complex reality. Annu Rev Cell Dev Biol.;24:105-29.

O'Sullivan RJ, Karlseder J. **2010** Telomeres: protecting chromosomes against genome instability. Nat Rev Mol Cell Biol. Mar;11(3):171-81.

Palm W, de Lange T. **2008** How shelterin protects mammalian telomeres. Annu Rev Genet.;42:301-34.

Paro R, Hogness DS. **1991** The Polycomb protein shares a homologous domain with a heterochromatin-associated protein of Drosophila. Proc Natl Acad Sci U S A. Jan 1;88(1):263-7.

Partridge JF, Borgstrøm B, Allshire RC. **2000** Distinct protein interaction domains and protein spreading in a complex centromere. Genes Dev. Apr 1;14(7):783-91.

Peng JC, Karpen GH. **2007** H3K9 methylation and RNA interference regulate nucleolar organization and repeated DNA stability. Nat Cell Biol. Jan;9(1):25-35.

Perrini B, Piacentini L, Fanti L, Altieri F, Chichiarelli S, Berloco M, Turano C, Ferraro A, Pimpinelli S. **2004** HP1 controls telomere capping, telomere elongation, and telomere silencing by two different mechanisms in Drosophila. Mol Cell. Aug 13;15(3):467-76.

Peters AH, O'Carroll D, Scherthan H, Mechtler K, Sauer S, Schöfer C, Weipoltshammer K, Pagani M, Lachner M, Kohlmaier A, Opravil S, Doyle M, Sibilia M, Jenuwein T. **2001** Loss of the Suv39h histone methyltransferases impairs mammalian heterochromatin and genome stability. Cell. Nov 2;107(3):323-37.

Peters JM, Tedeschi A, Schmitz J. **2008** The cohesin complex and its roles in chromosome biology. Genes Dev. Nov 15;22(22):3089-114.

Pidoux AL, Allshire RC. **2005** The role of heterochromatin in centromere function. Philos Trans R Soc Lond B Biol Sci. Mar 29;360(1455):569-79.

Platero JS, Hartnett T, Eissenberg JC. **1995** Functional analysis of the chromo domain of HP1. EMBO J. Aug 15;14(16):3977-86.

Razin A, Riggs AD. **1980** DNA methylation and gene function. Science. Nov 7;210(4470):604-10.

Rea S, Eisenhaber F, O'Carroll D, Strahl BD, Sun ZW, Schmid M, Opravil S, Mechtler K, Ponting CP, Allis CD, Jenuwein T. **2000** Regulation of chromatin structure by site-specific histone H3 methyltransferases. Nature. Aug 10;406(6796):593-9.

Reinhart BJ, Bartel DP. **2002** Small RNAs correspond to centromere heterochromatic repeats. Science. Sep 13;297(5588):1831.

Reuter G, Spierer P. **1992** Position effect variegation and chromatin proteins. Bioessays. Sep;14(9):605-12.

Riedel CG, Katis VL, Katou Y, Mori S, Itoh T, Helmhart W, Gálová M, Petronczki M, Gregan J, Cetin B, Mudrak I, Ogris E, Mechtler K, Pelletier L, Buchholz F, Shirahige K, Nasmyth K. **2006** Protein phosphatase 2A protects centromeric sister chromatid cohesion during meiosis I. Nature. May 4;441(7089):53-61.

Riggs AD and Porter TN. **1996** Overview of epigenetic mechanisms. In Epigenetic Mechanisms of Gene Regulation (ed. VEA Russo *et al.*, Cold Spring Harbor Laboratory Press, Woodbury,).

Riggs AD. **1975** X inactivation, differentiation, and DNA methylation. Cytogenet Cell Genet.;14(1):9-25.

Riha K, Heacock ML, Shippen DE. **2006** The role of the nonhomologous end-joining DNA double-strand break repair pathway in telomere biology. Annu Rev Genet.;40:237-77.

Ritou E, Bai M, Georgatos SD. **2007** Variant-specific patterns and humoral regulation of HP1 proteins in human cells and tissues. J Cell Sci. Oct 1;120(Pt 19):3425-35.

Ruhl DD, Jin J, Cai Y, Swanson S, Florens L, Washburn MP, Conaway RC, Conaway JW, Chrivia JC. **2006** Purification of a human SRCAP complex that remodels chromatin by incorporating the histone variant H2A.Z into nucleosomes. Biochemistry. May 2;45(17):5671-7.

Salic A, Waters JC, Mitchison TJ. **2004** Vertebrate shugoshin links sister centromere cohesion and kinetochore microtubule stability in mitosis. Cell. Sep 3;118(5):567-78.

Sarma K, Reinberg D. **2005** Histone variants meet their match. Nat Rev Mol Cell Biol. Feb;6(2):139-49.

Sarthy J, Bae NS, Scrafford J, Baumann P. **2009** Human RAP1 inhibits non-homologous end joining at telomeres. EMBO J. Nov 4;28(21):3390-9.

Schmiedeberg L, Weisshart K, Diekmann S, Meyer Zu Hoerste G, Hemmerich P. **2004** High- and low-mobility populations of HP1 in heterochromatin of mammalian cells. Mol Biol Cell. Jun;15(6):2819-33.

Schotta G, Lachner M, Sarma K, Ebert A, Sengupta R, Reuter G, Reinberg D, Jenuwein T. **2004** A silencing pathway to induce H3-K9 and H4-K20 trimethylation at constitutive heterochromatin. Genes Dev. Jun 1;18(11):1251-62.

Schübeler D. **2009** Epigenomics: Methylation matters. Nature. Nov 19;462(7271):296-7.

Schultz, J. **1939** The function of heterochromatin. Proc. VII Int. Congr. Genet pp. 257–262.

Serrano A, Rodríguez-Corsino M, Losada A. **2009** Heterochromatin protein 1 (HP1) proteins do not drive pericentromeric cohesin enrichment in human cells. PLoS One.;4(4):e5118.

Serrano M, Lin AW, McCurrach ME, Beach D, Lowe SW. **1997** Oncogenic ras provokes premature cell senescence associated with accumulation of p53 and p16INK4a. Cell. Mar 7;88(5):593-602.

Serrano M, Blasco MA. **2001** Putting the stress on senescence. Curr Opin Cell Biol. Dec;13(6):748-53.

Sharma GG, Hwang KK, Pandita RK, Gupta A, Dhar S, Parenteau J, Agarwal M, Worman HJ, Wellinger RJ, Pandita TK. **2003** Human heterochromatin protein 1 isoforms HP1(Hsalpha) and HP1(Hsbeta) interfere with hTERT-telomere interactions and correlate with changes in cell growth and response to ionizing radiation. Mol Cell Biol. Nov;23(22):8363-76.

Singh PB, Miller JR, Pearce J, Kothary R, Burton RD, Paro R, James TC, Gaunt SJ. **1991** A sequence motif found in a Drosophila heterochromatin protein is conserved in animals and plants. Nucleic Acids Res. Feb 25;19(4):789-94.

Smogorzewska A, van Steensel B, Bianchi A, Oelmann S, Schaefer MR, Schnapp G, de Lange T. **2000** Control of human telomere length by TRF1 and TRF2. Mol Cell Biol. Mar;20(5):1659-68.

Srinivasan SV, Mayhew CN, Schwemberger S, Zagorski W, Knudsen ES. **2007** RB loss promotes aberrant ploidy by deregulating levels and activity of DNA replication factors. J Biol Chem. Aug 17;282(33):23867-77.

Strahl BD, Allis CD. **2000** The language of covalent histone modifications. Nature. Jan 6;403(6765):41-5.

Sullivan BA, Karpen GH. **2004** Centromeric chromatin exhibits a histone modification pattern that is distinct from both euchromatin and heterochromatin. Nat Struct Mol Biol. Nov;11(11):1076-83.

Takanashi M, Oikawa K, Fujita K, Kudo M, Kinoshita M, Kuroda M. **2009** Heterochromatin protein 1gamma epigenetically regulates cell differentiation and exhibits potential as a therapeutic target for various types of cancers. Am J Pathol. Jan;174(1):309-16.

Tang Z, Shu H, Qi W, Mahmood NA, Mumby MC, Yu H. **2006** PP2A is required for centromeric localization of Sgo1 and proper chromosome segregation. Dev Cell. May;10(5):575-85.

Tang Z, Sun Y, Harley SE, Zou H, Yu H. **2004** Human Bub1 protects centromeric sister-chromatid cohesion through Shugoshin during mitosis. Proc Natl Acad Sci U S A. Dec 28;101(52):18012-7.

Thiru A, Nietlispach D, Mott HR, Okuwaki M, Lyon D, Nielsen PR, Hirshberg M, Verreault A, Murzina NV, Laue ED. **2004** Structural basis of HP1/PXVXL motif peptide interactions and HP1 localisation to heterochromatin. EMBO J. Feb 11;23(3):489-99.

Torras-Llort M, Moreno-Moreno O, Azorín F. **2009** Focus on the centre: the role of chromatin on the regulation of centromere identity and function. EMBO J. Aug 19;28(16):2337-48.

Trimarchi JM, Lees JA. **2002** Sibling rivalry in the E2F family. Nat Rev Mol Cell Biol. Jan;3(1):11-20.

Tschiersch B, Hofmann A, Krauss V, Dorn R, Korge G, Reuter G. **1994** The protein encoded by the Drosophila position-effect variegation suppressor gene Su(var)3-9 combines domains of antagonistic regulators of homeotic gene complexes. EMBO J. Aug 15;13(16):3822-31.

Tsukiyama T, Daniel C, Tamkun J, Wu C. **1995** ISWI, a member of the SWI2/SNF2 ATPase family, encodes the 140 kDa subunit of the nucleosome remodeling factor. Cell. Dec 15;83(6):1021-6.

Ueno M, Murase T, Kibe T, Ohashi N, Tomita K, Murakami Y, Uritani M, Ushimaru T, Harata M. **2004** Fission yeast Arp6 is required for telomere silencing, but functions independently of Swi6. Nucleic Acids Res. Feb 2;32(2):736-41.

Uhlmann F, Nasmyth K. **1998** Cohesion between sister chromatids must be established during DNA replication. Curr Biol. Oct 8;8(20):1095-101.

Vakoc CR, Mandat SA, Olenchock BA, Blobel GA. **2005** Histone H3 lysine 9 methylation and HP1gamma are associated with transcription elongation through mammalian chromatin. Mol Cell. Aug 5;19(3):381-91.

van Steensel B, de Lange T. **1997** Control of telomere length by the human telomeric protein TRF1. Nature. Feb 20;385(6618):740-3.

Varga-Weisz PD, Wilm M, Bonte E, Dumas K, Mann M, Becker PB. **1997** Chromatin-remodelling factor CHRAC contains the ATPases ISWI and topoisomerase II. Nature. Aug 7;388(6642):598-602.

Volpe TA, Kidner C, Hall IM, Teng G, Grewal SI, Martienssen RA. **2002** Regulation of heterochromatic silencing and histone H3 lysine-9 methylation by RNAi. Science. Sep 13;297(5588):1833-7.

Waddington CH. **1939** An Introduction to Modern Genetics (Allen & Unwin, London)

Waddington CH. **1942** Endeavour 1, 18–20.

Waizenegger IC, Hauf S, Meinke A, Peters JM. **2000** Two distinct pathways remove mammalian cohesin from chromosome arms in prophase and from centromeres in anaphase. Cell. Oct 27;103(3):399-410.

Watrin E, Schleiffer A, Tanaka K, Eisenhaber F, Nasmyth K, Peters JM. **2006** Human Scc4 is required for cohesin binding to chromatin, sister-chromatid cohesion, and mitotic progression. Curr Biol. May 9;16(9):863-74.

Wirth KG, Wutz G, Kudo NR, Desdouets C, Zetterberg A, Taghybeeglu S, Seznec J, Ducos GM, Ricci R, Firnberg N, Peters JM, Nasmyth K. **2006** Separase: a universal trigger for sister chromatid disjunction but not chromosome cycle progression. J Cell Biol. Mar 13;172(6):847-60.

Wreggett KA, Hill F, James PS, Hutchings A, Butcher GW, Singh PB. **1994**A mammalian homologue of Drosophila heterochromatin protein 1 (HP1) is a component of constitutive heterochromatin. Cytogenet Cell Genet.;66(2):99-103.

Wu L, Multani AS, He H, Cosme-Blanco W, Deng Y, Deng JM, Bachilo O, Pathak S, Tahara H, Bailey SM, Deng Y, Behringer RR, Chang S. **2006** Pot1 deficiency initiates DNA damage checkpoint activation and aberrant homologous recombination at telomeres. Cell. Jul 14;126(1):49-62.

Xin H, Liu D, Wan M, Safari A, Kim H, Sun W, O'Connor MS, Songyang Z. **2007** TPP1 is a homologue of ciliate TEBP-beta and interacts with POT1 to recruit telomerase. Nature. Feb 1;445(7127):559-62.

Yamagishi Y, Sakuno T, Shimura M, Watanabe Y. **2008** Heterochromatin links to centromeric protection by recruiting shugoshin. Nature. Sep 11;455(7210):251-5.

Ye JZ, Hockemeyer D, Krutchinsky AN, Loayza D, Hooper SM, Chait BT, de Lange T. **2004** POT1-interacting protein PIP1: a telomere length regulator that recruits POT1 to the TIN2/TRF1 complex. Genes Dev. Jul 15;18(14):1649-54.

Zarebski M, Wiernasz E, Dobrucki JW. **2009** Recruitment of heterochromatin protein 1 to DNA repair sites. Cytometry A. Jul;75(7):619-25.

Zeng W, de Greef JC, Chen YY, Chien R, Kong X, Gregson HC, Winokur ST, Pyle A, Robertson KD, Schmiesing JA, Kimonis VE, Balog J, Frants RR, Ball AR Jr, Lock LF, Donovan PJ, van der Maarel SM, Yokomori K. **2009**

Specific loss of histone H3 lysine 9 trimethylation and HP1gamma/cohesin binding at D4Z4 repeats is associated with facioscapulohumeral dystrophy (FSHD). PLoS Genet. Jul;5(7):e1000559.

Zhang R, Liu ST, Chen W, Bonner M, Pehrson J, Yen TJ, Adams PD. **2007** HP1 proteins are essential for a dynamic nuclear response that rescues the function of perturbed heterochromatin in primary human cells. Mol Cell Biol. Feb;27(3):949-62.

Zhang R, Poustovoitov MV, Ye X, Santos HA, Chen W, Daganzo SM, Erzberger JP, Serebriiskii IG, Canutescu AA, Dunbrack RL, Pehrson JR, Berger JM, Kaufman PD, Adams PD. **2005** Formation of MacroH2A-containing senescence-associated heterochromatin foci and senescence driven by ASF1a and HIRA. Dev Cell. Jan;8(1):19-30.

Zheng L, Flesken-Nikitin A, Chen PL, Lee WH. **2002** Deficiency of Retinoblastoma gene in mouse embryonic stem cells leads to genetic instability. Cancer Res. May 1;62(9):2498-502.

Abstract

Heterochromatin protein 1 (HP1) proteins are fundamental units of heterochromatin packaging that are enriched at the centromeres and telomeres of nearly all eukaryotic chromosomes. HP1 homologues are found in a variety of organisms and are involved in the establishment and maintenance of higher-order chromatin structures by specifically recognizing and binding to (*tri*- and *di*-) methylated lysine 9 on histone H3. In mammals, there are three HP1 homologues termed HP1α (*Cbx5*), HP1β (*Cbx1*), and HP1γ (*Cbx3*). Among these three isoforms HP1β is the best characterized. Murine HP1β is essential for organismal survival. *Cbx1*$^{-/-}$ knockout mice are perinatal lethal and exhibit aberrant cerebral cortex development, reduced proliferation of neuronal precursors, widespread cell death and edema. *Cbx1*$^{-/-}$ neurospheres cultured *in vitro* show a dramatic genomic instability.

This study demonstrates that *Cbx1*$^{+/-}$ and *Cbx1*$^{-/-}$ mouse embryonic fibroblasts (MEFs) escape senescence crisis that is associated with gross chromosomal aberrations including aneuploidy, premature chromosome separations and telomere-telomere fusions. Telomeres of *Cbx1*$^{-/-}$ MEFs show reduced binding of the shelterin protein TRF1 with no change in the cellular localizations of POT1a, POT1b and TPP1 proteins compared to wild type (WT) cells. Telomere length analysis revealed that the telomeres of late passage *Cbx1*$^{-/-}$ MEFs are longer (~20 kb) than the WT controls. There was no change in the localization of cohesin protein SMC3, spindle assembly checkpoint protein BUB1 and SGO1. In an *in vitro* model of oncogene-induced senescence (OIS), introduction of *Cbx1*$^{-/-}$ mutation in cells expressing H-ras^{V12} oncogene did not result senescence bypass. *In vivo* experiments utilizing the inducible K-ras^{V12} oncogene expression in *Cbx1*$^{+/-}$ mice resulted in increased malignant adenocarcinomas in lungs, which were negative for the markers of senescence. Taken together these data indicate that HP1β acts as a tumour suppressor rather than mediating senescence in response to oncogenic stress. GST pull down experiments with WT HP1β, HP1β mutants and recombinant histone H3 showed that the binding of HP1β to histone H3 is resistant to 0.75 M NaCl concentrations and that HP1β chromoshadow domain is sufficient for this interaction. Isothermal calorimetry experiments confirmed that the binding affinity of HP1β for recombinant histone H3 was 4 times higher than its affinity for H3K9me3. V23M and F45E ("aromatic cage") mutations in the HP1β chromo domain were also shown to inhibit binding to H3K9me3 while retaining binding to histone H3.

In this study, the role of murine HP1β protein in the regulation of genome stability and senescence has been investigated, which provided insights into the role of HP1β in both processes. It has been shown that there is a high affinity binding of HP1β to the histone H3 histone-fold domain that is stronger than the affinity to H3K9me3. It is proposed that the loss of this high affinity interaction might result in the perinatal lethal phenotype seen in *Cbx1*$^{-/-}$ mice.

Zusammenfassung

Heterochromatin-Protein-1- (HP1-) Proteine sind grundlegende strukturelle Komponenten des Heterochromatins, die bevorzugt in den Centromeren und Telomeren fast aller eukaryotischer Chromosomen vorkommen. HP1-Homologe finden sich in zahlreichen Organismen und sind an der Bildung und Aufrechterhaltung von Chromatinstrukturen höherer Ordnung beteiligt. Dazu erkennen und binden sie spezifisch (*tri-* und *di-*) methylierte Lysin-9-Reste am Histon H3. In Säugern gibt es drei HP1-Homologe, nämlich HP1α (*Cbx5*), HP1β (*Cbx1*) und HP1γ (*Cbx3*), von denen HP1β das am besten charakterisierte darstellt. Das murine HP1β ist unabdingbar für das Überleben des Organismus. *Cbx1*$^{-/-}$-Nullmutanten sind perinatal letal und zeigen eine anomale Entwicklung des cerebralen Cortex, eine verringerte Proliferation von neuronalen Vorläuferzellen, ausgedehnten Zelltod und Ödeme. *In vitro* kultivierte *Cbx1*$^{-/-}$-Neurosphären weisen eine signifikante genomische Instabilität auf.

Diese Arbeit zeigt, dass murine embryonale Fibroblasten (MEF) der Genotypen *Cbx1*$^{+/-}$ und *Cbx1*$^{-/-}$ der Seneszenzkrise entkommen, die mit erheblichen Chromosomenanomalien einschließlich Aneuploidie, vorzeitiger Chromosomenseperation und Telomer-Telomer-Fusionen einhergeht. Telomere von *Cbx1*$^{-/-}$-MEF zeigen eine verringerte Bindung des Shelterin-Proteins TRF1, aber keine Veränderung der zellulären Lokalisation der Proteine POT1a, POT1b und TPP1 im Vergleich zu Wildtyp- (WT-) Zellen. Eine Analyse der Telomerlängen ergab, dass die Telomere von späten *Cbx1*$^{-/-}$-MEF-Passagen ~20 kb länger waren als WT-Kontrollen. Es konnten dabei keine Änderungen der Lokalisationen des Kohesinproteins SMC3, des Spindelkontrollpunkt-Proteins BUB1 sowie des SGO1-Proteins festgestellt werden. In einem *In-vitro*-Modell der Onkogen-induzierten Seneszenz (OIS) resultierte die Einführung der *Cbx1*$^{-/-}$-Mutation in H-ras^{V12}-Onkogen exprimierende Zellen nicht in einer Umgehung der Seneszenz. *In-vivo*-Experimente mit Hilfe einer induzierbaren K-ras^{V12}-Onkogenexpression in *Cbx1*$^{+/-}$-Mäusen führten zum vermehrten Auftreten maligner Adenokarzinome der Lunge, wobei diese keine Seneszenzmarker aufweisen. Zusammengenommen weisen diese Daten darauf hin, dass HP1β keine Induktion der Seneszenz als Antwort auf onkogenen Stress bewirkt, sondern vielmehr als Tumorsuppressor fungiert. GST-*pull-down*-Experimente mit WT-HP1β oder HP1β-Mutanten und rekombinantem Histon H3 zeigten, dass die Bindung von HP1β an Histon H3 resistent gegenüber einer Konzentration von 0.75 M NaCl ist und dass die *Chromoshadow*-Domäne ausreichend für diese Interaktion ist. Isothermale Kalorimetrie-Experimente zeigten, dass die Bindungsaffinität von HP1β zu rekombinantem Histon H3 viermal höher liegt als die Affinität zu H3K9me3. V23M- und F45E- ("aromatischer Käfig-") Mutationen in der HP1β-*Chromo*-Domäne zeigten weiterhin eine Inhibition der H3K9me3-Bindung während die Bindung zu Histon H3 erhalten bleibt.

In dieser Arbeit wurde die Rolle des murinen HP1β-Proteins bei der Regulation der Genomstabilität und Seneszenz untersucht, wobei sich Einblicke in die Involvierung von HP1β in beide Prozesse ergaben. Es wurde gezeigt, dass HP1β eine hohe Affinität zur *histone-fold*-Domäne des Histons H3 besitzt, welche über der Affinität zu H3K9me3 liegt. Hieraus ergibt sich, dass der Verlust dieser hochaffinen Interaktion den perinatal letalen Phänotyp von *Cbx1*$^{-/-}$-Mäusen bedingen könnte.

Acknowledgements

The work presented in this thesis would not be possible without the help and encouragement of many valuable people I would like to mention below.

First of all, I would like to thank **Dr. Prim Singh** for giving me the opportunity to work on a very exciting project and for his continuous guidance, support and advice throughout this thesis. His extraordinary example as a scientific investigator, a mentor and as an intellectual person is contagious and continuously boosted my motivation for science. I had learned a lot from the many conversations we had and enjoyed his roaring sense of humour. He taught me a great deal about "good" and "bad" science and I will always be indebted to him for this. The readability of this thesis has also benefited considerably from his feedback... *Thank you Prim, it was a privilege working with you!*

Prof. Johannes Gerdes deserves a special gratitude for his initial support in me and in this project. *Danke für alles Hannes!*

I would like to thank **Prof. Silvia Bulfone-Paus** for her support, trust and for taking the responsibility of being my supervisor.

Thank you, **Dr. Jörn Bullwinkel**, for bearing up with my never-ending questions, for your kind support, patience and proofreading this thesis. I am inspired by your work ethics, precision, and aim for perfection. I am also glad you introduced me in the art of drinking tea! *Danke Jörn!*

Without the support of the members of the lab group Immunoepigenetics, this work could have never been accomplished. I would like to thank **Ms Bettina Baron-Lühr** for her initial guidance and patience with me. I have learned many things from her including but not limited to culturing cells, organization and the art of saying "*tschüss*"... **Ms Anja Lüdemann** was always supportive and introduced me into many techniques used in this study. It would not be possible to organize hundreds of litres of bacterial cultures without the help of **Ms Tanja Mengden**. I am grateful to **Dr. Jeremy Brown** for the clarity of his mind and for his help in opening up mine. **Ms Katja Vertein** deserves special thanks for her dedication and hard work in protein expression. I must not forget **Ms Fabiana Fabretti** for her valuable assistance in the lab during her practical work. I also thank **Mr. Philipp Schneider, Mr. Giovanni Canu and Ms Kristina Jungius** for providing not only a scientifically motivating environment but also a perfect lab atmosphere.

I wish to acknowledge my collaborators for their excellent experimental contribution and stimulating scientific interest, especially **Prof. Hans Bartunik**, **Prof. Wolfgang Fischle**, **Prof. Yoichi Shinkai**, **Prof. Tim Brummendorf, Prof. Tej Pandita, Dr. Keiji Okamoto**, **Dr. Melanie Balabanov** and **Dr. Ute Brassat**.

I would like to thank **Ms Birgit Kullmann** and **Ms Doreen Beyer** for helping me in finding things whenever I needed them!

Prof. Ekkehard Vollmer and **Dr. Torsten Goldmann** deserve special thanks for their help and valuable support in histopathological analysis and access to state-of-the-art equipment. I am also indebted to **Ms Jasmin Tiebach** for her excellent support in sample preparation.

I wish to acknowledge the help of **Dr. Thomas Scholzen** in microscopy, in radioactive work and for proofreading this thesis.

I am grateful **to Dr. Sven Müller-Loennies** for his help in access to ITC equipment and data analysis. Many thanks go to **Ms Lena Heinbockel** for valuable conversations during culturing bacteria.

I would like to thank **Dr. Ilka Monath** and the **animal facility staff** for their support in animal experiments.

I am grateful to all past and present members of **Research Centre Borstel** for creating a scientifically motivating environment, providing help whenever needed, for many discussions and criticism and of course for the fun.

And of course, **Ms Gudrun Lehwark-Yvetot** deserves special thanks, for welcoming me in Borstel and for making the first few months run as smooth as possible. I must not forget my dear friends in *Ausländerbande* who made life in Borstel much colourful and enjoyable with their presence.

I would like to thank my gorgeous family, for their endless support and love: My mom, **Emel Billur**, who encouraged me so much in life and helped me become the person I am today. Families **Seifert**, **Lehmann**, **Trunte** and **Dr. Loysa** have always shown me so much love and caring. I feel quite fortunate having such wonderful people around me.

Special thanks go to my dear wife, **Diana**, for always being there for me in good and in bad times. I wouldn't have come so far without her love.

Last but not least, I would like to acknowledge **DFG** for financing this project and making it all possible in the first place.

Curriculum Vitae

Name: **Mustafa**
Surname: **Billur**
Date of birth: **04/01/1982**
Place of birth: **Famagusta, Cyprus**
Nationality: **Cypriot**

EDUCATION

2006-2010 PhD student
Division of Immunoepigenetics, Research Center Borstel, Germany

2004-2005 MSc in Applied Biosciences - Biotechnology
The Nottingham Trent University, Nottingham, UK

1999-2003 BSc in Biology majored in Zoology
Ege University, Faculty of Sciences, Biology Department, Izmir, Turkey

1996-1999 High School
Türk Maarif Koleji, Nicosia, Cyprus

1993-1996 Secondary School
Bayraktar Türk Maarif Koleji, Nicosia, Cyprus

Publications

Brown JP, Bullwinkel J, Baron-Lühr B, **Billur M**, Schneider P, Winking H, Singh PB. HP1gamma function is required for male germ cell survival and spermatogenesis. Epigenetics Chromatin. 2010 Apr 27;3(1):9.

Billur M, Bartunik HD, Singh PB. The essential function of HP1 beta: a case of the tail wagging the dog? Trends Biochem Sci. 2010 Feb;35(2):115-23.

Aucott R, Bullwinkel J, Yu Y, Shi W, **Billur M**, Brown JP, Menzel U, Kioussis D, Wang G, Reisert I, Weimer J, Pandita RK, Sharma GG, Pandita TK, Fundele R, Singh PB. HP1-beta is required for development of the cerebral neocortex and neuromuscular junctions. J Cell Biol. 2008 Nov 17;183(4):597-606.

Eidesstattliche Erklärung

Ich erkläre hiermit, dass die vorliegende Arbeit ohne unzulässige Hilfe Dritter und ohne Benutzung anderer als der angegebenen Hilfsmittel angefertigt wurde. Die aus anderen Quellen direkt oder indirekt übernommenen Daten und Konzepte sind unter Angaben der Quelle gekennzeichnet.

Weitere Personen, außer den angegebenen, waren an der inhaltlichen materiellen Erstellung der vorliegenden Arbeit nicht beteiligt. Insbesondere habe ich hierfür nicht die entgeltliche Hilfe von Vermittlungs- bzw. Beratungsdiensten (Promotionsberater oder andere Personen) in Anspruch genommen. Niemand hat von mir unmittelbar oder mittelbar geldwerte Leistungen für Arbeiten erhalten, die im Zusammenhang mit dem Inhalt der vorgelegten Dissertation stehen.

Ich erkläre dass diese Arbeit unter Einhaltung der Regeln guter wissenschaftlicher Praxis der Deutschen Forschungsgemeinschaft entstanden ist.

Die Arbeit wurde bisher weder im In- noch im Ausland in gleicher oder ähnlicher Form einer anderen Prüfungsbehörde vorgelegt.

Ich versichere, dass ich weder an der CAU Kiel noch anderweitig versucht habe, eine Dissertation einzureichen oder mich einer Doktorprüfung zu unterziehen.

Mustafa Billur

. …… ……

(Ort, Datum) (Unterschrift)

Appendix

Sequences of GST fusion proteins

Color code : GST sequence HP1 sequence

Full length HP1α in pGEX-4T-1 vector

DNA sequence:

ATGTCCCCTATACTAGGTTATTGGAAAATTAAGGGCCTTGTGCAACCCACTCGACTTCTTTTGGAATATCTTGAA
GAAAAATATGAAGAGCATTTGTATGAGCGCGATGAAGGTGATAAATGGCGAAACAAAAAGTTTGAATTGGGTTTG
GAGTTTCCCAATCTTCCTTATTATATTGATGGTGATGTTAAATTAACACAGTCTATGGCCATCATACGTTATATA
GCTGACAAGCACAACATGTTGGGTGGTTGTCCAAAAGAGCGTGCAGAGATTTCAATGCTTGAAGGAGCGGTTTTG
GATATTAGATACGGTGTTTCGAGAATTGCATATAGTAAAGACTTTGAAACTCTCAAAGTTGATTTTCTTAGCAAG
CTACCTGAAATGCTGAAAATGTTCGAAGATCGTTTATGTCATAAAACATATTTAAATGGTGATCATGTAACCCAT
CCTGACTTCATGTTGTATGACGCTCTTGATGTTGTTTTATACATGGACCCAATGTGCCTGGATGCGTTCCCAAAA
TTAGTTTGTTTTAAAAAACGTATTGAAGCTATCCCACAAATTGATAAGTACTTGAAATCCAGCAAGTATATAGCA
TGGCCTTTGCAGGGCTGGCAAGCCACGTTTGGTGGTGGCGACCATCCTCCAAAATCGGATCTGCTGGTTCCGCGT
GGATCCCCGGAATTCGATAAGCTTGACATGGGAAAGAAGACCAAGAGGACAGCCGACAGCTCTTCTTCAGAGGAT
GAGGAGGAATATGTGGTGGAAAAGGTGTTGGACAGGCGCATGGTTAAGGGGCAAGTGGAATATCTGTTGAAGTGG
AAAGGCTTTTCTGAGGAGCACAATACTTGGGAACCTGAGAAGAACTTGGATTGTCCTGAACTAATTTCTGAGTTT
ATGAAAAAGTATAAGAAGATGAAGGAGGGTGAAAACAATAAGCCCAGGGAGAAATCAGAAGGAAACAAGAGGAAA
TCCAGTTTCTCCAACAGCGCTGATGATATTAAATCTAAAAAAAAGAGAGAGCAAAGCAATGATATCGCTCGGGGC
TTTGAGAGAGGACTGGAACCAGAAAAGATCATCGGAGCAACAGATTCCTGCGGTGACTTAATGTTCTTAATGAAA
TGGAAAGACACAGATGAAGCTGACCTGGTTCTTGCAAAAGAAGCTAACGTGAAGTGTCCACAGATTGTGATAGCA
TTTTATGAAGAGAGACTGACGTGGCACGCATATCCAGAGGATGCGGAAAACAAAGAAAAAGAAAGCGCGAAGAGC
TAA

Amino acid sequence:

MSPILGYWKIKGLVQPTRLLLEYLEEKYEEHLYERDEGDKWRNKKFELGLEFPNLPYYIDGDVKLTQSMAIIRYI
ADKHNMLGGCPKERAEISMLEGAVLDIRYGVSRIAYSKDFETLKVDFLSKLPEMLKMFEDRLCHKTYLNGDHVTH
PDFMLYDALDVVLYMDPMCLDAFPKLVCFKKRIEAIPQIDKYLKSSKYIAWPLQGWQATFGGGDHPPKSDLVPRG
SPEFDKLDMGKKTKRTADSSSSEDEEEYVVEKVLDRRMVKGQVEYLLKWKGFSEEHNTWEPEKNLDCPELISEFM
KKYKKMKEGENNKPREKSEGNKRKSSFSNSADDIKSKKKREQSNDIARGFERGLEPEKIIGATDSCGDLMFLMKW
KDTDEADLVLAKEANVKCPQIVIAFYEERLTWHAYPEDAENKEKESAKS.

Full length HP1β in pGEX-3X vector

DNA sequence:

ATGTCCCCTATACTAGGTTATTGGAAAATTAAGGGCCTTGTGCAACCCACTCGACTTCTTTTGGAATATCTTGAA
GAAAAATATGAAGAGCATTTGTATGAGCGCGATGAAGGTGATAAATGGCGAAACAAAAAGTTTGAATTGGGTTTG
GAGTTTCCCAATCTTCCTTATTATATTGATGGTGATGTTAAATTAACACAGTCTATGGCCATCATACGTTATATA
GCTGACAAGCACAACATGTTGGGTGGTTGTCCAAAAGAGCGTGCAGAGATTTCAATGCTTGAAGGAGCGGTTTTG
GATATTAGATACGGTGTTTCGAGAATTGCATATAGTAAAGACTTTGAAACTCTCAAAGTTGATTTTCTTAGCAAG
CTACCTGAAATGCTGAAAATGTTCGAAGATCGTTTATGTCATAAAACATATTTAAATGGTGATCATGTAACCCAT
CCTGACTTCATGTTGTATGACGCTCTTGATGTTGTTTTATACATGGACCCAATGTGCCTGGATGCGTTCCCAAAA
TTAGTTTGTTTTAAAAAACGTATTGAAGCTATCCCACAAATTGATAAGTACTTGAAATCCAGCAAGTATATAGCA
TGGCCTTTGCAGGGCTGGCAAGCCACGTTTGGTGGTGGCGACCATCCTCCAAAATCGGATCTGATCGAAGGTCGT
GGGATCCCCCTGGCGGGTACTATGGGGAAAAAGCAAAACAAGAAGAAAGTGGAGGAGGTACTAGAAGAAGAGGAA
GAGGAATATGTGGTGGAAAAAGTTCTTGATCGGCGAGTTGTCAAGGGCAAGGTGGAATATCTTCTAAAGTGGAAG
GGTTTCTCAGATGAGGACAACACTTGGGAGCCAGAAGAGAATCTGGATTGCCCTGACCTTATTGCTGAGTTTCTA
CAGTCACAGAAAACAGCTCATGAGACAGATAAGTCAGAGGGAGGCAAGCGCAAAGCTGATTCTGATTCTGAAGAT
AAAGGAGAGGAAAGCAAACCAAAGAAGAAGAAAGAAGAGTCAGAAAAGCCACGAGGCTTTGCCCGGGGTTTGGAG
CCAGAGCGGATTATTGGAGCTACTGACTCCAGTGGAGAGCTCATGTTCCTGATGAAATGGAAAAACTCTGATGAG
GCTGACCTGGTCCCTGCCAAGGAAGCCAATGTCAAGTGCCCACAGGTTGTCATATCCTTCTATGAGGAAAGGCTA
ACGTGGCATTCCTACCCCTCAGAGGATGATGACAAAAAAGACGACAAGAATTAG

Amino acid sequence:

MSPILGYWKIKGLVQPTRLLLEYLEEKYEEHLYERDEGDKWRNKKFELGLEFPNLPYYIDGDVKLTQSMAIIRYI
ADKHNMLGGCPKERAEISMLEGAVLDIRYGVSRIAYSKDFETLKVDFLSKLPEMLKMFEDRLCHKTYLNGDHVTH
PDFMLYDALDVVLYMDPMCLDAFPKLVCFKKRIEAIPQIDKYLKSSKYIAWPLQGWQATFGGGDHPPKSDLIEGR
GIPLAGTMGKKQNKKKVEEVLEEEEEEYVVEKVLDRRVVKGKVEYLLKWKGFSDEDNTWEPEENLDCPDLIAEFL
QSQKTAHETDKSEGGKRKADSDSEDKGEESKPKKKKEESEKPRGFARGLEPERIIGATDSSGELMFLMKWKNSDE
ADLVPAKEANVKCPQVVISFYEERLTWHSYPSEDDDKKDDKN.

Mutants of GST-HP1β:

V23M : valine 23 to methionine, GTG to ATG

R29/30Q : arginine 29 and 30 to glutamine, CGGCGA to CAACAA

K33Q : lysine 33 to glutamine, AAG to CAG

F45E : phenylalanine 45 to glutamic acid, TTC to GAA

T51A : threonine 51 to alanine, ACT to GCT

I161E : isoleucine 161 to glutamic acid, ATA to GAG

V23M & I161E : valine 23 to methionine, GTG to ATG and isoleucine 161 to glutamic acid, ATA to GAG

R29/30Q & I161E : arginine 29 and 30 to glutamine, CGGCGA to CAACAA and isoleucine 161 to glutamic acid, ATA to GAG

K33Q & I161E : lysine 33 to glutamine, AAG to CAG and isoleucine 161 to glutamic acid, ATA to GAG

F45E & I161E : phenylalanine 45 to glutamic acid, TTC to GAA and isoleucine 161 to glutamic acid, ATA to GAG

T51A & I161E : threonine 51 to alanine, ACT to GCT and isoleucine 161 to glutamic acid, ATA to GAG

Full length HP1γ in pGEX-3X vector

DNA sequence:

ATGTCCCCTATACTAGGTTATTGGAAAATTAAGGGCCTTGTGCAACCCACTCGACTTCTTTTGGAATATCTTGAA
GAAAAATATGAAGAGCATTTGTATGAGCGCGATGAAGGTGATAAATGGCGAAACAAAAAGTTTGAATTGGGTTTG
GAGTTTCCCAATCTTCCTTATTATATTGATGGTGATGTTAAATTAACACAGTCTATGGCCATCATACGTTATATA
GCTGACAAGCACAACATGTTGGGTGGTTGTCCAAAAGAGCGTGCAGAGATTTCAATGCTTGAAGGAGCGGTTTTG
GATATTAGATACGGTGTTTCGAGAATTGCATATAGTAAAGACTTTGAAACTCTCAAAGTTGATTTTCTTAGCAAG
CTACCTGAAATGCTGAAAATGTTCGAAGATCGTTTATGTCATAAAACATATTTAAATGGTGATCATGTAACCCAT
CCTGACTTCATGTTGTATGACGCTCTTGATGTTGTTTTATACATGGACCCAATGTGCCTGGATGCGTTCCCAAAA
TTAGTTTGTTTTAAAAAACGTATTGAAGCTATCCCACAAATTGATAAGTACTTGAAATCCAGCAAGTATATAGCA
TGGCCTTTGCAGGGCTGGCAAGCCACGTTTGGTGGTGGCGACCATCCTCCAAAATCGGATCTGATCGAAGGTCGT
GGGATCCCCCTGGCGGGTACTATGGCCTCCAATAAAACTACATTGCAAAAAATGGGAAAGAAACAAAATGGAAAG
AGTAAAAAAGTTGAAGAGGCAGAGCCTGAAGAATTTGTGGTAGAAAAAGTACTGGACCGTCGTGTAGTGAATGGG
AAGGTGGAGTATTTCCTGAAGTGGAAGGGGTTCACAGATGCTGATAATACTTGGGAACCAGAAGAAAATTTAGAT
TGTCCAGAATTAATTGAAGCATTTCTTAATTCTCAAAAAGCTGGTAAAGAAAAAGATGGTACAAAAAGGAAATCT
TTATCTGACAGTGAATCTGATGATAGCAAATCGAAGAAGAAGAGAGATGCTGCTGACAAACCAAGGGGCTTTGCC
AGAGGTCTCGACCCTGAACGAATAATCGGCGCCACAGACAGCAGCGGAGAGTTAATGTTTCTCATGAAGTGGAAG
GACTCGGACGAGGCCGACTTGGTGCTGGCAAAGGAGGCGAACATGAAGTGTCCTCAGATTGTCATTGCCTTCTAC
GAGGAGCGGCTGACTTGGCATTCTTGTCCTGAAGATGAAGCACAATAA

Amino acid sequence:

MSPILGYWKIKGLVQPTRLLLEYLEEKYEEHLYERDEGDKWRNKKFELGLEFPNLPYYIDGDVKLTQSMAIIRYI
ADKHNMLGGCPKERAEISMLEGAVLDIRYGVSRIAYSKDFETLKVDFLSKLPEMLKMFEDRLCHKTYLNGDHVTH
PDFMLYDALDVVLYMDPMCLDAFPKLVCFKKRIEAIPQIDKYLKSSKYIAWPLQGWQATFGGGDHPPKSDLIEGR
GIPLAGTMASNKTTLQKMGKKQNGKSKKVEEAEPEEFVVEKVLDRRVVNGKVEYFLKWKGFTDADNTWEPEENLD
CPELIEAFLNSQKAGKEKDGTKRKSLSDSESDDSKSKKKRDAADKPRGFARGLDPERIIGATDSSGELMFLMKWK
DSDEADLVLAKEANMKCPQIVIAFYEERLTWHSCPEDEAQ.

C-terminal HP1β in pGEX-3X vector

DNA sequence:

ATGTCCCCTATACTAGGTTATTGGAAAATTAAGGGCCTTGTGCAACCCACTCGACTTCTTTTGGAATATCTTGAA
GAAAAATATGAAGAGCATTTGTATGAGCGCGATGAAGGTGATAAATGGCGAAACAAAAAGTTTGAATTGGGTTTG
GAGTTTCCCAATCTTCCTTATTATATTGATGGTGATGTTAAATTAACACAGTCTATGGCCATCATACGTTATATA
GCTGACAAGCACAACATGTTGGGTGGTTGTCCAAAAGAGCGTGCAGAGATTTCAATGCTTGAAGGAGCGGTTTTG
GATATTAGATACGGTGTTTCGAGAATTGCATATAGTAAAGACTTTGAAACTCTCAAAGTTGATTTTCTTAGCAAG
CTACCTGAAATGCTGAAAATGTTCGAAGATCGTTTATGTCATAAAACATATTTAAATGGTGATCATGTAACCCAT
CCTGACTTCATGTTGTATGACGCTCTTGATGTTGTTTTATACATGGACCCAATGTGCCTGGATGCGTTCCCAAAA
TTAGTTTGTTTTAAAAAACGTATTGAAGCTATCCCACAAATTGATAAGTACTTGAAATCCAGCAAGTATATAGCA
TGGCCTTTGCAGGGCTGGCAAGCCACGTTTGGTGGTGGCGACCATCCTCCAAAATCGGATCTGATCGAAGGTCGT
GGGATCCCCCTGGCGGGTACTCGGGGTTTGGAGCCAGAGCGGATTATTGGAGCTACTGACTCCAGTGGAGAGCTC
ATGTTCCTGATGAAATGGAAAAACTCTGATGAGGCTGACCTGGTCCCTGCCAAGGAAGCCAATGTCAAGTGCCCA
CAGGTTGTCATATCCTTCTATGAGGAAAGGCTAACGTGGCATTCCTACCCCTCAGAGGATGATGACAAAAAAGAC
GACAAGAATTAG

Amino acid sequence:

MSPILGYWKIKGLVQPTRLLLEYLEEKYEEHLYERDEGDKWRNKKFELGLEFPNLPYYIDGDVKLTQSMAIIRYI
ADKHNMLGGCPKERAEISMLEGAVLDIRYGVSRIAYSKDFETLKVDFLSKLPEMLKMFEDRLCHKTYLNGDHVTH
PDFMLYDALDVVLYMDPMCLDAFPKLVCFKKRIEAIPQIDKYLKSSKYIAWPLQGWQATFGGGDHPPKSDLIEGR
GIPLAGTRGLEPERIIGATDSSGELMFLMKWKNSDEADLVPAKEANVKCPQVVISFYEERLTWHSYPSEDDDKKD
DKN.

N-terminal HP1β in pGEX-4T-3 vector

DNA sequence:

ATGTCCCCTATACTAGGTTATTGGAAAATTAAGGGCCTTGTGCAACCCACTCGACTTCTTTTGGAATATCTTGAA
GAAAAATATGAAGAGCATTTGTATGAGCGCGATGAAGGTGATAAATGGCGAAACAAAAAGTTTGAATTGGGTTTG
GAGTTTCCCAATCTTCCTTATTATATTGATGGTGATGTTAAATTAACACAGTCTATGGCCATCATACGTTATATA
GCTGACAAGCACAACATGTTGGGTGGTTGTCCAAAAGAGCGTGCAGAGATTTCAATGCTTGAAGGAGCGGTTTTG
GATATTAGATACGGTGTTTCGAGAATTGCATATAGTAAAGACTTTGAAACTCTCAAAGTTGATTTTCTTAGCAAG
CTACCTGAAATGCTGAAAATGTTCGAAGATCGTTTATGTCATAAAACATATTTAAATGGTGATCATGTAACCCAT
CCTGACTTCATGTTGTATGACGCTCTTGATGTTGTTTTATACATGGACCCAATGTGCCTGGATGCGTTCCCAAAA
TTAGTTTGTTTTAAAAAACGTATTGAAGCTATCCCACAAATTGATAAGTACTTGAAATCCAGCAAGTATATAGCA
TGGCCTTTGCAGGGCTGGCAAGCCACGTTTGGTGGTGGCGACCATCCTCCAAAATCGGATCTGCTGGTTCCGCGT
GGATCCAGAAAGCTGGCGGGTACTATGGGGAAAAAGCAAAACAAGAAGAAAGTGGAGGAGGTACTAGAAGAAGAG
GAAGAGGAATATGTGGTGGAAAAAGTTCTTGATCGGCGAGTTGTCAAGGGCAAGGTGGAATATCTTCTAAAGTGG
AAGGGTTTCTCAGATGAGGACAACACTTGGGAGCCAGAAGAGAATCTGGATTGCCCTGACCTTATTGCTGAGTTT
CTACAGTCACAGAAAACAGCTCATGAGACAGATAAGTCAGAGGGAGGCAAGCGCAAAGCTGATTCTGATTCTGAA
GATAAAGGAGAGGAAAGCAAACCAAAGAAGAAGAAAGAAGAGTCAGAAAAGCCACGAGGCTTTGCCCGGGTCGAC
TCGAGCGGCCGCATCGTGACTGACTGA

Amino acid sequence:

MSPILGYWKIKGLVQPTRLLLEYLEEKYEEHLYERDEGDKWRNKKFELGLEFPNLPYYIDGDVKLTQSMAIIRYI
ADKHNMLGGCPKERAEISMLEGAVLDIRYGVSRIAYSKDFETLKVDFLSKLPEMLKMFEDRLCHKTYLNGDHVTH
PDFMLYDALDVVLYMDPMCLDAFPKLVCFKKRIEAIPQIDKYLKSSKYIAWPLQGWQATFGGGDHPPKSDLVPRG
SRKLAGTMGKKQNKKKVEEVLEEEEEEYVVEKVLDRRVVKGKVEYLLKWKGFSDEDNTWEPEENLDCPDLIAEFL
QSQKTAHETDKSEGGKRKADSDSEDKGEESKPKKKKEESEKPRGFARVDSSGRIVTD.

Mutants of GST-N-terminal HP1β

V23M : valine 23 to methionine, GTG to ATG

R29/30Q : arginine 29 and 30 to glutamine, CGGCGA to CAACAA

K33Q : lysine 33 to glutamine, AAG to CAG

F45E : phenylalanine 45 to glutamic acid, TTC to GAA

T51A : threonine 51 to alanine, ACT to GCT

Sequences of His fusion proteins

Color code: Hexahistidine tag sequence HP1 sequence

Full length HP1β in pQE-30 vector

DNA sequence:

ATGAGAGGATCGCATCACCATCACCATCACGGATCCATGGGAAAAAAGCAAAACAAGAAGAAAGTGGAGGAGGTA
CTAGAAGAAGAGGAAGAGGAATATGTGGTGGAAAAAGTTCTTGATCGGCGAGTTGTCAAGGGCAAGGTGGAATAT
CTTCTAAAGTGGAAGGGTTTCTCAGATGAGGACAACACTTGGGAGCCAGAAGAGAATCTGGATTGCCCTGACCTT
ATTGCTGAGTTTCTACAGTCACAGAAAACAGCTCATGAGACAGATAAGTCAGAGGGAGGCAAGCGCAAAGCTGAT
TCTGATTCTGAAGATAAAGGAGAGGAAAGCAAACCAAAGAAGAAGAAAGAAGAGTCAGAAAAGCCACGAGGCTTT
GCCCGGGGTTTGGAGCCAGAGCGGATTATTGGAGCTACTGACTCCAGTGGAGAGCTCATGTTCCTGATGAAATGG
AAAAACTCTGATGAGGCTGACCTGGTCCCTGCCAAGGAAGCCAATGTCAAGTGCCCACAGGTTGTCATATCCTTC
TATGAGGAAAGGCTAACGTGGCATTCCTACCCCTCAGAGGATGATGACAAAAAAGACGACAAGAATTAGAAGCTT
AATTAG

Amino acid sequence:

MRGSHHHHHHGSMGKKQNKKKVEEVLEEEEEEYVVEKVLDRRVVKGKVEYLLKWKGFSDEDNTWEPEENLDCPDL
IAEFLQSQKTAHETDKSEGGKRKADSDSEDKGEESKPKKKKEESEKPRGFARGLEPERIIGATDSSGELMFLMKW
KNSDEADLVPAKEANVKCPQVVISFYEERLTWHSYPSEDDDKKDDKN.

Mutants of His HP1β

V23M : valine 23 to methionine, GTG to ATG

F45E : phenylalanine 45 to glutamic acid, TTC to GAA

T51A : threonine 51 to alanine, ACT to GCT

I161E : isoleucine 161 to glutamic acid, ATA to GAG

Results from collaborations are outlined when discussing the respective data

Telomere FISH and Giemsa Staining

was done in collaboration with Prof. T. Pandita (WUSOM, St. Louis, USA)

Transient expression of EGFP fusion proteins and immunofluorescence staining

was done in collaboration with Dr. K. Okamoto (Scripps, San Diego, USA)

FLOW-FISH analysis

was done in collaboration with Dr. U. Brassat/Prof. T. Brummendorf (UKE, Hamburg, Germany)

Retroviral transduction of RAS and proliferation assay

was done in collaboration with Dr. M. Balabanov/Prof. T. Brummendorf (UKE, Hamburg, Germany)